Binding and characterization of fluorescent nano-aggregates on structured surfaces

TECHNISCHE UNIVERSITÄT
CHEMNITZ

von der Fakultät für Naturwissenschaften der
Technischen Universität Chemnitz genehmigte
Dissertation zur Erlangung des akademischen Grades

doctor rerum naturalium
(Dr. rer. nat.)

vorgelegt von Dipl. Phys. Thomas Baumgärtel
geboren am 17.11.1982 in Karl-Marx-Stadt
eingereicht am 20.02.2012

Gutachter: Prof. Dr. Christian von Borczyskowski
Prof. Dr. Robert Magerle

Tag der Verteidigung: 10.07.2012

URL: http://nbn-resolving.de/urn:nbn:de:bsz:ch1-qucosa-91552

Bibliographische Angaben

Baumgärtel, Thomas
Binding and characterization of optically active nano-aggregates on structured surfaces
Dissertation, Technische Universität Chemnitz, 2012
137 Seiten, 54 Abbildungen, 3 Tabellen, 186 Literaturverweise

Referat

Im Mittelpunkt dieser Arbeit steht die selektive Funktionalisierung von Siliziumoxidnanostrukturen auf alkyl-passivierten Siliziumoberflächen welche durch rasterkraftmikroskopisch induzierte lokale anodische Oxidation (LAO) erzeugt werden. Bei der gezielten Immobilisierung von funktionalen Molekülen auf den Strukturen werden zwei verschiedene Routen verfolgt Anbindung von ionischen Farbstoffen über elektrostatische Wechselwirkungen sowie stufenweise kovalente chemische Anbindung von bi-funktionalen Verbindermolekülen und Farbstoffen. Eine Untersuchung der hergestellten funktionalen Strukturen erfolgt mittels Rasterkraftmikroskopie, Raster-Kelvin-Mikroskopie sowie zeitaufgelöster Fluoreszenzmikroskopie und-spektroskopie. Durch zwei unabhängige Methoden kann gezeigt werden dass die Ladungen im lokalen Oxide vergleichsweise stabil sind und die elektrostatische Anbindung somit auch noch nach Tagen möglich sein sollte. Das Verhalten der elektrostatisch angebundenen Farbstoffe hängt stark von deren Art ab. Während es bei Rhodamin 6G nur zu einer minimalen spektralen Änderung im Vergleich zur Lösung kommt so zeigen spermin-funktionalisierte Perylenbisimidfarbstoffe eine deutliche H-Aggregation und Ausbildung von Excimerzuständen. Diese Zustände sind eindeutig thermisch aktiviert und zeigen eine wesentlich höhere Aktivierungsenergie als bei allen anderen bisher untersuchten Perylenaggregaten sowie eine Hysterese bei Temperaturveränderung. Die physikalische Ursache für dieses Phänomen liegt allem Anschein nach in der elektrostatischen Anbindung selbst welche ein instabiles Gleichgewicht mit der Wechselwirkung der Moleküle untereinander bildet. Eine geordnete kovalente Anbindung von funktionalen Silanmolekülen an die mittels LAO erzeugten Strukturen erfordert sehr definierte Prozessparameter. Die spektroskopische Untersuchung von an die funktionalen Silane chemisch angebundenen Fluoresceinfarbstoffen lässt indirekte Schlüsse auf deren Belegungsdichte und damit die Qualität der Silanmonolage zu.

Schlagwörter

Lokale Anodische Oxidation, AFM-Lithographie, KPFM, Rhodamin 6G, Perylenbisimid, E-Excimer, Tieftemperatur, zeitaufgelöste optische Spektroskopie, Silanisierung, Fluoresceinthioisocyanat, Funktionalisierung, Nanostrukturen

Contents

List of Figures

List of Tables

Glossary

AFM	atomic force microscopy
AC	alternating current
di-4-ANEPPS	aminonaphthylethenylpyridinium
APD	avalanche photo diode
APTES	aminopropyltriethoxysilane
BS	beam splitter
CCD	charge coupled device
CPD	contact potential difference
DC	direct current
FITC	fluorescein-5-isothiocyanate
KPFM	Kelvin probe force microscopy
LAO	local anodic oxidation
LP	long pass (filter)
LSCM	laser scanning confocal microscope
NC-APM	non-contact mode atomic force microscopy
ND	neutral density (filter)

OTS	octadecyl-trichlorosilane
PBI	perylene-bisimide
PL	photoluminescence
PMMA	poly(methyl methacrylate)
R6G	rhodamine 6G
RH	relative humidity
RMS	root mean square
RT	room temperature
SAM	self-assembled monolayer
sf-PBI	spermine-functionalized perylene-bisimide
SOI	silicon on insulator
SPD	surface potential difference
SSCM	sample scanning confocal microscope

1 General Introduction

Nanotechnology is a relatively young branch of natural science but has met with constantly growing interest within the last three decades. By informal definition it deals with the fabrication of structures, materials or whole devices sizing from 1 to 100 nanometers in at least one dimension. Thus nanotechnology is a tool to advance towards an ultimate frontier: a targeted manipulation of matter at the very bottom scale of our tangible world - at a molecular or an atomic level. Depending on the used materials and the employed phenomena or methods there is a huge variety of different applications such as nanomaterials, nanomedicine, nanorobotics, nanoelectronics and nanochemistry. Accordingly, nanotechnology involves knowledge and application of multiple fields of science like surface physics, molecular biology, micro- or nanofabrication, semiconductor physics and chemistry. Basically, the concepts used to create nanostructures can be divided into two groups: top-down and bottom-up approaches.

In a top-down approach a larger device is used to create or arrange a smaller structure. Through remarkable progresses within the last years, many conventional semiconductor device fabrication techniques are nowadays capable of creating not only thin films within the nanometer regime but also lateral nanostructures down to several tens of nm. Besides parallel approaches which use masks, etching and epitaxy, scanning methods as atomic force microscopy (AFM) [Tsen05] or focused ion beam [Watt05] based lithography are widely-used especially within basic research. Here a local manipulation of the sample surface is achieved by a scanning tip or a particle beam. Material can be selectively removed, deposited or even chemical reactions can be induced locally. In comparison with parallel techniques using e.g. parallel projection or stamps, scanning methods are much slower, thus not suitable for mass production, but on the other hand they offer a much greater versatility and adaptivity.

In contrast to top-down nanostructuring which is essentially a miniaturization of concepts from macroscopic technology, bottom-up approaches have been adopted from biology and supramolecular chemistry. In a bottom-up process smaller building blocks are used to form larger and more complex assemblies. This concept is omnipresent in living nature e.g. in order to form cell membranes or protein complexes. The interaction of the single blocks can be realized through different binding mechanisms such as hydrogen bonds, hydrophilic/hydrophobic interactions,

electrostatic interactions or covalent bonds. A very promising bottom-up method is molecular self-assembly where single molecules automatically arrange into a desired conformation. This can be achieved in a very controllable and reliable way by so called 'click'-chemistry [Kolb01] which employs concepts of supramolecular chemistry and molecular recognition. By synthesis of molecules with different functional and anchoring groups, site-selective chemical reactions enable the functionalization even of inorganic surfaces.
Furthermore it is possible to combine both approaches in a successive manner. A pre-structuring of the surface via top-down methods can be followed by a bottom-up functionalization of the structures or vice versa. However, an implementation of such multi-step processes is quite challenging as every single stage is critical and requires a high degree of precision and control. Especially for miniaturization of electronics or devices, it is desirable not only to be able to build nanoscopic entities but also to selectively create, position or arrange them in a highly defined environment. The silicon surface is a very suitable system for such a purpose as it is one of the best-investigated materials in modern science and basis of our state of the art electronics (integrated circuits). Nanostructuring of silicon surfaces via various top-down methods is still of much interest and is studied by many groups [Chie10, Mo09, Albo08, Yang09, Han09, Lu07]. A promising approach is to terminate the silicon by a self-assembled monolayer (SAM) prior to the structuring. This not only provides the means to protect the reactive silicon against ambient oxygen but also enables to create surfaces with a desired physicochemical functionality. By using AFM anodization lithography, the monolayers or moreover the silicon beneath can be oxidized locally thus resulting in structures with lateral dimensions in the range of a few tens of nanometers and a height up to a few nanometers. These structures can be used as template for further bottom-up functionalization with manifold materials as metal or semiconductor nanoparticles, single molecules or biological macromolecules. Especially interesting for such purposes are optically active materials, which means in the context of this work molecules or nanoparticles that show luminescence emission of light upon optical excitation. By a controlled binding of these entities to a nanostructured substrate, nanoscopic fluorescence emitters can be easily created. Such systems may be used as basis for the design of sensors (lab-on-a-chip), photonic circuits or molecular electronics. Thus, the current work focusses on the immobilization of xanthene and perylene dyes molecules on silicon oxide nanostructures that have been created by local anodic oxidation of monolayer-terminated silicon. Thereby the specific binding has been realized by electrostatic attraction of rhodamine 6G or spermine functionalized perylene bisimide as well as covalent binding of fluorescein-5-isothiocyanate. Both classes, xanthene as well as perylene dyes are characterized by a high quantum yield and distinctive fluorescence properties. Furthermore their binding and aggregation behavior has been investigated in numerous studies.

This thesis continues the research which I started with my diploma thesis 'AFM-induced nanolithography on alkyl-terminated silicon for selective binding of dye molecules'. The preceding work was mainly about the investigation of local anodic oxidation of alkyl-terminated silicon at diverse parameters and a characterization of the formed alkyl SAMs. The present work focuses on a more detailed investigation about how a combination of top-down and bottom-up nanostructuring can be successfully utilized to create optically active one- and two-dimensional nanostructures on silicon surfaces. It will not only provide insights into the different chemical functionalization routes but will also reveal new aspects of the optical properties of nanoscopic dye-assemblies. As the presented realizations are rather specialized, novel and interdisciplinary approaches, the relevant and associated literature will be reviewed in the respective chapters separately.

Outline of the thesis

The primary scope of this thesis is to show how different functionalization routes can be used to create optically active nanostructures and to characterize these structures by atomic force and Kelvin probe force microscopy as well as photoluminescence spectra and life time measurements. Here, a special focus is on the explanation of the results from a physiochemical point of view. Chapter 2 provides experimental details about the experimental techniques and setups that have been used in this work to fabricate and characterize the discussed samples and processes. In chapter 2, specific basics are elucidated and an overview is given about major works of other groups connected to the general scope of this thesis. Parts of this section have already been published as a book chapter in [Baum11a]. Sections 4 to 7 form the scientific core of the thesis:

- In chapter 4 the nature and stability of the negative space charge within the created local anodic oxide nanostructures will be investigated. This is a crucial question especially for the functionalization via electrostatic attraction of positively charged dye molecules. Combining the results of both Kelvin probe force microscopy and optical spectroscopy of a charge sensitive dye, this is the first time that such a stability study has been conducted. Furthermore, the water adsorption kinetics on a nanoscale could be observed and explained with known models. This chapter has been published recently in Nanotechnology [Baum12].

- Chapter 5 was also published in Nanotechnology in the year 2010 [Baum10]. Here a detailed analysis of rhodamine 6G functionalized local anodic oxide nanostruc-

tures has been conducted. The investigations include photoluminescence intensity, spectra and bleaching experiments which have been performed using wide field and confocal fluorescence microscopy and spectroscopy. The wide field and the bleaching data have thereby been obtained during my diploma thesis.

- Similar investigations are presented in chapter 6, yet here a special perylene derivative has been used as optically active material. Also the scope of experimental techniques was enlarged by fluorescence life time and low-temperature spectral investigations. The findings are discussed and classified in the known frameworks of perylene aggregation and excimer formation as well as a semiconductor fluorescence quenching theory.

- While the previous chapters deal with the electrostatic binding of cationic dye molecules, part 7 is about another functionalization route: the covalent binding of fluorescein-5-isothiocyanate to the nanostructures by functional silane linker molecules. This work was inspired by a 6 months research period at the 'Molectronics' lab of Prof. Hirokazu Tada at Osaka University in Japan. There, first investigations about the functionalization of silicon(111) surfaces have been carried out which later on could be successfully implemented on the silicon oxide nanostructures.

Finally, in chapter 8, the major findings of this thesis are summarized and prospects as well as open questions are briefly discussed.

2 Fundamentals

Within this section, the basic physical and chemical principles will be introduced which have been used for the generation and investigation of the functional nanostructures. However, due to their diversity and number, not all methods can be explained in full detail here and the intrigued reader is asked to refer to the denoted literature. Parts of this section have also been published as a review in form of a book chapter [Baum11a].

2.1 Local anodic oxidation nanolithography via AFM

In local anodic oxidation (LAO) nanolithography [Snow94, Daga95, Avou97] the AFM tip and the substrate form the electrodes of a nanoscopic electrochemical cell, modifying the surface by a chemical reaction (oxidation). Water is commonly used as electrolyte for the cell but also other oxygen-containing liquids can be utilized [Tell03]. Under ambient conditions, there is always an adsorption layer of water both covering the tip and the sample surface. If the tip is close to the surface (some nanometers) and a voltage is applied between probe and sample, water molecules are polarized by the electric field and follow the field gradient. They will accumulate at the terminus of the tip where the field strength is maximal. If the voltage is above a certain threshold value, a stable water bridge (meniscus) between tip and sample surface is formed (figure 2.1A). In the case of direct physical contact between tip and surface no voltage is needed in order to form a water meniscus. If the electrical field strength is high enough, water is dissociated into protons and hydroxyl anions (OH^-) or even oxy anions (O_2^-). Considering the small distance between tip apex and substrate ($\sim$nm) as well as the small tip curvature radius ($\sim$10 nm), such field strength is reached even for relatively small voltages in the range of some volts. The positive protons are dragged to the tip (cathode) where they are reduced and finally form molecular hydrogen. The negatively charged hydroxyl anions are pulled to the silicon anode (figure 2.1B). Reaching the bulk silicon they

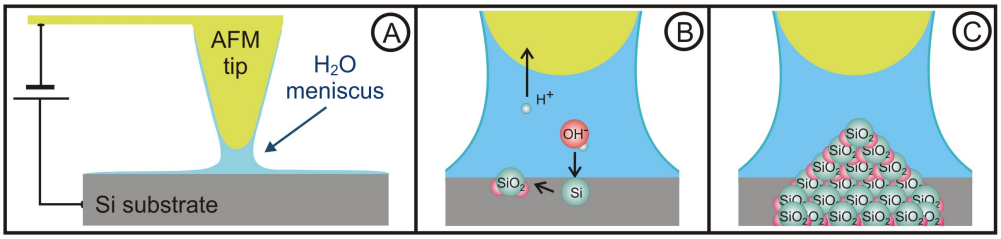

Figure 2.1: Principle of local anodic oxidation of a silicon substrate with an AFM tip. **A**: Ambient humidity and application of a DC voltage lead to the formation of a stable wmater meniscus between tip and surface. **B**: Water molecules are dissociated through the electric field; hydroxyl anions migrate to the substrate and react with the silicon atoms under formation of silicon oxide. **C**: A silicon oxide structure is forming under the tip position due to volume increase (SiO_2 is more spacious than silicon).

react with it and form silicon oxide according to the following equation [Daga98]:

$$Si + 2OH^- + 4h^+ \longrightarrow SiO_2 + 2H^+ \tag{2.1}$$

whereby h^+ denotes a hole in the bulk silicon. As a silicon oxide molecule is more spacious than a single silicon atom ($V_{Si}/V_{SiO_2} = 20$ Å^3/45 Å^3 [Avou97]), there is an increase in volume expanding in vertical direction. Due to strain relaxation which is possible only in upward direction, an oxide protuberance forms (figure 2.1C). The ratio of height to total oxide thickness was determined to a value of 0.6 [Font98] which means that 40% of the oxide is below the surface plane and 60% is a topographically detectable elevation. This oxidation process is self-limited and saturates after an oxide thickness of a few nanometers [Avou97]. Dagata *et al.* and Dubois *et al.* developed models that explain the self-limitation through the build-up of space charge within the LAO oxide [Daga98, Dubo00] which reproduced the experimentally obtained data very well. In order to reach the underlying silicon, the OH^- anions have to migrate through the already formed oxide. Some of them will be trapped at unsaturated bonds within the oxide leading to a growing accumulation of a space charge. This hinders the migration of further hydroxyl anions by Coulomb repulsion as the oxide grows which finally stops the oxidation. The size and shape of the formed oxide structures is strongly related to the extent of the water meniscus and therefore to the humidity in the surrounding atmosphere. The smaller the meniscus the narrower is the electrochemical cell. With a more confined reaction, the formed oxide features are expected to be laterally smaller in size. Especially using non-contact AFM the water meniscus can be tuned to be very small yielding to oxide structure width below 20 nm [Call00]. Detailed investigations of various LAO structuring parameter dependencies have been published within the last two decades [Font98, Teus95, Snow00, Kura03, Graa08a,

Yang06a, Park04, Call00, Ley96, Oria06, Daga04, Baum11b]. It should be mentioned that oxidation of silicon takes also place under ambient conditions where oxygen in the atmosphere reacts with the silicon forming a thin native oxide layer with a thickness between 1 and 2 nm. However, the reachable oxide thickness using local anodic oxidation is about one order of magnitude larger depending on the applied voltage and environmental conditions. LAO can not only be performed on hydrogen-passivated silicon or silicon covered with a native oxide film but also on silicon substrates with a thin protecting surface layer. Self-assembled monolayers (SAMs) formed through covalent binding of 1-alkenes to silicon [Siev98] are a promising system for LAO structuring. Such SAMs are very thin (around a few nanometers depending on the alkyl chain length) but also densely packed [Fauc07] and very stable [Sung97, Linf95], thus preventing the oxidation of the silicon by atmospheric oxygen. Nevertheless, they allow for local anodic oxidation. If local anodic oxidation is carried out on an alkyl-SAM terminated silicon substrate, first the SAM is at least partially oxidized and degraded until the hydroxyl anions reach the silicon and the oxidation of silicon takes place as mentioned above. Under so-called 'soft' oxidation conditions (low voltage, short duration), the process can be tuned in a way that only the upper parts of the alkene molecules are locally oxidized resulting e.g. in COOH terminal groups [Wout03]. Monolayers are not only a suitable resist for lithographic purposes but they also allow for tuning the surface properties of the substrate, e.g. surface hydrophobicity [Pols10]. This can be used to influence the formed water meniscus and therefore the shape of the resulting oxide structures [Baum11b]. If molecules with special anchoring groups are used as building blocks for the monolayer, a physicochemical functionality of the surface can be achieved. Different routes for such a chemical functionalization will be discussed in the next chapter.

2.2 Chemical functionalization of nanostructured surfaces

Once a local nanostructuring of the substrate has been realized, the desired materials have to be selectively immobilized on the structures. Depending on the type of structures, a multitude of chemical routes are in discussion and have partially been proven as applicable in a substantial number of publications [Daga95, Wout09, Ravo09, Gu04, Sugi09, Wout03]. However, most cases involve either a local mild oxidation of the monolayer only or an etching of the silicon oxide after LAO lithography respectively. A general schematic overview of LAO structuring and functionalization of SAM terminated silicon is given in figure 2.2. The dif-

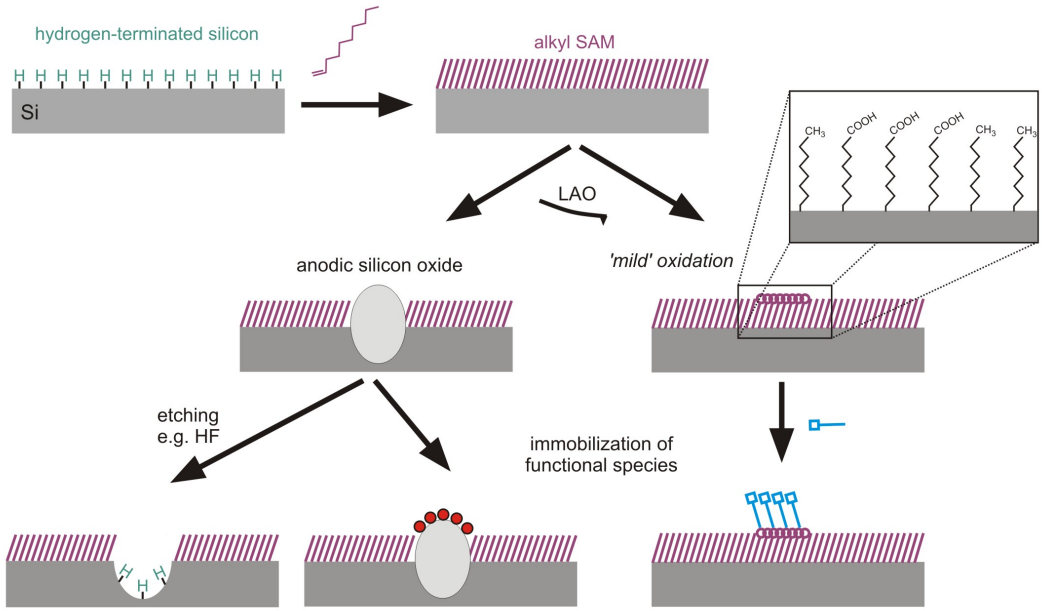

Figure 2.2: Different routes towards functional nanostructures on alkyl-terminated silicon substrates by LAO. Starting from alkyl-SAM formation on hydrogen-terminated silicon (top) local anodic oxidation is performed either resulting in silicon oxide structures or oxidizing only the terminal groups of the monolayer (middle). Bottom: the silicon oxide can be etched away resulting in hydrogen-terminated silicon or functional species can be immobilized by appropriate routes. The carboxylic groups on the monolayer can also act as anchoring points for chemical reactions.

ferent binding mechanisms that can be used for the selective functionalization of local anodic oxidation patterns on monolayer-terminated silicon can be classified into three major groups:

- Intermolecular interactions
- Electrostatic / ionic interactions
- Covalent bonds

Intermolecular interactions in this context is a general term for the forces between uncharged molecules in close proximity such as dipole interactions, hydrogen bonds or van-der-Waals forces. Such forces can be used for the selective binding of materials to surfaces. The surface energy of a nonpolar molecule at a

nonpolar interface is smaller than on a polar interface, for example. If a mixture of polar and nonpolar species (which have to be sufficiently mobile; e.g. in solution) is exposed to a surface containing areas with different surface polarity, this leads to a phase separation which can be used for site-selective deposition of molecules (e.g. cyclopentane lubricants [Mo09]) or nanoparticles (e.g. CdSe/ZnS nanocrystals with passivating ligands [Graa07]). However, intermolecular interactions are mostly characterized by a much lower binding energy compared to covalent bonds and electrostatic interactions and are also only limited to short ranges. Thus their selectivity is not as distinctive as for the other binding mechanisms and the immobilized molecules or particles can be removed easily from the structures (e.g. by rinsing with a solvent). This means that a multi-step functionalization with different species is very difficult in many cases, which is the reason why this binding mechanism has not been employed in this thesis. Electrostatic interactions on the other hand are much more long-ranged and thus are particularly applicable for the selective immobilization of ionic materials. Local oxidation of an alkyl monolayer under mild conditions leads to the formation of polar -COOH surface groups that possess a negative partial charge. It has been shown that cationic molecules like quaternary ammonium salts or positively charged gold nanoparticles can be bound selectively to such groups [Wout03]. Also other metal ions like Fe_2^+ can be bound in a similar way using the negative surface polarity of carboxyl groups generated by local anodic oxidation [Hoep05]. Electrostatic attachment of particles is also possible if not only the monolayer is oxidized but also the underlying silicon. The presence of residual negative charges within local anodic silicon oxide has been demonstrated by electrostatic force microscopy [Wout05] and Kelvin probe force microscopy [Chie10]. The negative partial charge can be used to bind cationic species to the surface e.g. positively charged dye molecules, thus leading to dye-functionalized nanostructures [Graa07, Baum10]. Unfortunately, there are no investigations concerning the stability of such an electrostatic binding. A competitive mechanism between different cationic species and partial reversibility of the binding has to be expected which makes this method also not suitable for multi-step processing. Covalent attachment of molecules on the other hand is a highly desired method for functionalization since covalent bonds possess comparable high dissociation energy (several 100 kJ/mol) and with the knowledge about their successful implementation on nanostructures, the whole realm of modular chemistry can be applied (so called 'Click'-chemistry [Kolb01]). LAO on SAM-terminated silicon is an ideal system for multi-step surface chemistry. An inert monolayer can be used to protect the silicon against environmental influences and with the local oxidation technique the monolayer is chemically altered or locally removed which leads to the formation of nanoscopic oxide. It has to be regarded that only such chemical reactions are suitable for functionalization of these silicon oxide structures which do not corrode the monolayer (e.g. reactions in alkaline environment). Another

important fact is that due to the confined geometry, some reactions cannot proceed like in an isotropic solution because of steric hindrance. A short overview over the successful chemical binding routes on confined surfaces is given in the following. A feasible way to generate functionalized nanostructures via LAO is the mild oxidation of the monolayer surface groups without destruction of the monolayer or the creation of anodic oxide. It has been demonstrated that vinyl-terminated silane SAMs can be formed selectively after the tip-induced electrochemical patterning of an OTS terminated silicon substrate which results in the formation of a bilayer [Maoz00a]. Using different chemical routes the vinyl groups can be converted to thiol groups or carboxyl groups. Thus metals (e.g. gold or silver [Maoz00b]) or semiconductors (e.g. CdSe [Maoz00a]) can be deposited on the structures using wet-chemical processes. Also other silanes can be bound this way which allows for the design of laterally confined multilayer-systems [Maoz99, Haen09]. Alternatively, oxidation and reduction reactions can also be employed for preparation of amine and thiol-terminated structures by local de-protection of a monolayer. Typically, α,α-dimethyl-3,5-dimethoxybenzyloxycarbonyl groups are used for protection of amines and thiols. These groups can be removed by AFM induced anodic oxidation, which leads to amine- [Fres04] or thiol-terminated [Fres05] nanostructures that can be functionalized with dendrimers or small gold nanoparticles. It should be noted that these kinds of selective de-protection reactions are only possible under inert atmosphere. Of course also the inverse procedure is possible: LAO can be used to locally render a surface inert to a certain chemical treatment. Mild scanning probe oxidation on N-hydroxysuccinimide ester-terminated monolayers on silicon yields to the local cleavage of the functional ester groups [Yang09]. The rest of the unoxidized surface can be functionalized through a reaction with $N_3(EO)_3NH_2$. Only where LAO has been carried out, no molecules can attach to the surface which is observed as an apparent height decrease [Yang09]. Another approach than mild oxidation of monolayers is to degenerate the SAM completely and produce local oxide which is etched subsequently. The etched surface is hydrogen-terminated and can be functionalized via attachment of e.g. alkene molecules [Ara02a]. Instead of etching, the generated oxide also could be used as anchoring point for the attachment of silane molecules (e.g. octadecyl trichlorosilane, OTS). However, a direct functionalization of the oxide seems to be much more difficult. Most likely due to the rough nature of the anodic oxide surface as well as its non-uniform stoichiometric composition, a formation of a densely packed and smooth monolayer on the oxide has not been reported yet.

2.3 Optical investigation of the functionalized structures

Fluorescence microscopy and spectroscopy is a versatile tool which has become a standard technique in many branches of physics, chemistry and biology. One of the most advantageous qualities of these methods is that the measured photophysical properties of the investigated entities (e.g. dye molecules or nanocrystals) allow a deep insight into other fundamental physical or chemical processes within themselves or their direct environment. Thus fluorescent molecules or other particles can be utilized as probes which are reliable, comparably cheap and relatively easily accessible by experiment. However, the interpretation of the measured data is in many cases not trivial. Fluorescence is a quantum-mechanical process originating from the electronic structure of matter. Especially for organic molecules,

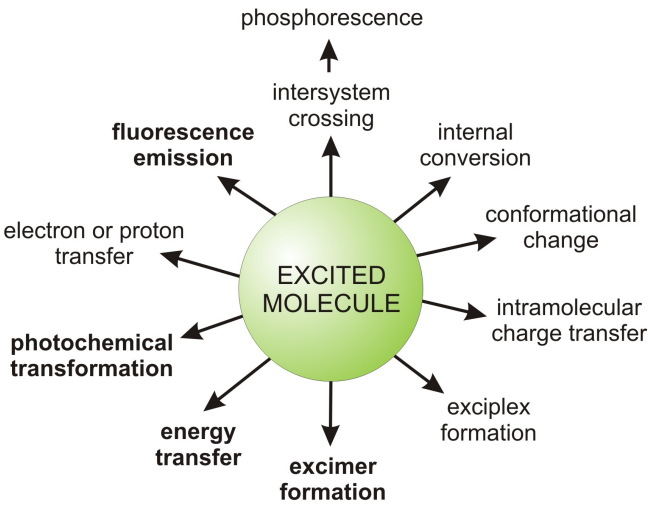

Figure 2.3: Possible de-excitation pathways of excited molecules. Adopted from [Vale02], p. 10.

there is a strong interplay between their electronic structure, molecular geometry and the electronic structure of the environment. Once the molecule has been excited, there are different de-excitation pathways in which fluorescence is only one amongst many. Figure 2.3 gives an overview of the involved processes. Of course, these pathways are not independent from each other but often connected, e.g. an energy transfer or an excimer formation may require a conformational change or rearrangement of the involved molecules [Kash65]. The time scales on that those processes take place can also be very different, ranging from 10^{-12} s for vibrational relaxations to seconds for triplet relaxation (phosphorescence) [Vale02]. Usually,

it is only possible to measure few of these mechanisms by experiment (often: fluorescence). If other pathways are involved which are not directly accessible by experiment, then models have to be conceived and certain assumptions about the other processes have to be made, which generally require a detailed knowledge about the investigated system in a molecular picture. In the following, the relevant properties and processes for the measurements and explanations used in this thesis are presented briefly. There are three major characteristics of the fluorescence emission: photoluminescence (PL) intensity, PL spectrum and PL life time. The PL spectrum originates from the transitions of electrons between different molecular energy levels (orbitals) or states and thus represents the electronic structure of the emitters. The life time is a measure for the rates (or probability) for the transitions between the energy levels. It is important to remember, that in most cases there is a competition between different de-excitation pathways, each with a different probability or rate. If the molecule is in the excited state S_1, then the measured life time τ_s of this state is given by the following formula:

$$\tau_s = \frac{1}{k_r + k_{nr}} \tag{2.2}$$

with k_r being the rate constant for radiative de-excitation of S_1 with emission of fluorescence emission and k_{nr} being the rate constant for non-radiative de-excitation of S_1. For multiple non-radiative processes, k_{nr} is the sum of the rates of the respective sub-processes. If the probability for non-radiative processes is very high ($k_{nr} \gg k_r$), the measured life time τ_s becomes very small which is denoted as fluorescence quenching. The relation between radiative and non-radiative rates determines also the PL intensity. However, the absolute measured intensity of the fluorescence emission depends not only on the quenching but also on other factors such as excitation power, excitation wavelength, dipole orientation and re-absorption, whereas τ_s does not. In the case of an aggregation or self-assembly of organic dye molecules on nanostructures, these entities can no longer be regarded as single (or 'free') emitters but there is often an interaction between the molecules which may have a strong influence on their electronic and therefore optical properties. The interaction of the forming molecular aggregates can be described by different approaches such as quantum mechanical wave function formalisms or molecular orbital theory [Kash65] and a substantial amount of theoretical works have been engaged with this topic. Many effects, however, could be understood with the help of a quasi-classical vector exciton model mainly developed by Kasha and coworkers [Kash65]. Here, the excited state resonance interaction is understood as the electrostatic interactions of the molecular transition dipole moments. For reasons of simplicity, the following considerations are made for a dimer formation. For higher oligomers the general concept is the same, though the mathematical solutions become much more complicated. The energy of the excited state of a dimer splits into the two levels E' and E'', depending on the relative orientation of the

transition dipoles of the two involved molecules. Figure 2.4 illustrates this in an exciton band energy diagram. For parallel transition dipoles (figure 2.4a), the out-

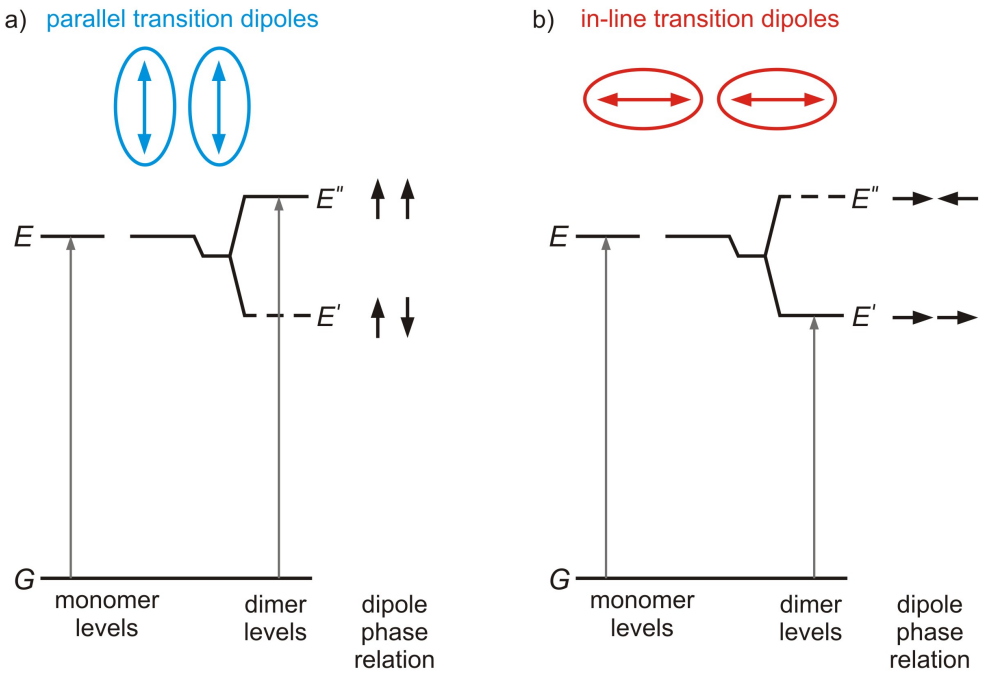

Figure 2.4: Exciton band energy diagram for a molecular dimer with a) parallel and b) in-line transition dipoles. Adopted from [Kash65].

of-phase dipole arrangement corresponds to the lower energy E' and an in-phase orientation to the higher energy E''. Due to the conservation of oscillator strength, only the transition between ground state and the state with in-phase orientation of the dipoles is allowed (= transition to or from the higher energy level E''). Such dimers with parallel transition dipole moments are also called H-aggregates. They are usually characterized by a hypsochromic shift (to lower wavelengths) in the absorption spectrum. For in-line transition dipoles on the other hand, the in-phase arrangement (and therefore allowed transition) corresponds to the low energy state E' (figure 2.4b). Those so called J-aggregates are characterized by a bathochromic shift (to longer wavelengths). For any orientation of the dipoles apart from these two border cases, the energies of the respective levels change intermediately according to certain relations which are not stated here but can be found in the respective literature [Kash65]. It has to be noted, that for H-aggregates, an emission from the energetic higher level E'' does not necessarily mean a blue-shift of the dimer fluorescence compared to the monomer emission. This is due to the Franck-Condon principle. The energy of each electronic state of a molecule is a function

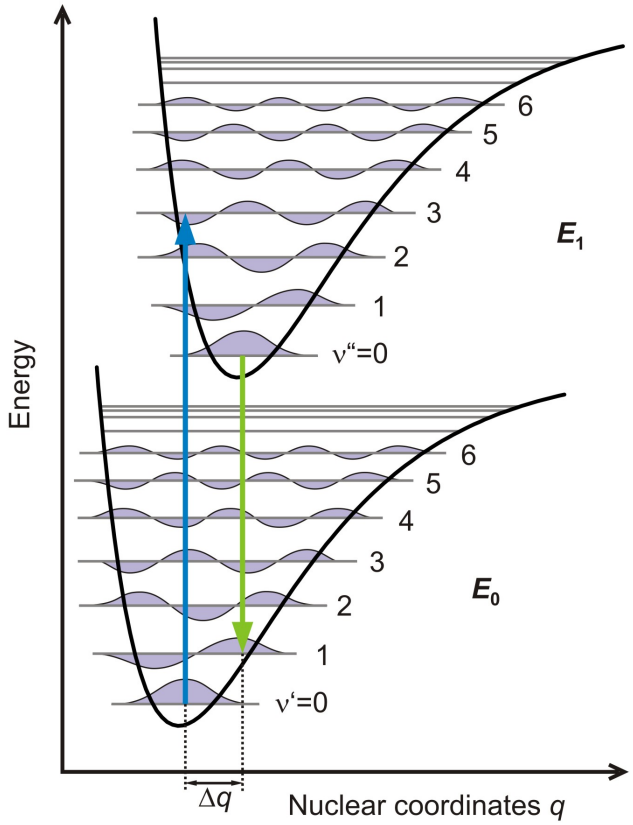

Figure 2.5: Energy diagram for the explanation of the Franck-Condon principle in the case of a diatomic molecule. Adopted from [Vale02, Somo06].

of the nuclear coordinates and can be described by a Morse potential curve (figure 2.5). According to the model of a quantum mechanical oscillator, different vibronic states exist within this potential. The electronic potential curve of the first excited state is shifted compared to the ground state, as the new configuration of the electrons in the molecular orbitals leads to a change in the equilibrium position of the nuclei constituting the molecule. As electronic transitions occur very fast (10^{-15} s) compared to the slower movement of the nuclei, only vertical transitions between the vibronic levels of ground state ν' and excited state ν'' occur. Quantum mechanically, this is explained by the fact that a such a transition is more likely if the vibrational wave functions overlap more significantly. According to Kashas rule the electrons in higher vibrational sub-levels will quickly relax into the vibrational ground state by non-radiative processes. Thus the optical transition is mainly originating from the vibrational ground state. As it can be easily seen in figure 2.5, the shift in nuclear coordinates upon excitation Δq leads to the typical

red-shift of the emission compared to the absorption. If for a parallel dimer (H-aggregated molecules), the change of the nuclear coordinates in the excited state is significantly larger than for the monomer, then its fluorescence emission may possess an even lower energy than the monomer emission. If the dimeric molecule is only formed if one of the both constituents is an electronic excited state, then it is referred to as excimer (**exci**ted di**mer**). For a detailed investigation of the involved energy levels, scientists usually employ a combination of concentration dependent spectroscopic measurements including absorption, excitation and emission spectra. Such experiments can be relatively easily obtained in ensemble measurements (e.g. in solution) but are hardly accessible for the investigated systems in this thesis. Absorption and excitation experiments require a transparent substrate, knowledge of the dye concentration and a well-defined excitation/detection geometry and tunability. As those conditions are not given for dye-functionalized nanostructures on silicon substrates, investigations remain limited to fluorescence emission, which complicates the interpretation of the spectroscopic data.

3 Experimental chapter

Most of the relevant experimental details are described in the respective experimental sections of chapters 4 to 7. This section will only provide exceeding information on used setups and methods.

3.1 Alkyl SAM formation on silicon substrates

As substrates for the alkyl monolayer formation double-side polished n-type silicon(100) has been used. The silicon wafers with a resistivity of $>$3000 Ωcm were delivered by the Center for Microtechnologies (ZfM/Fraunhofer ENAS) at the Chemnitz University of Technology and came cut in pieces of 1 cm x 1 cm. The monolayer preparation was carried out in three steps: cleaning, native oxide removal and monolayer formation (radical chain reaction). The substrates have been cleaned using acetone (C_3H_6O, "Uvasol for spectroscopy", Merck) and ethanol (C_2H_5OH, "Uvasol for spectroscopy", Merck). Acetone and ethanol treatment has been carried out in an ultrasonic bath under 40° C to increase the cleaning efficiency. Subsequently, the sample was sonicated in *Piranha* at 60°C. *Piranha* is the common name for an acid mixture consisting of 40% hydrogen peroxide (H_2O_2, 30% "Suprapur", Merck) and 60% sulfuric acid (H_2SO_4, 96% "Suprapur", Merck). Afterwards the samples have been rinsed thoroughly with *Millipore* (ultra-clean demineralized and deionized water, resistivity of $>$ 18 MΩcm) and dried in a nitrogen stream.
In a next step the samples were etched in aqueous hydrofluoric acid (HF, 40% "Suprapur", Merck) solution (3-4 % in volume) for 3 minutes at room temperature. This removes the native oxide covering the silicon and generates the hydrogen terminated silicon surface which is needed for the monolayer formation. Immediately after the etching the samples were transferred without further treatment into the liquid alkene.
All organo-silicon monolayers used during the presented experiments have been prepared using 1-dodecene ($C_{12}H_{25}$, for synthesis, Merck) in pure form. The alkene has been deoxygenated with argon gas at least 30 minutes prior to the re-

action and the argon flow was also sustained during the reaction. Eliminating the oxygen (and other reactive gases) from the solution is necessary to avoid an unwanted oxidation of the silicon surface and to prevent reactions with the radicals formed during the radical chain reaction. To activate the self-assembly reaction, the solution with the substrates was heated up to 190°C for at least 7 hours. Afterwards the samples with the formed densely packed and well-ordered monolayer have been sonicated for 5 minutes in dichloromethane (CH_2Cl_2, "Uvasol for spectroscopy", Merck) and ethanol followed by drying in a nitrogen stream.

3.2 AFM and KPFM

As far as not stated otherwise, AFM experiments have been carried out using an Anfatec Level AFM with a 24 bit DS4L controller. The scan range of the piezo stage of the AFM was about 55 µm x 55 µm in lateral direction and 5 µm in z-direction. The nominal resolution in x- and y-direction is about 0.45 nm and in z-direction roughly 0.08 nm. The controller outputs were amplified by several stabilized high voltage amplifiers. Samples have been mounted on the scanner by pinning them on a metal substrate holder with a small magnet. The used AFM tips possessed a tip radius of around 40 nm for metal coated tips ("NSC18 Ti/Pt", "CSC36 Pt", Mikromash) or 10 nm for pure silicon tips ("NSC15 HD", Mikromash). Image acquisition and instrument control have been carried out using the Anfatec Scan SXM software and drivers for the instrument. AFM image analysis was performed with "WSxM Scanning Probe Microscopy evaluation software" (Nanotec Electronica)[1].

[1] I. Horcas, R. Fernandez, J.M. Gomez-Rodriguez, J. Colchero, J. Gomez-Herrero and A. M. Baro. *Rev. Sci. Instrum.*, Vol. 78, 013705, 2007

3.3 Spectrally and temporally resolved fluorescence microscopy

3.3.1 Wide-field microscope setup

The home-built wide-field microscope setup is mounted on an optical table for vibration damping. A schematic of the instrument is shown in figure 3.1. The laser source (argon ion laser, "Innova 310", Coherent) is located on another table and the 514 nm laser line is coupled into a fiber optics and guided to the microscope table. Arrived at the microscope table, the laser light is intensity-stabilized using an electro-optic modulator ("E.O.Modulator 370", ConOptics Inc.). The linear polarized laser beam is circularly polarized with a $\lambda/4$ plate and spectral filtered using a 514 nm band-pass filter. Via a dichroic beam splitter ("525 DRLP", Omega) the laser light is passed through the objective ("Epiplan Neofluar", 100x, NA 0.9, Carl Zeiss AG, Germany) and is focused on the sample as a spot with a diameter of approximately 25 µm. The sample itself is placed on an x-y translation stage.

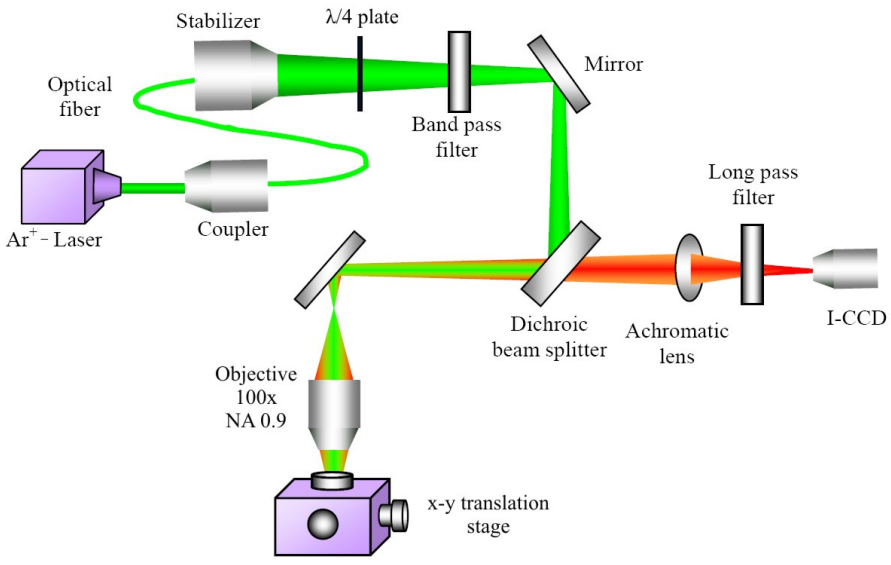

Figure 3.1: Schematic of the wide-field microscope setup. Adopted from A. Issac. *Photoluminescence Intermittency of Semiconductor Quantum Dots in Dielectric Environments*. PhD thesis, University of Technology Chemnitz, Germany, 2006.

The light emitted and reflected by the sample passes the same way back through the objective, passes the beamsplitter and is focused with an achromatic lens on an intensified CCD-camera (”Pentamax-512EFT”, ”Gen IV Intensifier”, Princeton Instruments, USA). To filter the fluorescence light, a long-pass filter (”3RDLP530”, Omega) has been used. The irradiance applied during the experiments was in the range of some 100 $W \cdot m^{-2}$. The CCD-chip in the camera has a resolution of 512 x 512 pixel and operates at a temperature of -25°C (thermoelectrically cooled). The image from the CCD-camera is transferred to the computer via a frame grabber card and could be viewed in real-time with the ”WinView” software (V 2.5.25.5, Roper Scientific).

3.3.2 Confocal microscope setups

Sample scanning confocal microscope (SSCM)

A schematic drawing of this home-built confocal microscope setup is shown in figure 3.2. The 465 nm excitation light from a pulsed laser diode (”LDH-P-C-470”, Picoquant GmbH) with adjustable repetition rate and a narrow pulse length of 75 ps, is focused on the sample using an objective lens (100x, 0.9 NA, ”EC Epiplan Neofluar” Carl Zeiss, Germany). The fluorescence light from the sample is collected with the same objective and separated from the reflected excitation light by a dichroic mirror (”z 470 RDC”, AHF Analysetechnik GmbH, Germany) and a fluorescence filter at 480 nm (Omega Optics Inc.). Using a beam splitter one part of the fluorescence light is focused on an avalanche photodiode (”SPCM-AQR-14”, Perkin Elmer), the other part is coupled into a spectrometer (”Shamrock SR-163/ SR1-GTR-600-500”, Andor Technology) with a thermoelectrically cooled CCD camera (”Newton DU971N-BV”, Andor Technology) as detector. The detection range of the spectrometer was adjusted to 480 nm to 655 nm. The triggering of the position controller of the piezo scan-stage as well as the read-out of the APD signal is realized by a home-written software. For easier retrieval of the structured surface region, the setup can be converted to a wide field operation mode via white light source, imaging camera and retractable mirror/beam splitter.

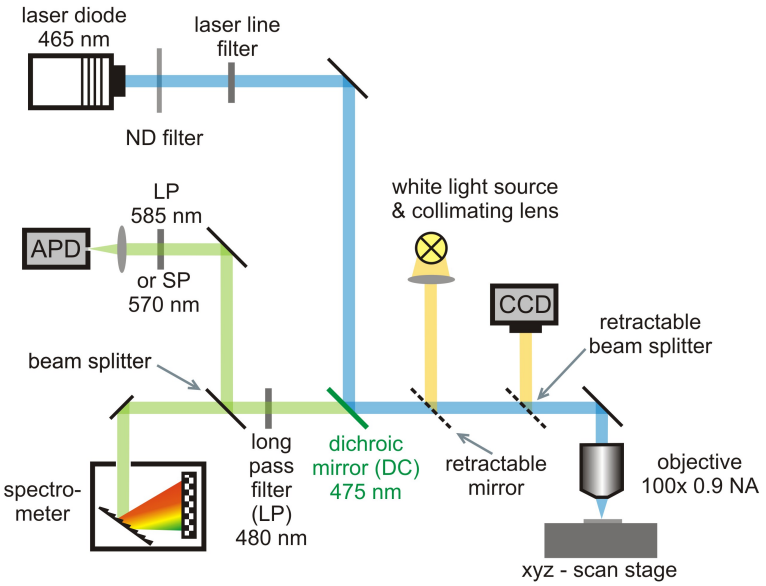

Figure 3.2: Scheme of the SSCM setup. For details see text. Abbreviations: ND neutral density, LP long pass filter, SP short pass filter, CCD - charge-coupled-device camera, APD avalanche photo diode.

Laser scanning confocal microscope (LSCM)

The LSCM setup is also home-built and schematically visualized in figure 3.3. The 488 nm line of an Ar/Kr laser (”Innova 70C-Spectrum”, Coherent) has been used as excitation light. The laser beam was focused on the sample by either a 63x cover-glass-corrected air-immersion objective (”LD Plan-Neofluar”, Carl Zeiss, Germany) with a numerical aperture of NA=0.75 for experiments using a cryostat or standard 100x objective (0.9 NA, ”EC Epiplan Neofluar”, Carl Zeiss, Germany) for experiments at ambient conditions. The sample was placed in a flow cryostat (”ST-500H”, Janis), evacuated to a pressure in the range of 10^{-5} mbar using a vacuum pump and cooled down using liquid nitrogen. An avalanche photo diode (”SPCM-AQR-16”, Perkin Elmer) with a very low dark count rate has been used as luminescence detector. The excitation light was blocked by a long pass filter (”502ALP”, Omega Optical) in the detection path. In front of the detector a beam splitter couples 75% of the fluorescence light into a spectrometer (”Acton SpectraPro-275”, Acton Research Corp.) with a liquid nitrogen cooled CCD camera (Princeton Instruments) as detector. A standard data acquisition and control board (”ME-SlyFoXX ME-4670”, Meilhouse Electronics) processes the detector signal from the APD. The scanning mirror is controlled by a motion controller

("XPS", Newport). Signal acquisition and scanning controls are operated by a home-written software. For easier retrieval of the structured surface region, the setup can be converted to a wide field operation mode via white light source, imaging camera and retractable mirror.

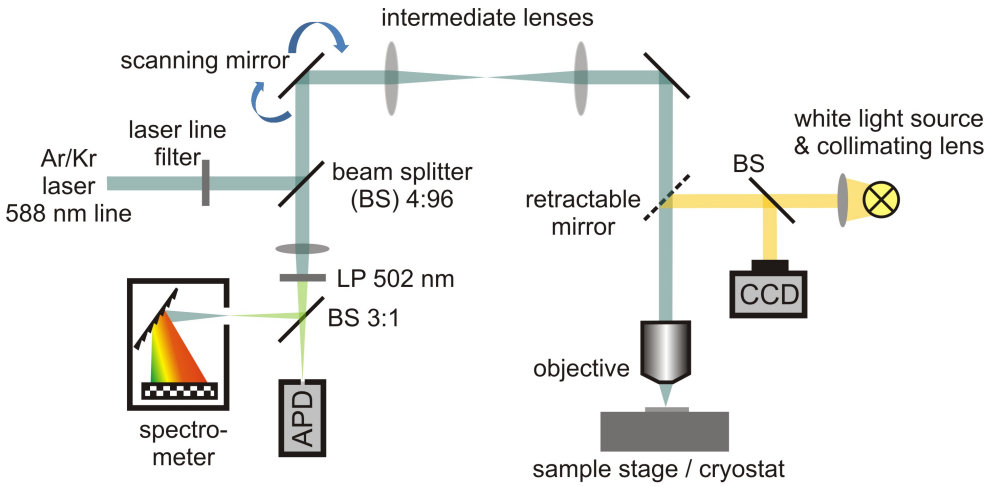

Figure 3.3: Scheme of the LSCM setup. For details see text. Abbreviations: BS beam splitter, LP long pass filter, CCD - charge-coupled-device camera, APD avalanche photo diode .

4 Detection and stability of nanoscale space charges in local oxidation nanolithography

Abstract

We report on the stability of space charges within nanoscale silicon oxide patterns generated by atomic force microscope tip-induced local anodic oxidation of alkyl-terminated silicon. Surface potentials of these structures are investigated using two different approaches: Kelvin probe force microscopy and spectroscopy of adsorbed charge-sensitive dye molecules. Both techniques prove that there is no decay of the space charge itself at least for several days. The apparent decrease of the surface potential measured with the Kelvin probe method is known to be influenced by the ambient humidity. It is supposed to be caused by a screening effect through the formation of a water layer. This is confirmed by our investigation of the surface potential decrease kinetics which could be well-fitted with an adapted model of water condensation. The fluorescence of the charge-sensitive dye di-4-ANEPPS, which is applied to the structures, shows a spectral shift of about 270 meV compared to uncharged silicon oxide surface. The high stability of the charges supports the use of local anodic oxidation patterns as templates for selective immobilization of cationic species.

The content of this chapter is published in [Baum12]:
T. Baumgärtel, C. v. Borczyskowski and H. Graaf, "Detection and stability of nanoscale space charges in local oxidation nanolithography." *Nanotechnology*, Vol. 23, p. 095707, 2012.

4.1 Introduction

Local anodic oxidation (LAO) nanolithography by atomic force microscope (AFM) is a reliable and versatile method to create nanoscaled patterns on metal or semiconductor surfaces [Garc06, Ara02b, Yang09, Baum11a]. The general working principle of LAO is an electrochemical reaction which is spatially confined by the AFM tip sample geometry (for details about the oxidation process see [Yang06b]. In the case of a silicon substrate, silicon oxide is formed which expands above the sample surface resulting in a topographic structure. Moving the AFM tip during oxidation and controlling the oxidation parameters such as speed and voltage enables to draw various structures which can be used as templates for further functionalization [Baum11a, Wout03] or to build electronic nano-devices [Mart08]. The oxidation process itself is self-limited and saturates after an oxide thickness of a few nm [Avou97]. Dagata *et al.* and Dubois *et al.* developed models that explain the self-limitation through the build-up of space charge within the LAO oxide which reproduced the experimentally obtained data very well [Daga98, Dubo00].
Recently, Chiesa and Garcia [Chie10] verified the existence and the sign of the space charge in local anodic oxide on silicon by Kelvin probe force microscopy (KPFM) [Nonn91, Pale06]. From their KPFM data they calculated charge densities of about 10^{17} cm^{-3} and found that the measured KPFM signal depends on the ambient humidity. For increasing ambient humidity there is a decrease of the measured surface potential which they attributed to a screening effect of the water which adsorbs on the oxide pattern. The negative space charge can be used to immobilize cationic species like dye molecules selectively on the structured surface [Baum10, Graa07]. For a possible application of the electrostatic attachment it is important to know how stable these charges are, which has not been investigated so far. It is known from AFM-induced charging experiments on silicon oxide films that the introduced charges dissipate rather quickly (usually within several minutes to hours) [Buh01, Enik04]. However, in such experiments electrons were deposited into more or less stoichiometric oxide where in the case of space charges within the LAO oxide, the charge carriers are OH- ions that are trapped within a nonstoichiometric environment. It is therefore reasonable to assume that the charges within the LAO oxide are much more stable than electrons or holes inserted in thermal silicon oxide.
Another important issue is the quantitative interpretation of KPFM measurements on insulating surfaces. In the case of metallic or semiconducting substrates, KPFM probes the contact potential difference (CPD) between tip and sample surface, whereby the measured surface potential is a convolution of the 'real' surface potential of the sample and a transfer function which is determined by the tip-sample geometry [Stra05]. However, for dielectric surfaces such as silicon oxide, the

CPD is not well-defined as insulating thin films cannot be regarded as equipotential and a simple capacitor model is no longer valid for the tip-sample system. Additionally, dielectrics may possess surface charge and dipole layers which contribute to the Coulomb interaction between tip and sample [Shen08]. Calculating the charge density in dielectrics directly from the measured KPFM data is generally not possible as it is an inverse potential problem with insufficient data [Shen08]. Therefore we also probed the potential of the charged LAO oxide by using a special dye molecule which is spectroscopically sensitive to electric fields. Such molecules have been successfully used to measure surface polarity[Macq99], membrane potentials[Mont89] or charge transfer processes in silicon nanoparticles [Mart05]. In this paper we will present results on the stability of the space charge in oxide nanostructures generated by LAO of alkyl-passivated silicon. The charge has been measured by KPFM at different humidities as well as by the fluorescence emission of the charge-sensitive dye di-4-ANEPPS.

4.2 Experimental

All local anodic oxidation experiments were carried out on weakly doped n-type silicon (resistivity $>3000\,\Omega$cm) substrates with a self-assembled monolayer (SAM) of dodecene molecules as surface coating. Details of the preparation process are described elsewhere [Baum10, Graa07, Linf95]. The SAM prevents the oxidation of the silicon by ambient oxygen and yields to a well-defined and adjustable surface chemistry. Yet local anodic oxidation is still possible, as the SAM is decomposed during the process. This leads to a silicon oxide nanostructure on a chemically different alkyl-terminated silicon surface. LAO experiments, topography and KPFM measurements were conducted with an Anfatec Level AFM (Anfatec GmbH, Germany) using platinum coated silicon tips (NSC18/Pt, resonant frequency 75 kHz, spring constant 3,5 N/m Mikromash, Estonia). For the generation of the investigated oxide structures, a voltage of -9 V was applied to the AFM tip while scanning a 3 µm x 3 µm image in contact mode with a tip velocity of 1 µm/s at a relative humidity (RH) of about 67%. Figure 4.1a shows a scheme of the local anodic oxidation on alkyl-terminated silicon. Topography and KPFM investigations were carried out simultaneously in non-contact operation (see figure 4.1b) and subsequent KPFM images were taken over at least 24 hours. To control the humidity of the ambient atmosphere the microscope was placed under a closed PMMA dome which can be purged with dry nitrogen or water vapor-saturated nitrogen. The humidity was measured using a SHT15 digital humidity sensor (Sensirion AG, Switzerland) For the optical investigations, a 50 µM solution of the charge-sensitive dye aminon-

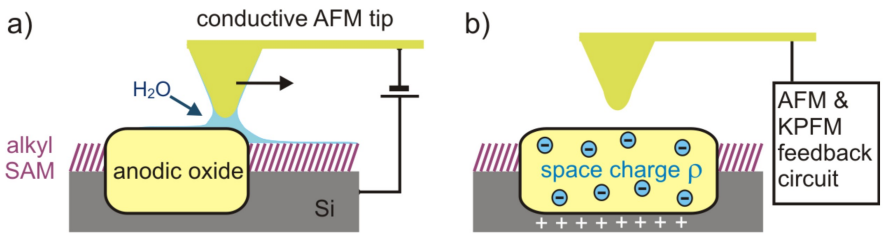

Figure 4.1: Schematic description of a) local anodic oxidation nanolithography of alky-terminated silicon and b) AFM and KPFM measurement of the space charge within the local oxide.

aphthylethenylpyridinium (di-4-ANEPPS, molecular probes, Invitrogen Inc., see figure 4.2) in ethanol was spincoated on the structured substrates as well as on a reference sample of silicon with a 4 nm thermally grown oxide layer. The reference sample was cleaned by an ultrasonic baths in acetone, ethanol and a mixture of H_2SO_4 and H_2O_2 (60:40 vol. %, Piranha solution) and afterwards thoroughly rinsed with MilliQ water. Optical measurements were performed using a home-built confocal microscope setup. The 465 nm excitation light from a pulsed laser diode (LDH-P-C-470, Picoquant GmbH) is focused on the sample using an objective lens (100x, 0.9 NA, Zeiss EC Epiplan Neofluar). The fluorescence light from the sample is collected with the same objective and separated from the reflected excitation light by a dichroic mirror (z 470 RDC, AHF Analysetechnik GmbH, Germany) and a fluorescence filter at 480 nm (Omega Optics Inc.). Using a beam splitter one part of the fluorescence light is focused on an avalanche photodiode (Perkin Elmer, SPCM-AQR-14), the other part is coupled into a spectrometer (Andor Technology, Shamrock SR-163/ SR1-GTR-600-500) with a thermoelectrically cooled CCD camera (Andor Technology, Newton DU971N-BV) as detector. The detection range of the spectrometer was from 480 nm to 655 nm.

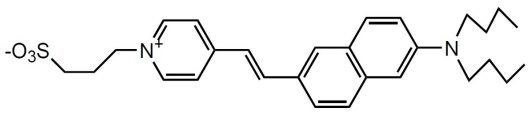

Figure 4.2: Chemical structure of di-4-ANEPPS.

4.3 Results and Discussion

4.3.1 KPFM investigations

Figure 4.3a shows the non-contact AFM image of a typical rectangular local oxide pattern on dodecyl-terminated silicon. The oxide height above the surface is about 3.5 nm. Since 40% of the oxide is below the silicon interface [Font98] and the dodecene monolayer (thickness $\approx$ 1.3 nm [Siev98]) decreases the apparent height (see experimental section, fig. 4.1), the total thickness of the LAO oxide can be calculated to about 8 nm.

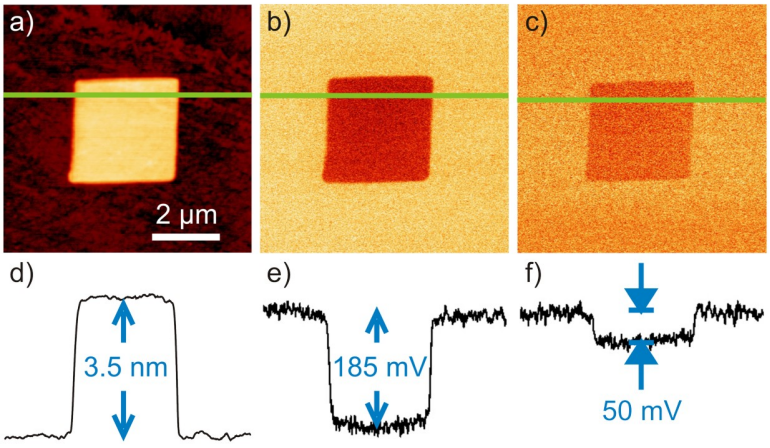

Figure 4.3: a) AFM non-contact topography image of a nanolithography oxide structure on a dodecyl-terminated silicon surface. b) KPFM image of the structure 47 min after generation at 51% RH. c) KPFM image of the same structure 1034 min after generation at 51% RH. d)-f) profile section along the green lines in the respective images in a)-c).

The KPFM image in figure 4.3b indicates that the structure is charged negatively as the surface potential of the local oxide is about 185 mV lower than of the dodecyl-terminated silicon. By solving the one-dimensional Poisson equation and assuming a uniform charge density, Chiesa and Garcia derived the following approximation for the relation between space charge ρ and measured surface potential Φ:

$$\phi = \frac{2\varepsilon_r \varepsilon_0}{d^2}\Phi \tag{4.1}$$

with ε_r being the relative permittivity of the LAO oxide, ε_0 the vacuum permittivity and d the total oxide thickness [Chie10]. With equation (4.1) and the assumption that ε_r = 3.9[Sze81], we can calculate a space charge density of 1.25 x 10^{18} cm^{-3} for the oxide structure in figure 4.3b. This is a higher value than in the experiments of Chiesa and Garcia who calculated charge densities in the order of $10^{17}cm^{-3}$ yet this deviation may be a result of the used silicon. Our experiments were conducted on weakly doped n-type silicon as substrates, whereas Chiesa and Garcia used higher doped silicon. As they also found a clear difference in the charge densities (about a factor two) for differently doped silicon (p-type and n-type), a strong effect of the silicon doping on the charge density within the local oxide has to be presumed. However, as it can be seen from figure 4.3c, 17 hours after the preparation of the structure, the measured surface potential decreased by about 73% (135 mV) when exposed to a relative humidity of 51%. It is known from previous KPFM studies on dielectric surfaces that water which adsorbs on the surface in a humid atmosphere shields the surface potential and thus decreases the KPFM contrast significantly [Sugi02]. In order to investigate the dynamics of this adsorption and shielding process on the charged oxide nanostructure, we continuously scanned a freshly prepared LAO structure for several hours, taking an image approximately every 47 minutes. This type of measurement was performed in an atmosphere with a relative humidity of 51% and for another sample under nitrogen flux ($< 4\%$ RH). For a precise determination of the surface potential difference (*SPD*) between oxide nanostructure and unstructured sample surface, histograms of the obtained KPFM image sections have been fitted with Gaussian curves. The *SPD* is the difference of the central values of the Gaussian peaks. The time dependent curves for the *SPD* for the two different relative humidities are displayed in figure 4.4. For better comparison, the *SPD* values have been normalized to the initial value at t = 48 min. It has to be noted that the absolute initial *SPD* values measured in humid atmosphere are about three times smaller than in dry atmosphere. In a dry nitrogen atmosphere, the surface potential difference is nearly constant even for long observation times t. There are some slight variations though, which may be connected to either small fluctuations of the ambient humidity below the detection limit of the humidity sensor or to a degeneration of the AFM tip (abrasion or accretion of contaminants). When exposed to a more humid environment however, there is a strong decrease of the *SPD* within the first 5 hours after the generation of the oxide structure. After 10 hours, the surface potential of the structure remains nearly constant yet it is unequal to zero but in the order of 50 mV (see also figure 4.3c). Obviously the water layer does not shield the surface potential of the structure completely but a small KPFM contrast remains detectable. Muster *et al.* investigated the water adsorption kinetics on silica nanoparticles and stated that the water uptake on the silicon oxide surface is governed by two first-order processes: (1) adsorption of water molecules onto surface hydroxyl groups occurring at sub-monolayer coverage and (2) condensa-

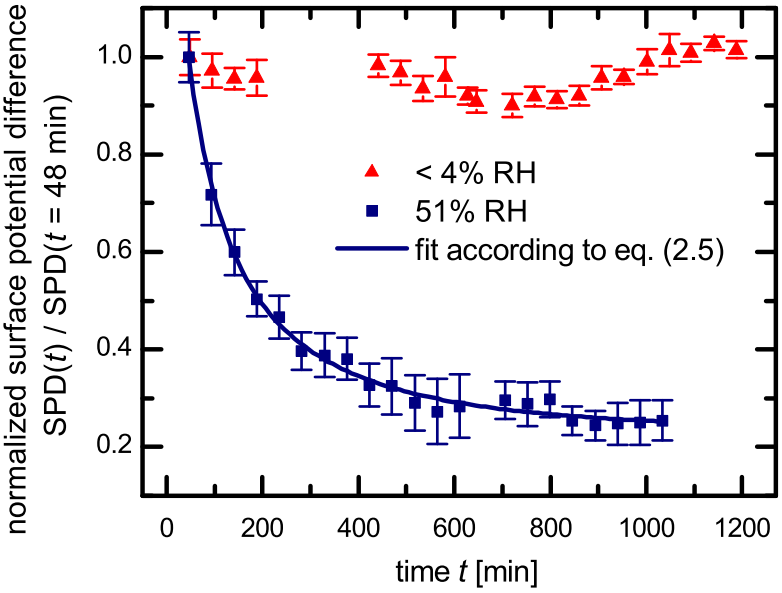

Figure 4.4: Surface potential difference as a function of time for dry (red triangles) and humid (blue squares) atmosphere. For better comparison the data has been normalized to the initial value at t = 48 min. The values for humid air have been fitted with an exponential decay according to equation 4.5

tion of water to form multilayers [Must01]. They proposed the following kinetic model for the amount of adsorbed water Γ_T at time t:

$$\Gamma_T = \Gamma_0 \left(1 - e^{-k_1 t}\right) + \Gamma_C \left(1 - e^{-k_2 t}\right) \tag{4.2}$$

where Γ_0 is the total amount of adsorbed water according to process (1) occurring with a rate constant k_1 and Γ_C is the equilibrium water uptake due to condensation (2) with the rate constant of condensation k_2. Assuming that the rate for adsorption on hydroxyl-groups is significantly larger than for condensation ($k_1 \gg k_2$), equation (4.2) can be simplified to:

$$\Gamma_T = \Gamma_0 + \Gamma_C \left(1 - e^{-k_2 t}\right) \tag{4.3}$$

Furthermore it is expected that the surface potential difference is indirectly proportional to the thickness of the adsorbed water film (or to the amount of adsorbed water since the surface area is constant):

$$SPD \sim \frac{1}{\Gamma_T} \tag{4.4}$$

Therefore the data for the humid environment in figure 4.4 was fitted using the following equation:

$$SPD(t) = \frac{1}{A + B\left(1 - e^{-k_2 t}\right)} \tag{4.5}$$

with the parameters A and B representing the respective effects of the water adsorption Γ_0 and Γ_C on the *SPD*. The fit via nonlinear regression is in good agreement with the experimental data. The obtained rate constant for condensation k_2 = 4.15 x 10^{-5} s^{-1} is about one order of magnitude smaller than found by Muster *et al.* for the silicon dioxide nanoparticles [Must01]. However, this is understandable since for their water adsorption measurements they used air with saturated water vapor (100% RH) while in our experiments the relative humidity was about 50%. From kinetic gas theory it can be derived that the flux of incident gas molecules on a unit surface area is directly proportional to the partial pressure of the gas above the surface (Hertz-Knudsen-Equation). As the partial water vapor pressure at 50% RH is half of the saturated water vapor pressure, the flux of incident molecules and therefore the condensation rate should be smaller by at least a factor of two. Another aspect that may further decrease the condensation rate is the unknown surface chemistry of the silicon oxide nanostructure itself. Time-of-flight secondary ion mass spectroscopic investigations revealed that silicon oxide nanostructures produced by anodic oxidation of silicon covered by an organic monolayer contain substantial amounts of organic C_xH_yO molecules [Pign03]. This suggests that the monolayer is not fully degraded during oxidation but parts of the organic molecules that formed the SAM are incorporated within the anodic oxide (presumably at the top layers of the oxide). Therefore the surface of the local anodic oxide on SAM-terminated silicon may possess areas with hydrophobic carbon chains that hinder the adsorption of water. The thickness of the water layer is clearly an equilibrium parameter which depends on the surrounding humidity. After the time series of the KPFM images at 51% RH was taken, the humidity inside the measurement chamber was reduced to below 5% starting from 1035 min for about 30 min. We found that the *SPD* increased about 63% after 78 minutes within the dry atmosphere which confirms an at least partial reversibility of the layer build-up.

4.3.2 Optical investigations using charge sensitive dye

Figure 4.5a shows a typical confocal microscope fluorescence image of a square LAO oxide structure after di-4-ANEPPS treatment. The charge sensitive dye is presumably deposited on the whole sample surface during the spin coating process but it can only be optically detected on the local oxide. Reason for this is a strong

quenching of the dye fluorescence by an effective energy transfer to the underlying silicon. The dye molecules on the oxide structure are separated from the silicon by the oxide (thickness = 8 nm) while the dye molecules on the rest of the surface are much closer to the silicon (1.3 nm = thickness of the dodecene monolayer). Since the energy transfer between the dye molecules and the silicon depends strongly on their spacing ([Sluc95]), molecules on the oxide structure show a detectable though weak fluorescence whereas the fluorescence from molecules on the unstructured surface is quenched below the detection limit. The emission spectrum of

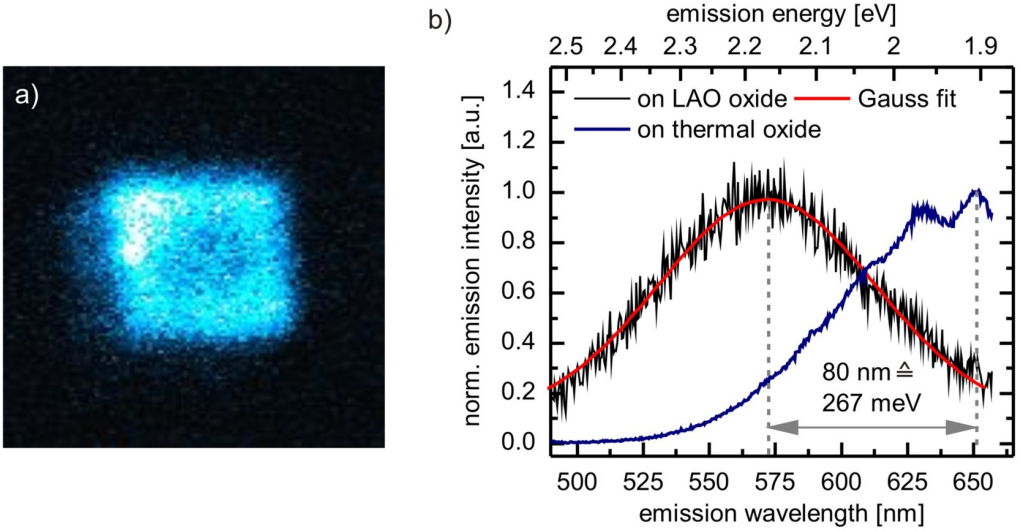

Figure 4.5: a) Confocal microscope image of di-4-ANEPPS spincoated onto a substrate containing a square LAO structure. The excitation power was about 2 µW and the integration time 5 ms for each pixel. b) Emission spectra of di-4-ANEPPS on the structure (black) and on an uncharged reference substrate with 4 nm thermal oxide (blue). Spectra were integrated over 5 s and 30 s respectively. The spectral range of the spectrometer is limited to 655 nm.

di-4-ANEPPS on the local anodic oxide structure is displayed in figure 4.5b (black curve). Compared to the emission of the dye deposited on uncharged thermal oxide of similar thickness (blue curve), there is a pronounced blue-shift of about 267 meV (80 nm). The double peak sub structure of the emission on thermal oxide is supposed to be a result of the piranha cleaning of the substrate which leaves the surface terminated with hydroxyl groups. Some of the di-4-ANEPPS molecules which are very close to those groups may be influenced by their partial negative charge thus showing a relatively small blue-shift. Other dye molecules which are not close to the hydroxyl groups possess a wavelength of maximum emission similar to that on quartz glass (around 650 nm[Mart05]). The strong blue-shift of the emission on the LAO oxide structure is most likely caused by the space charge within the

oxide. Reason for this is an electrochromic mechanism where the energy of the electronic transition is altered in presence of an external field [Fluh85, Loew78]. From experiments with di-4-ANEPPS bound to hemispherical lipid bilayers it is known that the fluorescence emission maximum changes from 640 nm to 540 nm (ΔE = 359 meV) upon a change of the transmembrane potential in the order of -100 mV [Fluh85]. Thus the shift of 267 meV in case of di-4-ANEPPS on the charged oxide structure would suggest a smaller absolute value of the surface potential. However, it should be noted that is not possible to directly compare both measurements quantitatively. The spectral response of an electrochromic dye on the electric field depends strongly on the orientation of the dipole moments of the ground and the photoexcited state and therefore on the orientation of the molecule [Loew78]. To correlate the spectral changes with a certain surface potential, a calibration measurement has to be performed for each system. For measurements where di-4-ANEPPS is used to monitor membrane potentials, the dye is incorporated into a lipid double layer. It will self-align, orienting its polar SO_3^- group towards the layers outer face and the hydrocarbon chains at the other end of the molecule towards the hydrophobic interior of the layer: the molecules orient with their long axis parallel to the surface normal and thus parallel to the electric field. The transition moment of di-4-ANEPPS is very likely aligned along the long axis of the π-system, as it was shown for other amino-pyridinium dyes [Loew81]. With the transition moment parallel to the electric field, a maximal spectral response is expected for the dye adsorbed into the bilayer membrane. In the case of di-4-ANEPPS on the charged local oxide, on the other hand, no perpendicular alignment to the surface is expected. The negatively charged SO_3^- group is repelled from the also negatively charged oxide and the hydrophobic and polar hydrocarbon chains at the other end of the molecule have also no affinity for the more hydrophilic and polar oxide surface. Thus the molecules should tend to adsorb rather parallel to the surface. This means their transition moment is less parallel to the electric field and therefore a smaller shift of the emission spectrum is expected even though the surface potential might be larger than in the case of the membrane measurements (-100 mV). Despite the lack of a definite quantification due to the unknown molecular orientation, nevertheless relative measurements of the time-dependence of the surface potential can be conducted. In order to investigate the stability of the charge, the emission spectra have been investigated 2 h, 5 h and 42 h after generation of the LAO structure (a continuous investigation of the same structure is not possible as the dye bleaches rapidly due to the necessity of a relatively high excitation power). The blue-shifted emission spectra have been fitted with a Gauss type distribution to determine the peak position more precisely (see figure 4.5b), red curve). Table 1 summarizes the results for different observation times after preparation as well as values from the literature. Even 42 h after the structure has been generated, the surface potential has not decreased but our results indicate a slight

enhancement as the blue-shift increases even further. As it is very unlikely that the number of charges within the oxide increases, this effect may be connected with a rearranging of either the dye molecules or the charges within the oxide. Since the optical probes have been deposited on the substrate directly after the generation of the oxide structures and are in closest proximity to the space charges, a possible condensation of ambient water has no strong influence. The water condenses on top of the di-4-ANEPPS film, and thus has no shielding effect for the local charge within the oxide.

Table 4.1: Fluorescence maximum position λ_{em}^{max} and E_{em}^{max} of di-4-ANEPPS on different systems.

surface / condition	λ_{em}^{max} [nm]	E_{em}^{max} [nm]
on quartz	655[a]	1.893
on thermal oxide ("piranha"-treated, 4 nm)	651	1.905
on LAO oxide		
- after 2 h	571 ± 2	2.171
- after 5 h	561 ± 2	2.210
- after 42 h	559 ± 2	2.218
on lipid membrane	640[b]	1.937
on lipid membrane at -100 mV membrane potential	540[b]	2.296

[a] from Ref. [Mart05] [b] from Ref. [Fluh85]

As far as any qualitative understanding of the observed effects is developed, until now it is still unclear which type of probing technique delivers the more correct quantification of the surface potential. On the one hand, electrochromic dyes as molecular probes are likely to possess a higher local sensitivity than KPFM. Yet the influence of the local electric field on the electronic structure of the chromophore is not easily assigned (unknown dipole orientation). At a first glance, KPFM data seems to be more reliable and easily evaluable as the electro-physical principles behind the measurement are well-understood. However, as mentioned above, there are many obstacles in the case of KPFM on dielectric materials as the work function is not defined, a simple capacitor model is not applicable and there may be a formation of surface charges or surface dipoles. Furthermore the KPFM signal is not only determined by the interactions between tip apex and underlying substrate but is also strongly affected by the electric coupling between the whole sample and the entire cantilever [Char08].

4.4 Conclusions

Summarizing, we investigated the influence of ambient humidity on the measured KPFM images of charged silicon oxide nanostructures. In a nitrogen atmosphere there is practically no decrease of the surface potential on the nanostructures which indicates a high stability of the incorporated charges. The time dependence of the KPFM signal in the case of a humid environment could be fitted using an adapted model from the kinetics of the adsorption water layer thickness. Together with the found partial reversibility of the KPFM signal decrease, the shielding effect of an adsorption water layer was further proved. The local space charge within the oxide was also probed using the charge-sensitive dye di-4-ANEPPS. A strong spectral blue-shift of about 270 meV was found for the dye emission on the charged oxide structure. The shift increases slightly within the first hours but is also stable for at least 42 h. While the results for the different probing techniques are qualitatively similar, our results indicate that an absolute quantification of the space charge remains difficult as both methods yield different values for the surface potential. The KPFM data shows a surface potential in the order of -200 mV whereas the spectral shift of the dye suggests a surface potential of above -100 mV. Though both methods are suitable tools for the qualitative investigation of the surface potential, special attention should be paid in order to understand and quantitatively interpret both, the KPFM measurements on dielectric surfaces as well as the influence of local electric fields on the spectral properties of electrochromic dyes.

Acknowledgement

The authors thank the Deutsche Forschungsgemeinschaft (DFG, GR 2695/4) for financial support.

5 Fluorescence studies of Rhodamine 6G functionalized silicon oxide nanostructures

Abstract

Selective anchoring of optically active molecules on nanostructured surfaces is a promising step towards the creation of nanoscale devices with new functionalities. Recently we could demonstrate the electrostatic attachment of charged fluorescent molecules on silicon oxide nanostructures prepared by AFM nanolithography via local anodic oxidation (LAO) of dodecyl-terminated silicon. In this article we report on our findings from a more detailed optical investigation of the bound dye rhodamine 6G. High sensitivity optical wide field as well as confocal laser microscopy have been used to characterize the rhodamine fluorescence emission. A highly interesting question is the interaction between an emitter close to a silicon surface because mechanisms like energy transfer and fluorescence quenching will occur which are still not fully understood. Since the oxide thickness can be varied during preparation continuously from 1 to $\sim$10 nm, it is possible to investigate the fluorescence of the bound dye in close proximity to the underlying silicon. Using confocal laser microscopy we were also able to obtain optical spectra from the bound molecules. Together with the results from an analysis of their photochemical bleaching behaviour, we conjecture that some of the rhodamine 6G molecules on the structure are interacting with the oxide causing a spectral shift and differences in their photochemical properties.

The content of this chapter is published in [Baum10]:
T. Baumgärtel, C. v. Borczyskowski and H. Graaf, "Fluorescence studies of Rhodamine 6G functionalized silicon oxide nanostructures." *Nanotechnology*, Vol. 21, p. 475205, 2010.

5.1 Introduction

Selective anchoring of optically active molecules on nanostructured surfaces is a promising step towards the creation of nanoscale devices with new functions and working principles. Light emitting and absorbing single particles or thin films could be used for transmitting energy as well as information. At first we have to understand the physics behind those processes in order to manipulate the behaviour of the investigated systems. Quantum physical phenomena and ordering effects play a crucial role in the nanometer regime and are yet only partially understood.
In order to investigate luminescence on the nanoscale and to build up functional structures, several requirements have to be fulfilled. First of all, the substrates have to be defect free, well defined, and ultra flat. We use silicon wafers as substrates, since they satisfy the above mentioned requirements because of their monocrystallinity and are also a well-investigated standard material for semiconductor technologies. Self-assembled monolayers (SAMs) can be used to passivate the silicon surface [Linf95]. The covalent Si-C bond, which is formed e.g. by the reaction between a 1-alkene and a hydrogen terminated silicon surface [Buri99, Siev00], is highly thermally [Sung97] and chemically stable [Linf95, Siev98]. As a next step an appropriate method is required to structure the silicon in the range of a few nanometers. Local anodic oxidation (LAO) via atomic force microscope (AFM) is a versatile and reliable method for the fabrication of nanometer-scale oxide patterns on alkyl-terminated silicon [Sugi97, Maoz99, Ara02a, Daga98, Graa07, Graa08a]. Last but not least we need a way to immobilize tracers (e.g. dye molecules) selectively on the generated structures. To achieve this, it is necessary to modify and adjust the chemical or physical properties of both the substrate and the structure independently. This is another advantage of the usage of SAMs since their surface properties can be tuned by the modification of the end groups of the molecules used as building blocks. A structuring of an e.g. dodecyl-terminated substrate via LAO results in a rather hydrophilic oxide pattern while the surrounding surface is hydrophobic. The oxide can also be modified by different chemical routes e.g. by etching the oxide [Ara02a] or binding species such as molecules or nanoparticles. However, since the structures are negatively charged due to the oxidation process, we applied electrostatic interactions to bind cationic molecules to the oxide pattern. Such a selective binding of molecules by electrostatic interactions is known from previous studies, where rhodamine 6G (R6G) molecules [Graa07] or organic semiconductors [Losi08, Losi09] have been bound to the silicon oxide structures. It should be noted that other binding concepts for oxide structures are also known from the literature. For example, differences in hydrophobic interactions have been used for attaching semiconductor nanoparticles [Patt09, Chen99] or the oxide sur-

face has been functionalized using silane molecules with anchoring groups for gold nanoparticles [Sheu05] or an even more complicated method has been used with a chemical reaction step in order to form an anchoring group and finally the attachment of gold clusters [Liu02]. Thus all these methods lead to a selective arrangement of functional units, the binding is not very stable or poorly uniform only. In other cases many synthesis steps are necessary, which complicates the preparation compared to our approach.
In the present study we will show the effect of nearby silicon on the luminescence of rhodamine 6G molecules for very small silicondye distances. Rhodamine 6G is used because it is a well-known cationic dye which is a standard emitter in laser applications, characterized by a high quantum yield [RF K82] and it has been the subject of previous investigations by many other groups, regarding its behavior at interfaces [Chen08, Tleu05, Arbe06, Cnos93].

5.2 Experimental

Dodecyl monolayers were prepared by reaction of hydrogenterminated silicon(100) (3000 Ωcm, n-type, phosphor doped) with a 1-dodecene solution in mesitylene (both from Merck, for synthesis grade). The details of the preparation are described elsewhere [Linf95]. The formed hydrogen and dodecylterminated silicon was controlled by measuring the water contact angle. For hydrogen-terminated silicon water contact angles of $78^\circ \pm 2^\circ$ and for dodecyl-terminated silicon contact angles of $109^\circ \pm 2^\circ$ were found (the measurements were performed with a "OCA 20 contact angle meter", Dataphysics, Germany). For the anodic oxidation process and the visualization of the sample surface, a "multimode scanning probe microscope" (AFM, Veeco with "Nanoscope IIIa controller") was used. A homemade program for the nanolithography was applied to the AFM software. The local anodic oxidation was performed with electrical platinum coated cantilevers ("NST-EF-R-S03-01", Nascatec, Kassel, Germany) in contact mode by applying different DC voltages to the cantilever with respect to the dodecyl-terminated silicon substrate (see figure 5.1). All AFM investigations were carried out at room temperature with controlled humidity. In the LAO process the AFM-tip and the substrate form the electrodes of a nanoscopic electrochemical cell, modifying the surface by a chemical reaction (oxidation). If the tip is close to the surface (some nanometers), applying a voltage between the conductive tip and the positively biased silicon substrate generates an electric field E. Under ambient conditions there is always an adsorption layer of water both covering the tip and the sample surface. With the applied voltage the water molecules are polarized by the electric field and

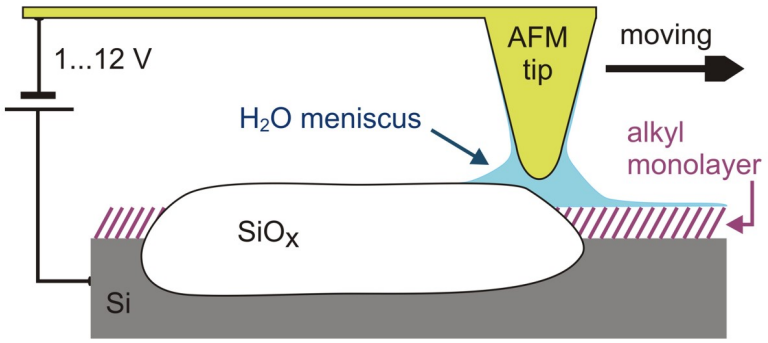

Figure 5.1: Schematic view of AFM-induced LAO for drawing oxide line patterns on alkyl-terminated silicon.

following the field gradient, they will accumulate at the terminus of the tip (where the field strength is at a maximum). If the voltage is above a certain threshold value, a stable water bridge (meniscus) between the tip and sample surface is formed and the water molecules are dissociated by the electric field into H^+ and OH^- ions. The positive H^+ ions will move to the tip (cathode) where they will be reduced and finally form hydrogen molecules, the negative OH^- ions are pulled towards the silicon (anode). After they have penetrated the termination layer (e.g. hydrogen molecules, already formed silicon oxide, or an organic monolayer), the hydroxide ions reach the native silicon and react with holes producing silicon oxide [Daga98]. As a silicon oxide complex is more spacious than a single silicon atom, there is an increase of volume which can only expand in the vertical direction and an elevated silicon oxide structure is formed. If the tip is moved laterally during the process, line structures can be written on the surface (see figure 5.1).
For the binding of cationic dyes the nanostructured sample was immersed directly after lithography in a solution of 3 mg rhodamine 6G (see figure 5.2, Radiant Dyes Laseraccessories, Germany) in 2 ml H_2O (purified water, specific resistance 18.2 MΩcm) for 90 min, followed by washing with methanol (Merck, spectroscopic grade). The samples were investigated both by AFM (contact mode for investigation of changes in height) and optical microscopy. Two different types of home built microscopes were used to observe the emission of the dye-functionalized structures, a wide field microscope and a laser scanning confocal microscope. For the wide-field setup the 515 nm excitation light (argon ion laser; Spectra) was stabilized by an electrooptical modulator (Conoptics) followed by a laser line filter at 515 nm (Omega). The laser light is directed into an objective lens (100x, 0.9 NA, Zeiss ”EC Epiplan Neofluar”) via a dichroic mirror (Omega, ”525 DRLP”). Fluorescent light was focused on an intensified frame transfer camera (Pentamax Roper Scientific), whereas excitation laser light was suppressed by a long pass filter (Omega ”3RD530LP”). In the laser scanning confocal microscope we used the

same laser for excitation as in the wide field setup. The laser beam was focused by a similar objective lens (Zeiss "EC Epiplan Neofluar") as was used for the wide field setup. An avalanche photodiode (Perkin Elmer, "SPCM-AQR-16") with a very low dark count rate served as the luminescence detector. Laser excitation light was blocked by an optical long pass filter (Omega Optics, 480 nm) in the detection path. In front of the detector an 8:2 beam splitter coupled part of the light into a spectrometer (Andor Technology, "Shamrock SR-163/SR1-GTR-600-500") with a Peltier cooled CCD camera (Andor Technology, "Newton DU971N-BV") as detector.

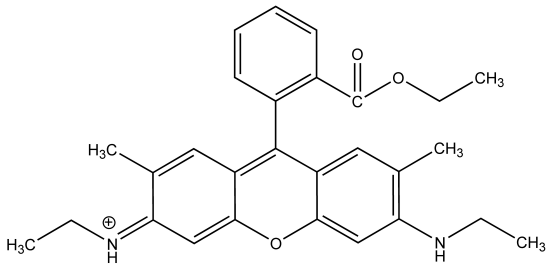

Figure 5.2: Chemical structure of the rhodamine 6G cation.

5.3 Results and Discussion

Figure 5.3 shows several oxide lines generated via LAO using different voltages from -8 to -4 V. The left part of figure 5.3 is an AFM height image of the oxide structures before attachment of the R6G molecules. The line width is below 100 nm and the line height is in the range from 1 to 4.5 nm. As we have shown previously, there is an increase in height of the oxide after attachment of R6G, indicating that there is about one monolayer of dye molecules on the oxide structure [Graa07]. The investigation of the same spot with an optical wide-field microscope shows a signal in the shape of the structures (figure 5.3, right image). Thus it can be concluded that the dye molecules attached to the silicon oxide can be excited optically and emit fluorescent light. However, the optical image is resolution-limited and thus not as sharp as the AFM image. The emission intensity from the dye-functionalized nanostructures is relatively low, which we attribute to a strong photoluminescence quenching. We determined an average value of 0.6 ns for the lifetime of the excited state which is considerably lower than the lifetime of R6G in diluted aqueous solution (3.7 ns). We evaluated the cross sections in figure 5.3 by fitting Gaussian functions to each peak, determining characteristic parameters of each line such as

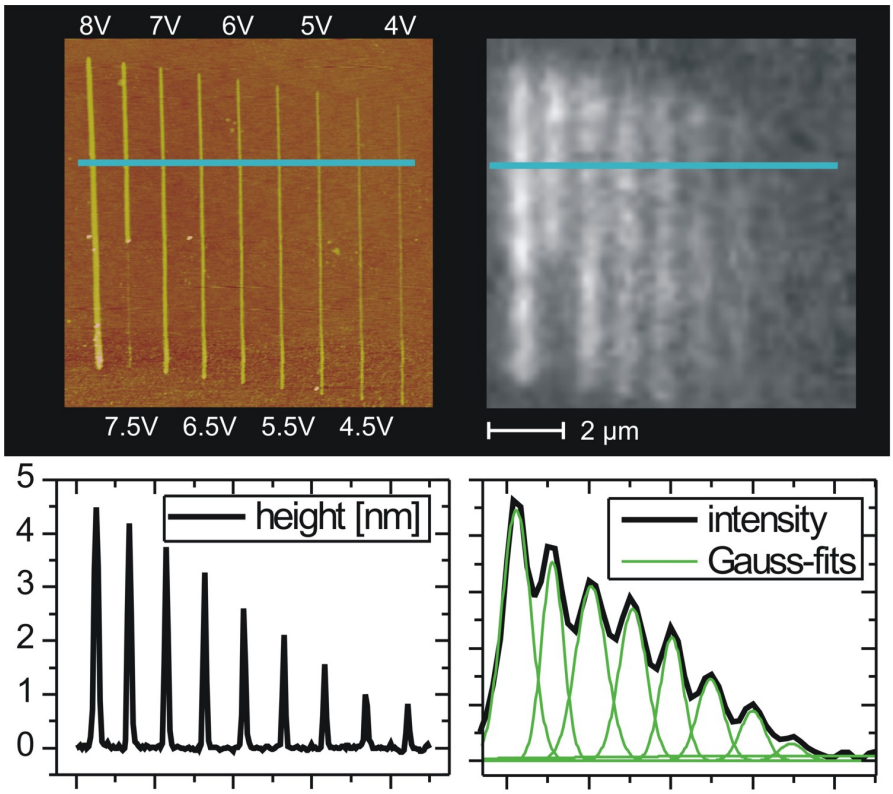

Figure 5.3: Oxide line patterns of different size on dodecyl-terminated silicon before and after dye attachment. **Left:** AFM height image before dye attachment (the corresponding lithography voltages are given above and below the lines). **Right:** optical wide-field microscope image of the same spot on the surface after dye attachment. The diagrams below correspond to a cross-section along the blue line in the above image.

height, width, and area under the curve. For the optical image, the Gauss fits reveal that the FWHM of the detected intensity for each line is below the line separation so that there is only a negligible contribution to the neighbouring line maximum. Figure 5.4 shows the height of the fitted Gaussian curves for both the topographical AFM image as well as the optical image for each line (every line corresponds to a different voltage used to generate the line). As it can be seen there is a linear correlation between oxide height and applied voltage, which is in full agreement with previous results from other groups [Graa08a, Yang06b, Teus95, Cava03]. Interestingly the peak photoluminescence (PL) intensity also decreases linearly with the oxide height and, accordingly, with the voltage. However, according to the classical theory of dipole-surface interaction, a d^{-3} dependence of the fluorescence resonance energy transfer (FRET) rate on the distance d between dye and semicon-

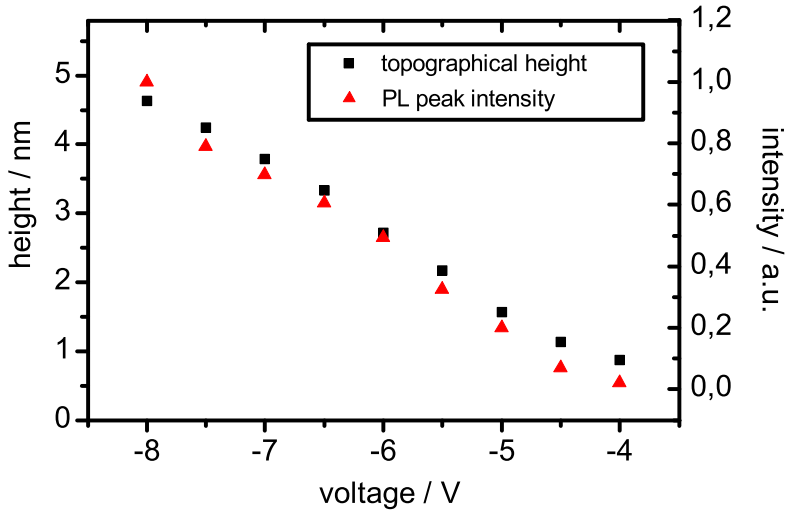

Figure 5.4: Topographical height (black squares) and peak PL intensity obtained from the Gaussians (red triangles) against the voltage at which the corresponding line was generated.

ductor is expected [Haya83, Whit83]. Yet deviations from this d^{-3} behavior have been reported by different groups for distances close to the semiconductor surface ($d < 10$ nm) [Haya83, Whit83, Sluc95, Barn98]. Since in our case the oxide height is below 10 nm, our observations confirm that for small distances a simple model of dipole-semiconductor energy transfer cannot be applied. Obviously in this case there is no inverse cubic correlation between distance to the semiconductor and energy transfer rate.

Also we did not find a straightforward relation between PL intensity and line width, which is proportional to the oxide surface on which dye molecules can bind. This, on the other hand, can be explained by the fact that the nature of the binding mechanism is not related to a surface interaction but to an electrostatic interaction. Due to the LAO the generated oxide is partially negatively charged by trapped OH^- ions. The cationic dye molecules are attracted by these charges and bind selectively to the oxide structures. The amount of trapped charges should be proportional to the volume of formed oxide. Since writing speed and length were constant for each line, the volume of each oxide line should also be proportional to its cross sectional area. Figure 5.5 shows a plot of the peak PL intensity against the line cross sectional area. The fluorescent light intensity increases nearly linearly with the cross sectional area, which is strong evidence for the assumption that the number of bound dye molecules is directly related to the number of trapped charges. The nonexistence of a d^{-3} dependence as well as the nearly linear relation between

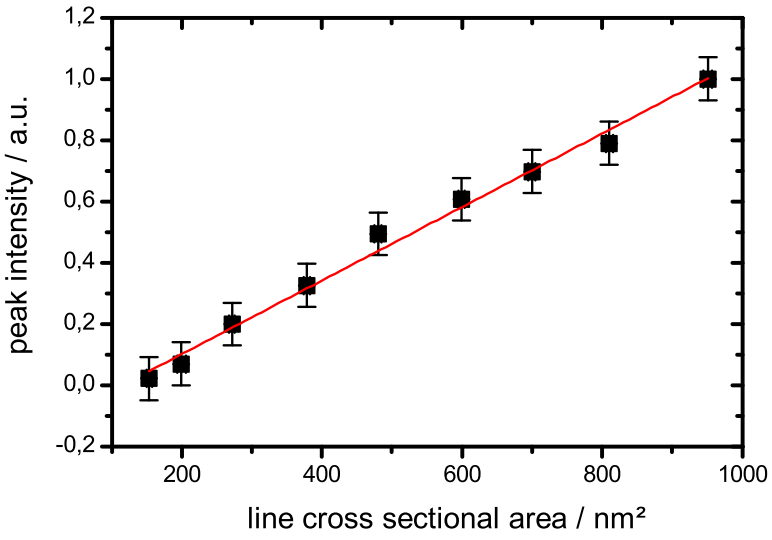

Figure 5.5: Photoluminescence peak intensity plotted against the line cross sectional area.

PL intensity and oxide volume leads to the conclusion that the increase of luminescence intensity is mainly attributed to the increase in the number of emitting molecules and not to a distance dependent quenching caused by the underlying silicon. We suggest the following rate equation, where the rate k for the relaxation of an R6G molecule from the excited state D^* to an unexcited state D is given by:

$$k = k_r + k_{nr}^{Si} + k_{nr}^{SiO_x} \tag{5.1}$$

where k_rr is the rate constant for the radiative decay, k_{nr}^{Si} for the non-radiative excitation energy transfer to the silicon, and $k_{nr}^{SiO_x}$ for a non-radiative decay mechanism to the silicon oxide. If the transfer process between the excited molecules and the silicon oxide is much faster than the energy transfer to the silicon ($k_{nr}^{SiO_x} \gg k_{nr}^{Si}$), the observed fluorescence intensity would not be dependent on the distance between the dye molecules and the semiconductor. As suggested in [Lian85], such a fast decay channel could be provided by e.g. surface states or other localized states near the interface that serve as electron acceptors on the silicon oxide. As the silicon oxide formed by the local anodic oxidation process contains, beside remaining oxyanions, also residuals of the alkyl monolayer [Pign03], the existence of various trap states at the surface and within the bulk is very reasonable.
In a next step we investigated the luminescence spectra of dye-functionalized nanostructures by scanning confocal microscopy. With confocal microscopy, spectral information can be sampled point by point. In figure 5.6 the emission spectrum of R6G on an oxide line structure (oxide height: 2.7 nm) is compared with that of R6G in aqueous solution and spin-coated on a silicon substrate with native oxide.

Because of the low signal-to-noise ratio of the spectra on the oxide lines, the PL spectrum has been measured on 15 different spots on different lines. The different spectra resemble each other in shape but vary slightly in position of the maximum. To account for these small deviations the spectra have been added up and the gained sum spectrum was subsequently normalized (figure 5.6, black line).

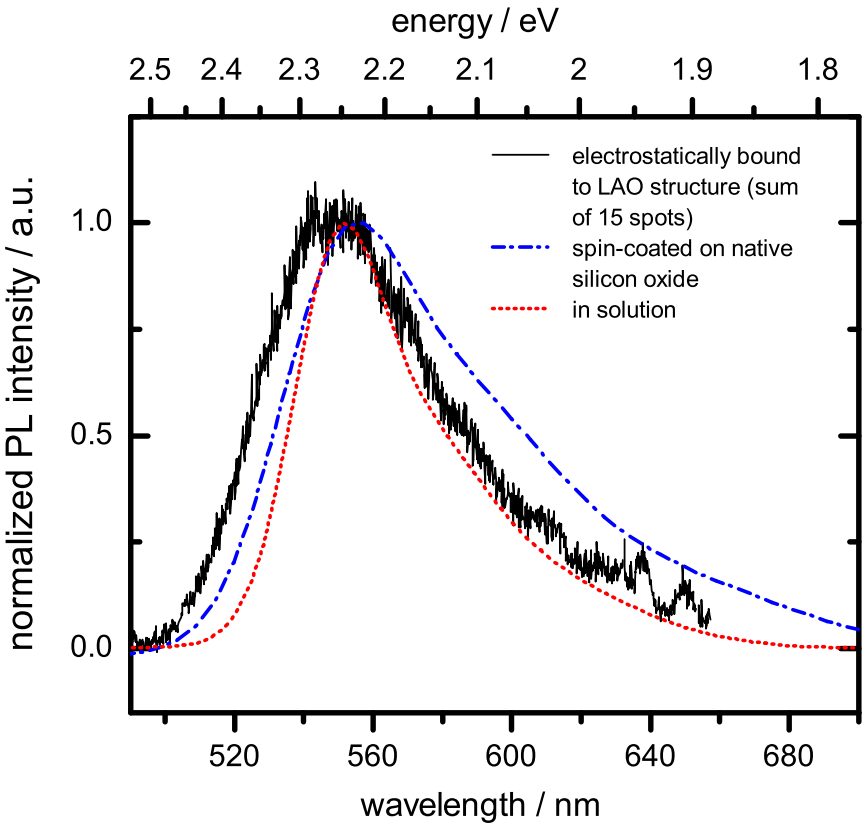

Figure 5.6: Emission spectra of R6G attached to an LAO-generated nanostructure (black), in diluted aqueous solution (red) and as a sub-monolayer on Si with a native SiO_x layer (blue). All spectra are normalized, the excitation wavelength was 465 nm and the excitation power 4 µW for the spectra measured by confocal microscopy.

The spectral shape of the emission from the oxide lines is similar to that in solution (figure 5.6, red dotted line) though there is clearly a spectral broadening especially towards blue wavelengths. The mean value of the peak position from all the different single spectra is 548.8 nm with a standard deviation of 2.4 nm. Though there is just a small difference of the spectral position on average because of the broaden-

ing effect and the mean variation, there are single spectra that are blue-shifted up to 9.5 nm ($\sim$40 meV). In particular, there is an additional flank in the blue part of the spectrum while in the red part the spectrum looks similar to that from the solution. The spectral shifts can be due to several reasons. First of all the dielectric environment of the R6G molecules on the surface is different from that of the molecules in solution. The dielectric surroundings influence the intermolecular energy levels and thus, if they are dissimilar, can cause a spectral shift. So we compared the spectra obtained from R6G on the LAO structures with that of a sub-monolayer of R6G on a silicon substrate with a native oxide layer prepared by spin-coating of the diluted solution of the dye in ethanol (figure 5.6, blue curve). The emission from the spin-coated R6G molecules, however, is shifted about 36 meV to the red with respect to the solution spectrum. Such an inhomogeneous broadening towards larger wavelengths has been reported before for R6G in close vicinity to metallic surfaces [Cnos93] and was explained as an effect of the reduced excited state lifetime on the homogeneous damping rate. In contrast, the emission from the nanostructures is shifted to blue wavelengths which can be explained by the difference between the LAO oxide and native or thermally grown oxide on silicon. It has been shown that for local anodic oxidation of alkyl-terminated silicon, C_nH_{2n} fragments of the organic monolayer are incorporated within the oxide [Pign03]. However, since the influence of this change in oxide composition on the intra-molecular energy structure is hardly unascertainable, we want to discuss some other possible and systematic reasons for the blue-shifted emission behaviour. It is known that some cationic dyes in solution undergo a spectral shift in the presence of anions to shorter wavelengths. This phenomenon is called metachromasia [Schu56] and is attributed to the formation of cationanion chargetransfer complexes [Pal73]. Since the oxide is negatively charged and the dye molecules are in proximity to the outermost negative space charges within the oxide, it is reasonable to assume that there is a strong coupling of the positively charged dye molecules with the negative space charges, which leads to a similar shift to shorter wavelengths for the absorption (and therefore emission) as it was found for charge-transfer complexes [Pal73].
Another possible explanation is that the molecules may form aggregates when they are bound to the oxide. However, in order to form aggregates that possess a blue-shifted emission (H-aggregates), the transition dipolemoments of the molecules have to be aligned parallel and the molecules need to be in a face-to-face arrangement [Gavr06]. Since we used a rather highly concentrated solution of R6G to functionalize the nanostructures, the formation of H-aggregates in solution and subsequent electrostatic binding of the aggregates to the LAO oxide is possible. Though the absorption of H-aggregates is strongly shifted to shorter wavelengths, they are known to be non-fluorescent and consequently a dimerization cannot be the reason for the blue-shift. Especially remarkable is the fact that other groups have found a red-shift of the R6G emission if the intermolecular distance is close

to the molecular FÖRSTER radius (5 nm in the case of R6G) due to resonance energy transfer [Zond03]. Since the molecules should be densely packed on the oxide structure because of the electrostatic binding mechanism, such behaviour should also be expected in our case, yet we found a blue-shift of the emission. So it can be concluded that the electric charge within the oxide influences the emission of the dye molecules. However, further systematic investigations and a detailed theoretical explanation of this phenomenon are still missing.
In a last step we investigated the photobleaching behaviour of the dye molecules. Bleaching is the irreversible conversion of a fluorescent particle into a non-fluorescent entity [Zond04]. The photobleaching mechanisms of organic dye molecules are highly complex and mostly unknown. It is supposed that they follow various pathways involving different intermediate states [Schu07]. If the dye bound to the silicon oxide structure is exposed to the excitation light for some time (seconds to minutes depending on the power of the excitation light beam), there is drastic decrease in the dye emission intensity. For long exposure times or very high excitation power the dye is bleached completely. Even after a long period without light excitation there is no recovery of the dye emission. Therefore we conclude that the observed decay of fluorescence is indeed due to permanent photobleaching. The bleaching of R6G was investigated by measuring the intensity of the fluorescent light for a period of 120 s with a time resolution of 0.5 s. In figure 5.7 the resulting bleaching curves for R6G electrostatically bound to an LAO line structure (total oxide thickness approximately 4 nm) and R6G spincoated on a silicon substrate with a 4 nm thermal oxide layer are compared with each other. For both systems the dye fluorescence decreases by roughly one order of magnitude after two minutes exposure to the excitation light. Furthermore both time traces can be well fitted with a bi-exponential decay according to $I_{PL} = I_0 + Ae^{-t/\tau_1} + Be^{-t/\tau_2}$. The determined time constants for the decays are shown in table 5.1. For R6G adsorbed on a semiconductor substrate, such a bi-exponential bleaching behaviour has been reported before [Lian84]. At present it is still unclear why the bleaching process is governed by two different characteristic times. It may be a hint for the existence of two different species or states of R6G molecules which show a dissimilar photochemistry that leads to their destruction. Though they are not identical, the characteristic time constants for bleaching of R6G bound to the LAO oxide and adsorbed on silicon oxide differ by less than a factor of 1.6. Considering, furthermore, the fact that both processes can be described by the same bi-exponential law, there seems to be no influence of the electrostatic binding mechanism on the bleaching of the dye molecules. The quantitative differences between the constants of the two systems may be explained by a slight difference in oxide thickness. It should be noted that the measured photobleaching data could also be fitted by a stretched exponential decay. This implies that there are not only two different time constants but a multitude of many different time constants. Such behaviour could

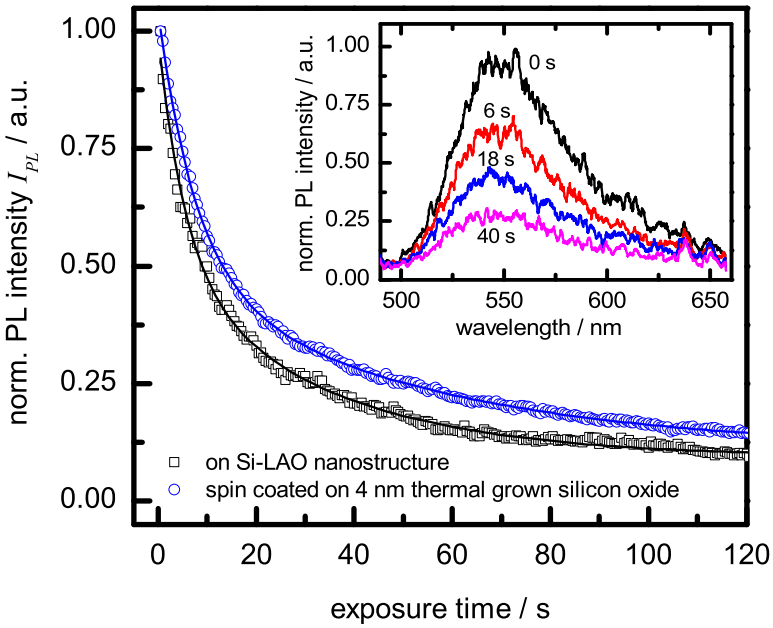

Figure 5.7: Photoluminescence intensity of a spot on a dye-functionalized oxide structure as a function of exposure time for R6G electrostatically attached to an LAO silicon oxide nanostructure with a total thickness of ∼4 nm (black squares) and spin-coated on silicon with a 4 nm silicon oxide layer (blue circles). The data have been fitted with second-order exponential functions (solid lines). In the inset related spectra of R6G on the LAO oxide are shown for different exposure times. The power of the excitation light was about 6.5 µW.

be understood in terms of a small variation of the nanoscopic chemical environment for each molecule.

Table 5.1: Time constants extracted from the bi-exponential fits in figure 5.7.

R6G on	τ_1 (s)	τ_2 (s)
LAO oxide nanostructure	5.6	33
Thermal oxide	7.7	52

5.4 Conclusions

We have shown that nanoscaled structures generated with AFM-induced local anodic oxidation of silicon can be functionalized with cationic dye molecules (R6G). The dye emission could be analysed via optical wide field and laser scanning confocal microscopy. The intensity of the emitted light is nearly proportional to the surface area of the dye-covered oxide structures which can be explained by a linear correlation between bound R6G molecules and the number of charges trapped within the oxide. The obtained dependency cannot be explained by fluorescence resonant energy transfer, so we conclude that another non-radiative energy transfer occurs. Regarding the emission spectrum of the dye, we found a blue-shift compared with the emission in solution. The reason for this is still unclear but presumably it is caused by a strong interaction of the dye molecules with the negative charges within the silicon oxide. Finally the dye molecules on the nanostructure are bleached during laser excitation. The bleaching follows a bi-exponential law and there seems to be no significant influence of the electrostatic binding on the photophysical degradation of R6G molecules.

Acknowledgement

The authors are grateful to the Deutsche Forschungsgemeinschaft (DFG, GR 2695/4) for financial support.

6 Functional perylene molecules bound to local oxide structures via electrostatic interactions

Abstract

Within this study silicon oxide nanostructures have been functionalized by selective binding of a positively charged perylene derivative. The structures were prepared by AFM nanolithography via local anodic oxidation (LAO) of dodecyl-terminated silicon and are negatively charged due to the production process. Therefore cationic spermine-functionalized perylene-bisimide (sf-PBI) molecules can be bound to the structures by electrostatic interactions. The assembly of the sf-PBI units on the LAO nanostructures is verified by AFM height measurements and means of fluorescence microscopy. Emission spectra from the dye-functionalized oxide show that the molecules are able to form excimers. These excimers are characterized by a broad and featureless red-shifted emission and an increased excited state life time. In contrast to the emission of sf-PBI films on uncharged silicon oxide, the excimer emission was found to decrease strongly for low temperatures. This may be explained by a very tight binding due to the electrostatic attraction of the molecules to the LAO oxide.

The content of this chapter is planned for publication:
T. Baumgärtel, C. v. Borczyskowski and H. Graaf: to be submitted

6.1 Introduction

Electrostatic binding of cationic dyes such as rhodamine 6G and cresyl violet [Baum10, Graa08a, Baum07] is a reliable and easily applicable method for a selective functionalization of LAO nanostructures on alky-passivated silicon. Though these dyes possess a high quantum yield, they bleach rather quickly upon photoexcitation. Therefore, another class of dyes was used for electrostatic binding: perylene tetracarboxylic acid bisimides (PBIs). Initially applied for industrial purposes as pigments [Herb97], PBI dyes have become one of the most promising and investigated system in basic and applied research. They are a highly photostable, chemically inert and show a high quantum yield which makes them an ideal system for single molecule spectroscopy [Kowe09, Krau11], light induced energy transfer processes [Prat01] and light collection [Wurt04]. Apart from their advantageous optical characteristics, PBI dyes display several other outstanding properties. For example, perylene bisimides show n-type semiconducting behavior due to the high electron affinity of rylene dyes [Lee99] and thus are a promising material for organic field effect transistors [Jone04]. Furthermore, they are known to form highly fluorescent J-type aggregates under certain conditions by hydrogen bonding and π-π stacking interactions [Kais09]. In recent studies, evidence was found for an efficient long-range transport of energy by exciton migration in such aggregates [Lin10] which could be very useful for photovoltaic devices or organic circuits. Another advantage of PBI is the possibility to rather easily introduce or tune different properties by chemical modification of the molecules. The addition of different functional side groups, such as alkyl chains, halogens or recognition units, can alter solubility [Zhan07, Ebel07], air-stability [Jone07] as well as the self-assembly behavior of perylene bisimides [Wurt04] in a directed manner. Recently, a novel type of perylene bisimide dyes which is functionalized with the polyamine spermine has been synthesized by the Würthner group [Rehm10]. The chemical structure of these spermine functionalized PBI molecules (sf-PBI) is shown in figure 6.1. The functional spermine groups are protonated, thus possessing a polycationic character. As they are bound to the perylene core in imide positions, the planar structure of the perylene core is sustained and the optical properties of the PBI unit are not altered. Also, an aggregation of the molecules via - stacking should still be possible. Furthermore, the amphiphilic sf-PBI molecules are highly soluble in water because of the spermine residues and can form self-assembled nanostructures [Rehm10]. The polycationic nature of the spermine groups combined with the advantageous optical properties of perylene bisimide dyes makes sf-PBI a very promising material for the electrostatic binding to negatively charged silicon oxide nanostructures.

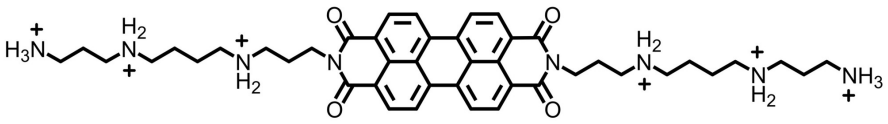

Figure 6.1: Chemical structure of the sf-PBI polycation.

6.2 Experimental

6.2.1 LAO sample fabrication and functionalization

The local anodic oxidation experiments have been carried out on weakly doped n-type silicon (resistivity >3000 Ωcm, Fraunhofer ENAS, Chemnitz) substrates with a self-assembled monolayer (SAM) of 1-dodecene molecules as surface coating. Details of the monolayer preparation process are described elsewhere [Baum11a, Linf95]. LAO experiments as well as topography measurements were conducted with an Anfatec Level AFM (Anfatec GmbH, Germany) using platinum coated silicon tips (”NSC18/Pt”, resonance frequency 75 Hz, spring constant 3,5 N/m, Mikromash, Estonia). The oxide structures were generated in contact mode operation with a voltage in the range of -7 V to -15 V applied between tip and substrate at a relative humidity (RH) of around 65%. To control the humidity of the ambient atmosphere the microscope was placed under a closed PMMA dome which can be purged with dry nitrogen or water vapor-saturated nitrogen. The humidity was measured using a ”SHT15” digital humidity sensor (Sensirion AG, Switzerland). Lithography of diverse patterns has been performed via different software protocols which have been written using a homemade software user interface. Functionalization of the structures was achieved by immersion of the freshly structured substrate in a 0.5 M solution of sf-PBI (provided courtesy of Prof. F. Würthner, University of Würzburg) in ethanol (Merck AG, spectroscopic grade) for approximately 90 minutes. After removing the sample from the solution, it was thoroughly rinsed with fresh ethanol and dried in a nitrogen stream.

6.2.2 Thin films on 100 nm silicon oxide

Sf-PBI thin films have been prepared on n-doped silicon with a resistivity of (5.9 - 7.3) Ωcm and a 100 nm-thick thermally grown silicon oxide layer (Fraunhofer ENAS, Chemnitz). Previous to film application, the substrates were cleaned with acetone and ethanol (both: Merck AG, spectroscopic grade) for 5 minutes in an

ultrasonic bath and rinsed with ultrapure water (Millipore DI). Subsequently, the substrates were heated for 30 s in a propane gas flame to remove any residual contaminants. The dye films were deposited by spin coating (3600 rpm, 20 s) 500 µl of ethanol solutions of sf-PBI with different concentrations on the cleaned substrates.

6.2.3 Optical investigations

Optical measurements on the surfaces were performed using home-built confocal microscope setups and spectral investigations in the liquid phase were carried out using a Varian "Cary Eclipse" fluorescence spectrometer with an excitation wavelength of 465 nm. Spectral measurements on the silicon substrates at low temperatures have been obtained with a laser scanning confocal microscope (LSCM). The 488 nm line of an Ar/Kr laser ("Innova 70C-Spectrum", Coherent) has been used as excitation light. The laser beam was focused on the sample by a 63x cover-glass-corrected air-immersion objective (Carl Zeiss Jena) with a numerical aperture of NA=0.75. The sample was placed in a flow cryostat ("ST-500H", Janis), evacuated to a pressure in the range of 10^{-5} mbar using a vacuum pump and cooled down using liquid nitrogen. An avalanche photo diode ("SPCM-AQR-16", Perkin Elmer) with a very low dark count rate has been used as luminescence detector. The excitation light was blocked by a long pass filter ("502ALP", Omega Optical) in the detection path. In front of the detector a beam splitter couples 75% of the fluorescence light into a spectrometer ("Acton SpectraPro-275", Acton Research Corp.) with a liquid nitrogen cooled CCD camera (Princeton Instruments) as detector. For time-resolved measurements a sample scanning confocal microscope (SSCM) setup with a 465 nm pulsed excitation has been used. Further details of the setup are described in chapter 3. The fluorescence decay curves were resolved by processing the detector signal using a "SPC-630" single photon counting board (Becker & Hickl). For spectral separation, a 570 nm short pass filter ("570SP", Omega Optical) or a 585 nm long pass filter ("585ALP", Omega Optical) could be placed in front of the detector. Both confocal setups have been expanded by a reflection wide field microscopy option in order to facilitate the retrieval of the structured spots on the sample surface.

6.3 Results and Discussion

6.3.1 AFM topography investigations

General remarks on the evaluation of comparative AFM height measurements

Atomic force microscopy is characterized by a very high resolution through the sub-nanometer positioning accuracy of the scanned probe by piezo drives [Binn86, Jali04]. The lateral precision is mainly limited by the curvature radius of the used AFM tip (usually around 10 nm to 20 nm) but the nominal resolution in z-direction is for most instruments within the Å range. Thus, the adsorption of additional molecular layers on the nanostructure should be detectable by AFM height measurements before and after the ex-situ functionalization step. However, there are some general issues concerning the measurement process that have to be addressed before evaluation of the obtained AFM images. First of all, though the mechanical positioning of the tip is very accurate, the feedback circuit that drives the piezos depends on many parameters (PID loop controller). The images for comparative height evaluation have been measured using non-contact mode operation of the AFM, which means that the cantilever is mechanically excited close to its resonance frequency and the interaction of the cantilever with the surface dampens the cantilever oscillation to a certain value which depends on the tip-sample distance [Tsuk98]. While scanning over the surface, the amplitude and therefore the tip-sample distance is kept at a given value (setpoint) by a feedback control of the z-piezo. As the transfer function between the 'real' sample topography and the z-piezo adjustment by the AFM feedback control system depends strongly on the driving frequency, driving amplitude, setpoint and the tip geometry, those parameters have to be kept implicitly constant when performing comparative height measurements [Hutt93]. Therefore all such measurements within this thesis have been conducted using equal software parameters and the same AFM tip. Unfortunately, even when using exactly the same parameters, the deposition of any material to the nanostructures alters their surface chemistry and therefore also the interactions between tip and structure surface [Send95, Noy97, Wilb95, Sasa01]. This is especially a problem if there is a strong chemical affinity between the new modified surface and the AFM tip (e.g. trichlorosilane or thiol surface groups which will bind to the silicon or metal tip [Noy95]). Yet the surface modifications used within this thesis should result in surfaces which are relatively inert towards the AFM tip. Another important factor is the formation of surface water layers as it was established in chapter 4. As all experiments have been conducted under ambient

conditions, a formation of such a water layer is very likely. As the rest of the substrate is very hydrophobic because of the alkyl monolayer, a pronounced wetting of more hydrophilic LAO structures could further distort the measurements if the effect of the water layer influences the tip-surface interactions sufficiently. Though such effects are known to exist [Weis89, Putm94], they have not been investigated deeply as their general quantitative impact on AFM height measurements is hardly determinable. Therefore, it has to be kept in mind that the following evaluations of the comparative height measurements may be biased beyond the physical positioning error of the used AFM hardware. Last but not least, for a reliable comparison it has to be assured that always the same part of the structures are compared to each other in order to exclude local variations. Since the shape of the LAO structures is sometimes slightly irregular, height profiles have been measured along defined paths over the sample without large local deviations. Furthermore the height profiles have been averaged over a width of 10 to 20 pixels and the global position of the profiles relative to the structure in successive images was adjusted as precisely as possible using topographic landmarks (e.g. distinctive 'bumps' on the structure). This ensures a positioning accuracy of the profile in the range of a few pixels.

Detection of bound sf-PBI via AFM

AFM height images of a square structure and a line structure before binding of sf-PBI are displayed in figure 6.2. After immersion in an ethanol sf-PBI solution and subsequent rinsing with ethanol and ultrapure water, there is a small but clearly detectable increase in height of the nanostructure only. Exemplarily topographic profiles are shown in figure 6.2C and 6.2D. In the case of the square structure, the height increase is about 0.7 nm and for the line structure 0.3 nm on average. As the height growth is very homogeneous and also the roughness of the residual surface does not change, a largely uniform deposition of sf-PBI on the LAO structure can be assumed. Furthermore, the height increase is rather small in comparison to the length of a single sf-PBI molecule (approximately 4 nm). Thus the molecules should be oriented rather flat on the surface and are not standing upright. This is also very plausible as the positive charges which are attracted towards the LAO oxide are located along both spermine side chains. Hence a flat orientation of the molecules on the surface brings the charges as close as possible to the negatively charged oxide. The measured height increase (0.3 nm to 0.7 nm) is within the range of the cross section diameter along the short axis of the molecule (0.5 nm). Due to the aforementioned uncertainties concerning the AFM height measurement however, it is not straightforward to draw conclusions about the orientation of the PBI cores with respect to the surface. Anyway, the AFM measurements show that there

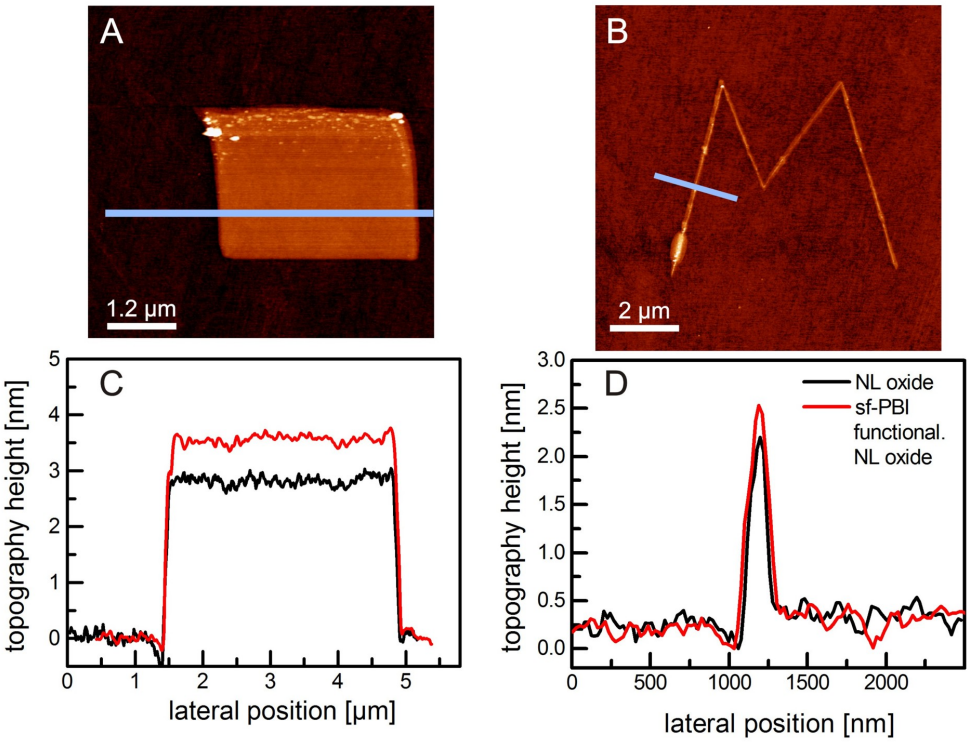

Figure 6.2: NC-AFM height images of a square (A) and line (B) oxide structure after generation by LAO. C and D show the topography profiles along the paths indicated in A and B before (black) and after (red) binding of sf-PBI. The profiles have been averaged over a width of 20 pixels.

is no formation of larger rod-like stacked aggregates as it has been demonstrated for sf-PBI films prepared from aqueous solution spin-coated on Mica substrates [Rehm10]. This is most likely due to the larger roughness and surface-chemical inhomogeneity of the LAO oxide and the strong electrostatic interaction between molecules and nanostructures which prevents an aggregation into larger structures / micelles.

6.3.2 Confocal microscopy and spectral investigation at room temperature

sf-PBI bound to LAO nanostructures

To confirm that the height increase is due to a binding of sf-PBI molecules, the samples have been investigated by confocal microscopy and spectroscopy. Similar to the findings for other cationic dyes (see chapter 5 and [Baum07]), there is a clear fluorescence signal originating only from the LAO nanostructures after the binding of sf-PBI. The signal is weak though, which is a result of the fluorescence quenching by the close proximity (several nm) of the dye molecules to the underlying silicon. Figure 6.3 shows the emission spectra of sf-PBI bound to LAO line structures which have been obtained with two different setups (black and blue curve). The inset in figure 6.3 shows a confocal microscope image of the investigated structure.

Both, the spectrum taken with the sample scanning confocal microscope (SSCM, black) as well as the laser scanning confocal microscope (LSCM, blue) are very similar in shape. Due to a larger spectrometer range the measurement with the LSCM extends up to 800 nm whereas the SSCM spectrum is limited to about 660 nm. The quite good congruence between the results of both setups emphasizes the true physical nature of the measured emission. The existence of small peaks in the low wavelength range (e.g. at 482 nm, 488 nm and 510 nm) on the other hand are experimental artifacts as they do not appear for both setups simultaneously. They might be caused by scattered light which is not sufficiently blocked by the used fluorescence light filters. Compared to the monomer fluorescence emission of sf-PBI in diluted solution (red curve), there is a red shift of the monomer-type fluorescence and the appearance of an additional emission in the long wavelength regime above 600 nm. The first peak at 540 nm can be attributed to the $S_1 \rightarrow S_0$ transition of the monomer as it resembles the first emission peak of the sf-PBI emission in solution except for the red shift of about 28 meV (540 nm compared to 533 nm in solution). This shift might be caused by the different dielectric environment of the dye molecules when bound to the charged oxide compared to the ethanol environment in solution. In the broad long wavelength part of the spectrum a substructure (a faintly visible peak) at 585 nm can be identified. This is attributed to the first vibronic progression of the $S_1 \rightarrow S_0$ transition (see figure 6.4) as the energetic separation from the main peak (also referred to as 'vibrational quantum') is about $\Delta E \approx (175 \pm 5)$ meV, which is in good agreement with typical values for perylenetetracarboxylic acid derivatives in solution or thin films [Bulo96, Henn99, Proe04].

The prominent broad peak in the low energy regime at about 640 nm is evidently

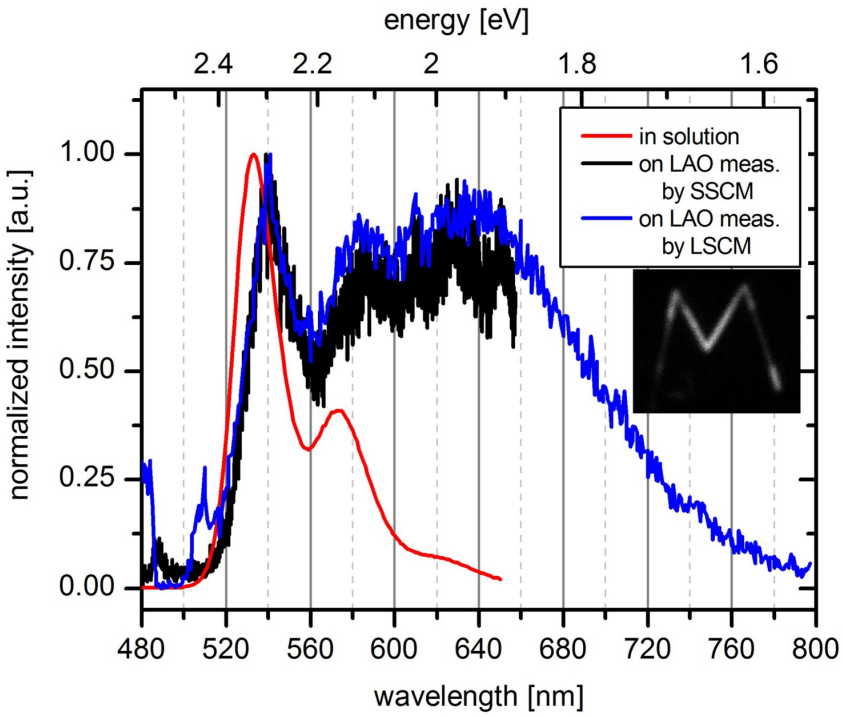

Figure 6.3: Emission spectra of sf-PBI in ethanol solution (red) and bound to a LAO nanostructure in shape of the letter 'M' (see confocal microscopic image as inset) measured with different setups. The black curve is the emission of the bound sf-PBI which was acquired using a sample scanning confocal microscope (SSCM) with an excitation wavelength of 465 nm. The blue curve has been acquired with a laser scanning microscope (LSCM) and an excitation wavelength of 488 nm.

not related to a monomer emission. The emission spectra of perylene dyes is known to change dramatically when prepared as films [Ahre04, Graa11], which is generally attributed to the formation of aggregates. In figure 6.5, the emission spectrum of an amorphous film of chlorinated N,N'-dimethyl-perylene-tetracarboxylic-acid-diimide (Cl_4MePTCDI) dye (red) is shown in comparison to the emission spectrum of sf-PBI bound to the LAO oxide (blue) from which the monomer emission spectrum in solution (figure 6.3) has been subtracted. Thereby the solvent shift has been corrected by shifting the monomer spectrum about 7 nm to longer wavelengths. The Cl_4MePTCDI data were taken from [Graa11]. Despite of a 40 meV red shift of the main peak of the Cl_4MePTCDI emission compared to the 640 nm band of sf-PBI on the oxide structure, both spectra are quite similar. In the shorter wavelength regime of the spectrum there is a larger deviation because

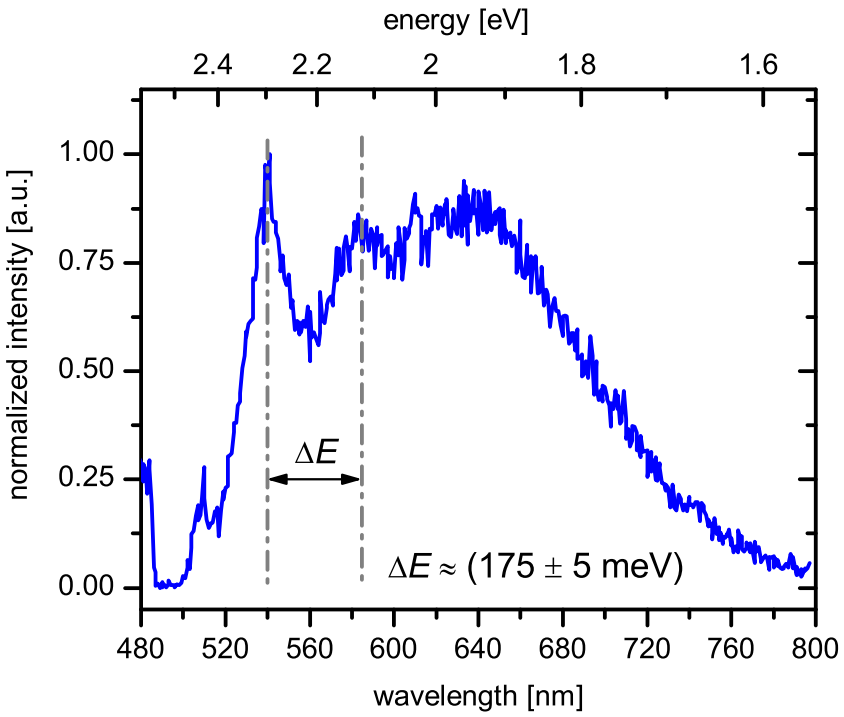

Figure 6.4: Emission spectrum of sf-PBI bound to a LAO nanostructure measured with a laser scanning confocal microscope (LSCM) at an excitation wavelength of 488 nm. Typical (red shifted) monomer bands (see figure 6.3, red curve) are indicated in the graph.

the solution (monomer) main peak is wider than the monomer peak on the structure. The red-shift is most likely caused by the much larger thickness in the case of the Cl_4MePTCDI films ($\sim$100 nm [Graa11] compared to less than 1 nm in case of sf-PBI on the LAO structure). Such an influence of the film thickness on the emission maximum position in perylene dye layers has been reported earlier and was attributed to a dielectric screening of the molecules within the layer [Proe04].

The typical emission spectrum of PBI derivatives in thin films with a broad peak at about 640 nm is explained by a stacking of the molecules in a vertical direction (plane-to-plane arrangement) which leads to an overlap of their π-orbitals (π-π stacking) and thus to a formation of H-aggregates [Proe04]. Spectral investigations of specially synthesized U-shaped PBI H-dimers (two PBI moieties held in a cofacial configuration by a linker molecule) led to results that are very similar to those for thin films [Giai08, Veld08]. Recently, Gao *et al.* were able to simulate the H-dimer spectrum in good agreement with experimental data by using an elaborate model which mixes Frenkel excitons (FE), intermolecular charge-transfer excitons

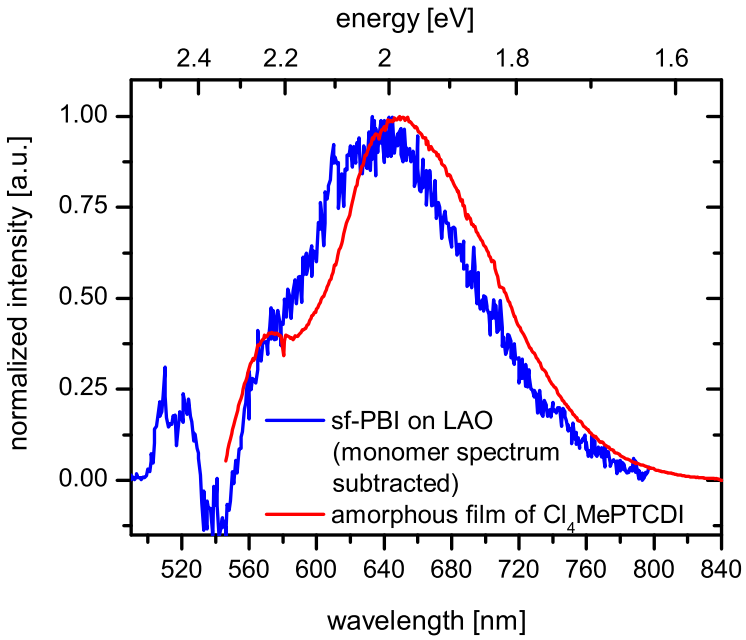

Figure 6.5: Blue curve: The fluorescence emission spectrum of sf-PBI bound to an LAO nanostructure from figure 6.4 after subtraction of a 7 nm red shifted monomer spectrum in solution (figure 6.3). Red curve: Fluorescence emission spectrum of an amorphous film of Cl_4MePTCDI (data from [Graa11]).

(CTE) and also includes electron-phonon coupling [Gao11]. They found that the broad and the strongly red-shifted emission of the H-dimers can be explained by a change in the optimal dimer geometry between ground state and excited state. Upon excitation, the H-dimer undergoes a relaxation to a new geometry which possesses a lower energy of the exciton. As the exciton life time in the optimal geometry is much longer than in the vertically excited state and the geometry relaxation is rather slow, there is an emission from both states (or any intermediate state) which extends the emission significantly.
It should also be mentioned that the smaller peak in the blue part of the Cl_4MePTCDI spectrum is most likely not related to the $S_1 \rightarrow S_0$ transition of the monomer as it may be assumed at first glance (e.g. not all the molecules in the film are dimerized) but seems to be an intrinsic transition of the dimer. This is evident as the blue peak also is present in the calculated emission spectra [Gao11] and measurements of chemically designed dimer PBIs [Giai08]. The blue peak at 540 nm in the spectrum of sf-PBI bound to the LAO nanostructures on the other hand, is much sharper and closely resembles the main peak of the monomer emission.

Comparison to sf-PBI monolayers on 100 nm oxide

In order to investigate the origin of the emission spectrum of sf-PBI bound to the nanostructures, sf-PBI was spincoated from solution onto silicon wafers with a thermal oxide layer of 100 nm thickness. Different concentrations of sf-PBI in ethanol have been used and the obtained emission spectra from these samples are shown in the left panel of figure 6.6. The measured confocal microscopy images (not shown) displayed a uniform emission over large parts of the surface which indicates the formation of homogeneous films of dye molecules. For very low dye

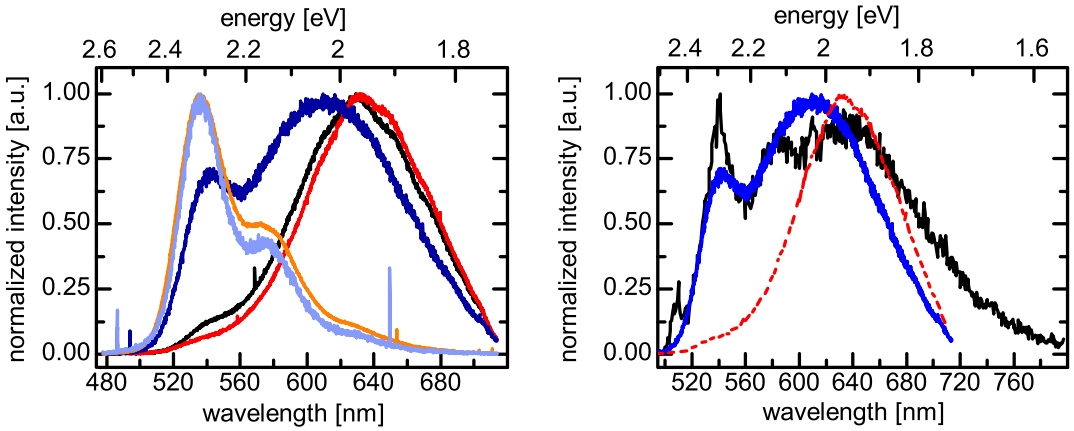

Figure 6.6: **Left:** Emission spectra of sf-PBI films on 100 nm thermal silicon oxide on silicon substrates for dye concentrations of $1.6 \cdot 10^{-7}$ M (light blue), $1.6 \cdot 10^{-6}$ M (orange), $1.6 \cdot 10^{-5}$ M (dark blue), $1.6 \cdot 10^{-4}$ M (red) and $1.6 \cdot 10^{-3}$ M (black) in the spincoated solution. **Right:** Comparison of the $1.6 \cdot 10^{-5}$ M (blue) and $1.6 \cdot 10^{-4}$ M (red dashed) spectrum with the emission of sf-PBI on a LAO nanostructure (black).

concentrations ($1.6 \cdot 10^{-7}$ M; light blue and $1.6 \cdot 10^{-6}$ M; orange), the fluorescence spectra from the sf-PBI films resembles that of the monomer emission (see figure 6.3). This is also the case for lower dye concentrations down to $1.6 \cdot 10^{-9}$ M which are not shown here for reasons of clarity. For higher dye concentrations ($1.6 \cdot 10^{-4}$ M; red and $1.6 \cdot 10^{-3}$ M; black), the emission is strongly red-shifted as well as broadened and similar to the fluorescence spectra of α-perylene crystals (denoted as E-type emission) [Sumi89]. Also for other perylene derivatives such an E-type-like emission has been found in the case of films [Graa08b, Graa11], designed H-dimers [Giai08, Veld08], stacks [Ford87, Bish96, Akim97] or polymers [Hern04]. Especially interesting is that for sf-PBI films from solutions with a concentration of $1.6 \cdot 10^{-5}$ M (dark blue), the emission seems to be a combination of a monomer and aggregate spectrum. Obviously there is a transition region of concentrations,

which is around 10^{-5} M for the used spincoating parameters, where both species of the sf-PBI molecules (monomers and dimers) coexist on the surface. However, the position of the peaks in the intermediate region is not the same as for the border cases of very low and very high concentrations. Thus it is no simple superposition of monomer and aggregate spectrum in the strict sense. Obviously, there is an interaction between both molecular states that influences the spectral properties and shifts the monomer peak to the red and the aggregate peak to the blue.
The right panel in figure 6.6 compares the emission from the $1.6 \cdot 10^{-5}$ M film (blue) and the $1.6 \cdot 10^{-4}$ M film (red dashed) to the fluorescence of sf-PBI electrostatically bound to an LAO nanostructure (black). The position of the monomer-like peak fits nicely for the black and the blue curve, though it is a little more pronounced for the nanostructure spectrum. It can also be seen that the peak in the low energy region of the spectrum coincides with the maximum intensity emission from the $1.6 \cdot 10^{-4}$ M film (red dashed). Only the spectral broadening in the case of sf-PBI bound to the LAO oxide is larger than for the films which may be caused by a more heterogeneous dielectric environment: Due to a non-stoichiometric composition, unsaturated bonds, trapped charges and residual hydro carbon residues [Pign03], the LAO oxide is much more diversified than the thermal oxide used for sf-PBI film preparation.
Considering the findings for the spincoated sf-PBI films, the spectrum of sf-PBI bound to the nanostructures seems to be a result of a formation of different sf-PBI species. Some of the molecules are forming H-dimers that exhibit the red-shifted E-type emission and some molecules exist in a monomer-like state. This assumption is also supported by the observation that the relative intensity of the 545 nm emission compared to the 640 nm peak varies for different prepared samples and oxide structures. The tendency of dimer formation may be influenced by different parameters such as oxide roughness or the magnitude of the space charge within the oxide. In order to confirm the above mentioned explanations, the spectral and time-resolved properties of sf-PBI bound to the nanostructures will be investigated in greater detail in the following chapters.

6.3.3 Confocal microscopy and spectral investigation at low temperatures

Using a microscope cryostat, a sample with a sf-PBI functionalized LAO nanostructure was cooled down to 77 K. The emission spectrum of the sf-PBI on the structure is shown in figure 6.7 for the three temperatures 298 K, 188 K and 77 K. The intensity ratio between monomer-like and E-excimer emission (at 644 nm) is clearly a function of the temperature, whereby the relative excimer emission is de-

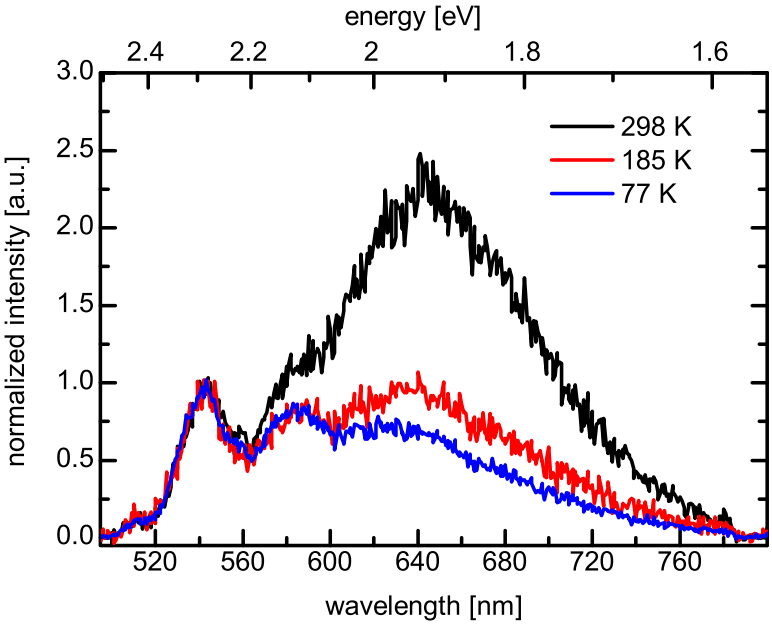

Figure 6.7: Emission spectra of sf-PBI bound to a square LAO nanostructure measured in vacuum at 298 K (black), 185 K (red) and 77 K (blue) using LSCM with an excitation wavelength of 488 nm. Spectra have been measured during cooling down from room temperature and are normalized to the monomer peak at 545 nm.

creasing for low temperatures. The spectra have been normalized to the monomer peak at 545 nm and only relative changes of the two peak intensities (monomer compared to excimer) can be deduced from the measurements. This is due to the fact that during cooling there is a rather large drift in all three spatial directions which has to be compensated manually. This requires a repeated scanning of the substrate in order to retrieve the structure. Furthermore by scanning the functionalized structures, the sf-PBI dyes bleach gradually. With the possibly bleached dyes and the uncertainty to adjust to exactly the same focal plane, an absolute quantitative measurement is not possible. Moreover, the drift and the bleaching is also the reason for the fact that a much finer temperature step size was practically impossible.

Investigations of α-perylene crystals also showed that for low temperatures the E-excimer emission vanishes and instead another emission at higher energies occurs which is denoted as Y-type emission and possesses a similar shape as the monomer spectrum [Frey78, Walk85, Sumi89]. Thereafter, the following phenomenological model, which is depicted in figure 6.8, has been developed and refined in order

to describe the excimer formation in perylene crystals [Walk85, Mahr94]. After

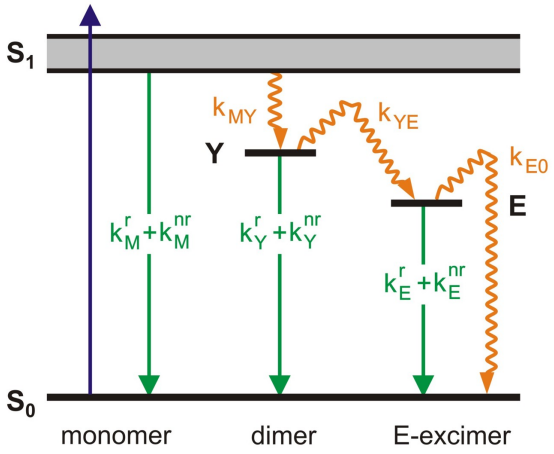

Figure 6.8: Energy scheme and kinetic rates for fluorescence decay processes in α-perylene including a two-step excimer formation after [Walk85]. Details are explained in the text.

excitation into the monomeric S_1 state, the perylene molecules can relax directly into the ground state S_0 ('normal' monomer relaxation at a radiative rate k_M^r and a non-radiative rate k_M^{nr}) or into the Y state with a rate k_{MY}. In the case of coupled perylene oligomers, k_M^{nr} and k_{MY} are much larger than k_M^r and there is nearly no monomer emission. The Y state decays either directly into S_0 by radiative and non-radiative processes or via thermal activation into the excimer states E at rates $k_Y^r + k_M^{nr}$ and k_{YE}, respectively. The E states are populated only via thermally activated energy transfer from the Y state and not directly from the S_1 state. Again, the E states decay by direct radiative or radiationless deactivation into S_0 but also indirectly after thermal activation at rates k_E^r , k_E^{nr} and k_{E0}, respectively. The obtained experimental observations for sf-PBI can be partly explained by this phenomenological model. The E-type emission at high temperatures is a result of the formation of E states upon excitation by a thermally activated change in the relative position of two coupled PBI molecules. The exact nature of the position change is thereby still not fully discovered and often discussed as either mainly related to the distance of the dimer subunits [Tana63, Sumi89] or caused by orientational and conformational changes [Veld08, Gao11]. At high temperatures (e.g. room temperature), the motional freedom of the molecules in the dimer allows such a position change which enables the formation of an excimer state. For lower temperatures, the thermal barrier cannot be overcome and a formation of the E state is not possible anymore. Considering the model, the monomer-like emission at 545 nm with its vibronic satellite should have to be interpreted as originating from the Y states rather than monomeric sf-PBI. In literature, the Y state is often interpreted as less relaxed

excimer state [Walk85]. However, in contrast to the E-excimer emission which is spectrally nearly identical for all studies, the shape of the Y-emission and its temperature behavior varies strongly for different perylene derivatives and preparation conditions. For unmodified or marginally altered perylene cores, the Y-emission is reported to be very similar to the monomer emission [Walk85, Mahr94, Weis92]. In α-perylene crystals, emission from the Y state does not occur for temperatures above 60 K and the E-emission completely vanishes only for temperatures below 30 K [Walk85]. In the case of highly concentrated Langmuir-Blodgett (LB) films of perylenyldodecaoic acid, the E-type emission does not disappear at all, even not for very low temperatures (2 K) [Mahr94, Weis92]. In contrast, for crystalline films of chlorinated dimethyl-perylene-tetracarboxylic-acid diimide (Cl_4MePTCDI) with a twisted aromatic core [Graa08b], or low-concentrated LB-films of peryleneyldodecanoic acid [Akim97], the Y-emission resembles more the E-emission in spectral shape and is energetically located between monomer and E-excimer. In the case of crystalline Cl_4MePTCDI [Graa08b] and MePTCDI films [Puec96], the rise of the Y-emission at low temperatures is not correlated with a decrease of the E-emission as it is the case for α-perylene crystals [Walk85] or concentrated LB films [Mahr94]. Thus the E-state seems not to be populated via the Y-state in such systems.

The partly contradictory findings for the different systems indicate that the true nature of the Y-emission is only poorly understood. Obviously, under certain conditions there is an additional emission at lower energies than the E-excimer for many systems, which is overall denoted as Y-emission. The origin and behavior of this emission, however, seems to depend on the molecular as well as the aggregation geometry. The Y-state found for the sf-PBI emission on the nanostructures is similar to the monomer emission and thus cannot be very different from the monomer excited state. It may also be valid to interpret this state as a monomeric state which is slightly altered by the environment of other sf-PBI molecules rather than a pure excimer state in which two PBI molecules are electronically involved. Nevertheless, the term 'Y-state' will be used within this thesis to describe the characteristic monomer-like emission at 545 nm, despite its ambiguous meaning.

As mentioned above, the transition from E- to Y-emission occurrs only for temperatures below 60 K in α-perylene crystals [Walk85] and highly concentrated LB films of perylenyldodecaoic acid [Mahr94, Weis92]. However, in the case of sf-PBI on the silicon oxide nanostructures, the E-type emission nearly vanishes at even higher temperatures and the Y-emission is visible even at room temperature. This is quite surprising as the order of the molecules on the rough and chemically inhomogeneous anodic oxide is not expected to be very high. In the following, the excimer formation kinetics of sf-PBI bound to the silicon oxide nanostructures will be discussed from a molecular point of view which accounts for a presumably heterogeneous nature of thin PBI films in contrast to a uniform crystal.

In an α-perylene crystal, the perylene units are aligned as depicted schematically in figure 6.9. The molecules are arranged in a coplanar orientation forming H-type dimers but there is a certain inclination between the two units due to the lattice structure. The centers of the molecules are shifted by 0.9 Å in the direction of the long molecular axis and by 1.3 Å in the direction of the short molecular axis [Mahr94]. It is generally argued that the E-emitting excited state corre-

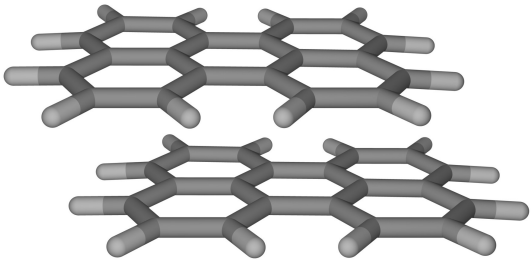

Figure 6.9: Geometry configuration of parallel perylene H-dimers in an α-perylene crystal.

sponds to a configuration where the distance between the molecular centers and also the interplanar distance is shortened, thus increasing the intermolecular overlap [Mahr94, Wars74, Veld08, Gao11]. According to standard exciton theory, a coplanar inclination of coupled parallel transition dipoles leads to a shift of the dimer energy levels [Kash65]. The thermal activation energy which is necessary for the E-type emission depends on the overlap of the perylene cores in the initial molecular configuration as well as the possibility of the perylene units to change their arrangement within their matrix towards the optimal E-excimer geometry. As the molecules align in a coplanar fashion with a certain inclination, they will need some thermal motion (e.g. lattice vibrations) in order to change their orientation to the E-type geometry. For sufficiently low temperatures, the system will freeze out and the E-emission vanishes. Due to the rather rigid nature of the crystalline structure, the E-type emission can only be observed for temperatures above 30 K.
In the case of sf-PBI bound to the LAO nanostructures the E-emission decreases drastically even for much higher temperatures (above 185 K, cf. figure 6.7) which can be explained by a very tight binding of the sf-PBI molecules to the nanostructure that prevents the reorientation of the perylene cores. This is most likely a result of the electrostatic attachment of the dyes. Each sf-PBI molecule is bound by six positive charges (three at both spermine groups) that will assemble in a minimum energy configuration within the electrostatic potential map of the negatively charged LAO oxide. The strong electrostatic interactions between the charged oxide and the comparably long polycationic spermine chains will dominate the ar-

rangement of the molecules on the surface of the nanostructures rather than the interactions between two perylene units. Therefore a large thermal energy is needed in order to allow for a reorientation of the perylene cores. For comparison, also the film of sf-PBI molecules which was spincoated from a 10^{-5} M solution on thermal oxide has been investigated at low temperatures (figure 6.10). Emission spectra

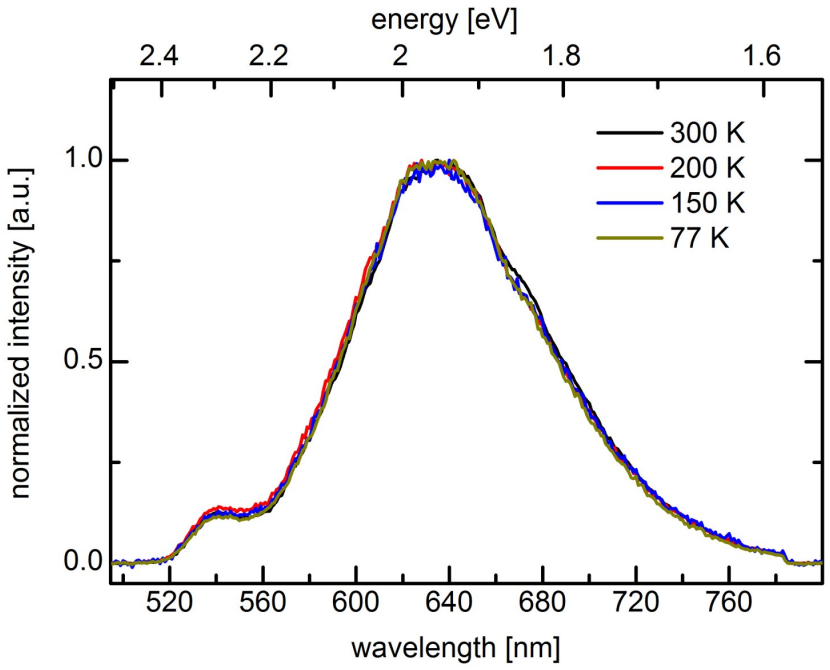

Figure 6.10: Normalized emission spectra of a sf-PBI dye film on 100 nm thermal silicon oxide substrates (dye concentrations of $1.6 \cdot 10^{-5}$ M in the spincoated solution) measured in vacuum at 300 K (black), 200 K (red), 150 K (blue) and 77 K (yellow) using LSCM with an excitation wavelength of 488 nm.

have been measured on at least 10 different positions on the substrate and have been averaged and normalized. Obviously there is no or only very little influence of the temperature on the E-type emission within the realizable temperature range. This indicates that even at 77 K the thermal energy is high enough in order to allow for configuration changes of the sf-PBI molecules within the thin films. This is also in agreement with the results both for perylene crystals as well as Langmuir-Blodgett thin films of different PBI molecules, where the decrease of the E-type emission occurs only at temperatures below 60 K [Walk85, Mahr94, Weis92]. The vanishing of the E-emission at comparable high temperatures for sf-PBI bound to LAO oxide, seems to be related to the special conditions in the case of electrostatic binding, which further endorses the considerations above. It should also be

remarked, that the non-vanishing E-type emission at low temperature does not necessarily mean that all the oligomers on the surface have to retain the possibility to undergo configurational changes into the E-type geometry. Mahrt *et al.* have proposed that in investigated LB films the majority of the PBI units form metastable or unstable dimer configurations and only a small fraction of the dimers are stable parallel dimers or able to relax into an E-excimer geometry [Mahr94]. They argue that these stable or E-excimer forming dimers function as traps and luminescence centers for the other excited molecules. The transition from E-type emission to Y-type emission at low temperatures would therefore be governed by an excitation energy transfer from the metastable or unstable dimers to these traps. However, this theory does not explain the difference of the temperature dependence of the emission spectra between spincoated films and sf-PBI electrostatically attached to the nanostructures and is therefore not elaborated any further.
The model from figure 6.8 does also not explain another experimental observation regarding the low-temperature behavior of bound sf-PBI. After cooling a sample with sf-PBI functionalized nanostructure down to 77 K, the temperature was increased gradually to 300 K within 1 h. However, this did not lead to an instant recovery of the E-excimer emission (see figure 6.11A). Only after 14 h at room temperature (RT), the E-emission reappeared though it is still weaker compared to the 545 nm peak than before the exposure to the low temperature (figure 6.11B). This is quite surprising as once the system has been heated up again to room temperature, the thermal motion should enable a change of the molecular configuration and a reoccurring of the E-emission. Yet, this is not the case and even after several hours the E-type emission is still quenched considerably. Therefore, the following simplified scheme has been derived for the sf-PBI fluorescence emission (see figure 6.12). After excitation and transition to the Y states, there is an energetic barrier for transition to the E state. This barrier can also be understood in terms of a thermal activation energy E_A which is necessary for the configuration changes. At room temperature, this barrier can be overcome and there is a prominent emission from E states (figure 6.12A). For lower temperatures, there is not enough thermal energy for the transition to the E states and instead a stronger emission from the Y states should occur. Unfortunately, this cannot be directly proven as only relative changes between E- and Y-type emission can be observed accurately (explanation see above). However, the decrease of the temperature must also mean an increase of the energy barrier (to a value of E_A^*) which is only slowly reversible (figure 6.12B). Thus, even for elevated temperatures, it is nearly impossible to form E states due to this energetic barrier. As it is evident from figure 6.7, there is a transient and not an abrupt vanishing of the E-emission. Furthermore, even at 77 K, the E-emission does not disappear completely but decreases in relative intensity and shifts slightly to smaller wavelengths (figure 6.11B). Obviously, this energy diagram is not identical for all the aggregates but there is a multitude of different

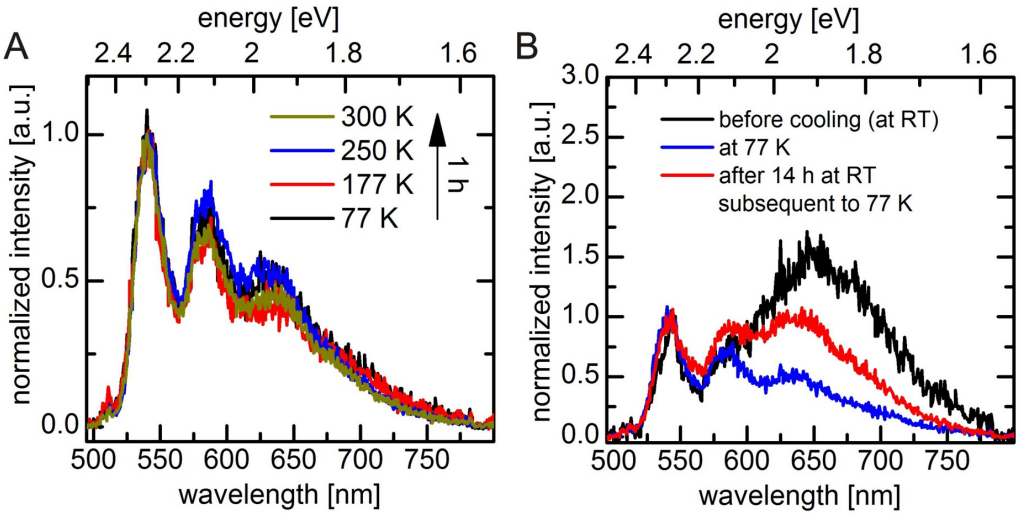

Figure 6.11: **A:** Emission spectra of sf-PBI bound to a LAO nanostructure measured in vacuum at 77 K (black), 177 K (red), 250 K (blue) and 300 K (yellow) using LSCM with an excitation wavelength of 488 nm. Spectra have been measured during heating up from 77 K to 300 K. **B:** Emission spectra of sf-PBI bound to a LAO nanostructure before cooling down (black), at 77 K (blue) and after 14 h at room temperature (RT) subsequent to cooling to 77 K (red).

energetic landscapes and barrier heights. The arrangement of the sf-PBI molecules on the LAO oxide is determined by an equilibrium between electrostatic attraction of the spermine chains towards the substrate at the one hand as well as a repulsion between the chains (figure 6.13A, red arrows) and the tendency of the perylene cores to form stacks on the other hand (figure 6.13A, blue arrows). The configuration of the sf-PBI molecules on the LAO structure is therefore an unknown and complicated function of those interactions and the temperature-dependent three-dimensional degrees of freedom of the molecular entities. Therefore, the discussed geometries below are just special cases which may be helpful to understand the underlying processes but are only a coarse simplification of the true conditions on the surface. Let us assume a molecular configuration of a sf-PBI dimer as depicted schematically in figure 6.13B. At room temperature, the thermal energy is high enough for the spermine chains to avoid the electrostatic repulsion between each other by bending upwards. This configuration also allows for a relaxation of the PBI cores into an optimal π-π-stacking or E-excimer geometry. If the temperature is reduced, there is not sufficient thermal energy to allow for a large bond angle motion of the spermine chains. Thus the chains bend down and the repulsion between them forces the molecule to rotate (figure 6.13C). Finally, the molecules

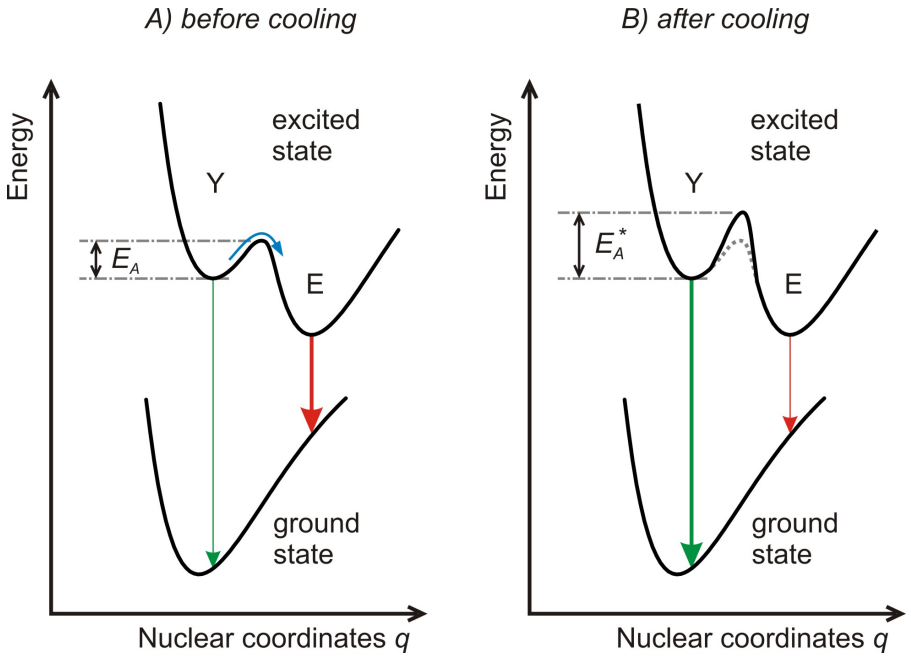

Figure 6.12: Schematic energy diagram for Y- and E-emission of aggregated sf-PBI molecules at room temperature A) before and B) after cooling down to low temperature.

orient in a new minimal energy configuration (6.13D) which is much more different from the optimal stacking or E-type geometry and also very stable because of the electrostatic binding of now all four spermine chains of the dimer. This stable configuration is also the reason for the very long recovery time of the E-emission once the substrate has been cooled down and heated up again. Of course, there may not only be a rotational re-orientation as depicted in the example above but also translational or angular changes which will lead to a re-organization of the molecules in a new minimum energy configuration within the negative potential surface. The surprisingly stable arrangement after cooling down is most likely also a result of the different distance dependencies of the involved interactions. The conventional understanding of π-π-stacking involves quadrupole interactions between the delocalized electrons in p-orbitals of aromatic compounds though true nature of the driving forces for this stacking is still debated controversially [Grim08]. A complete synopsis about this field is far beyond the scope of this chapter, but in summary, the interaction energy depends strongly on the inter-fragment distance R (at least $\sim R^{-6}$) [Grim08], which means that the stacking interaction is only strong for short separations of the perylene cores. The electrostatic forces between the spermine groups and the negatively charged substrate on the other hand possess a much longer ranged character (electrostatic force $\sim R^{-2}$). In conclusion, the strong

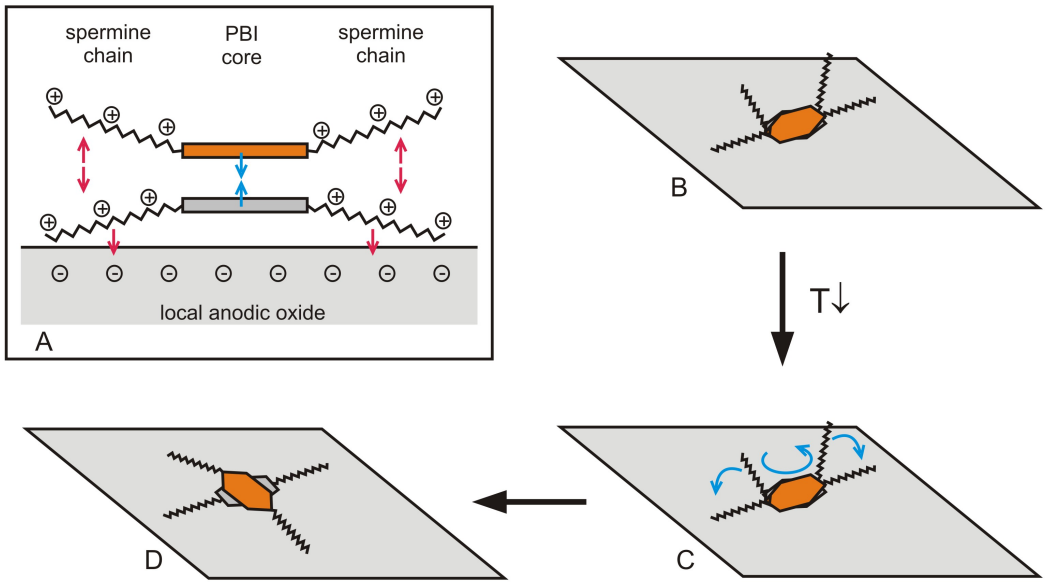

Figure 6.13: **A:** Schematic representation of different interactions governing the arrangement of sf-PBI dimers on local anodic oxide. Blue arrows denote π-π-interactions and red arrows symbolize electrostatic interactions. **B-D:** Exemplary configurational re-orientation of a sf-PBI dimer upon lowering of the temperature. At room temperature, the spermine chains can bend upwards and allow for a relaxation of the PBI cores into an optimal E-type geometry (B). Reduction of the temperature leads to a bending down of the chains and a reorientation of the monomeric units relative to each other (C). The final configuration (D) is much more different from the optimal E-type geometry and also especially stable because of the electrostatic binding of all of the spermine chains.

electrostatic interaction between the spermine chains and the substrate seems to be the reason for the hindrance of the relaxation into the π-π-stacking or E-excimer geometry. This is also substantiated by the observation that after storing sf-PBI thin film sample prepared from 10^{-5} M solution at RT, there is a slow gradual increase of the E-type emission. After two months, the relative intensity of the E-type emission increased by roughly a factor of four compared to the monomer emission which indicates rather slow kinetics of the reorganization processes within the thin film. In order to prove the theory of the configuration changes at low temperatures, an absolute measurement of the intensities of E-excimer and monomer emission would be very helpful. If the above considerations are true, then a decrease of the E-emission should also lead to an increase of the monomer emission. However, as stated above, such a quantitative measurement is very difficult for the investigated

systems.
The geometrical argumentation so far is the most likely but not the only possible explanation for the decrease of the E type emission. Another explanation may be provided by taking trapping mechanisms into account. Recent studies indicate that charge transfer (CT) states or CT excitons have a strong influence on the optical properties of perylene oligomers [Veld08, Gao11, Gang10]. When the excited dimerized sf-PBI molecules cannot undergo a fast conformational change into the E-excimer geometry due to the low thermal energy, the formation of CT excitons may be possible instead. If there are suitable trap states available in the environment of the perylene cores, electrons or holes could be localized there. With a trapped CT exciton, the dimer cannot be excited by the incident light anymore and the E-type emission is quenched effectively. In order to explain the observed slow recovery of the E-emission after cooling down, this trapping mechanism has to be very stable (long trapping times). There are many possible candidates for such traps in the case of sf-PBI on LAO nanostructures. The surface of the oxide structure is supposed to possess many unsaturated bonds due to the strong non-equilibrium nature of the oxidation process. Such dangling bonds are discussed as traps for electrons or holes in semiconductor nanocrystals that cause fluorescence intermittency phenomena [Kras11]. Also the negative charges within the oxide or the positively charged spermine groups may be traps for charge carriers if they are close to the CT excitons. At first glance, the spermine groups have to be ruled out, as for thin films of sf-PBI no temperature dependent vanishing of the E-emission was found. However, one has to keep in mind that the arrangement of sf-PBI on the LAO structures is without much doubt very different from that on uncharged oxide. On thermal oxide surfaces, the sf-PBI molecules can arrange more freely and will form different geometries. AFM-investigations of sf-PBI films on mica show that the molecules tend to form globular structures with a size of 2-3 nm [Rehm10]. This result was explained by molecular dynamic calculations and attributed to a self-aggregation of the molecules into micelle-like structures. Within those micelles, the perylene units constitute the (hydrophobic) core and the spermine residues form the (hydrophilic) shell. Consequently there is a clear separation of spermine and perylene entities whereby the perylene cores are much closer to each other than to the positive charges at the spermine chains and an occurring trapping event is rather unlikely. A similar micelle formation may also take place in the films prepared on thermal oxide. From the AFM investigations it must be concluded that sf-PBI does not form such structures when bound to the LAO nanostructure. The electrostatic interaction that drags the molecules towards the surface is stronger than the forces causing a phase separation and micelle formation. Thus it is also possible that a positively charged spermine group is close enough to a perylene core to act as a trap for the electrons of the CT exciton. In order to decide which of the both explanations is more adequate for the observed phenomena, a control experiment

has been devised in the following manner: A fluorescence spectrum of an sf-PBI-functionalized LAO nanostructure has been taken at room temperature, then the sample was cooled down to 77 K in an evacuated cryostat in complete darkness and kept at that temperature for 30 minutes. Afterwards the sample was heated up again to room temperature, removed from the cryostat and investigated once more by fluorescence microscopy. The obtained spectra before and after the cooling procedure are plotted in figure 6.14. In this case there is no perylene monomer-like spectrum detectable which leads to the assumption that on this structure nearly all of the sf-PBI molecules can change into the E-excimer geometry. Thus, a relative comparison of the E-emission and monomer emission is unfortunately not possible. Therefore the adjustment of the focus position was performed with the highest possible precision with a relatively low excitation power (250 nW) in order to minimize the bleaching of the dyes. As it can be seen from figure 6.14, there seems to be a decrease of the E-type emission once the sample has been cooled down to 77 K even if the sample is not excited optically at low temperatures. This would clearly contradict the explanation approach that the decrease in E-emission at low temperatures is caused by CT exciton trapping, because without illumination no such excitons are created which could be trapped. The experiment also indicates that there is no appearance of Y-emission upon decrease of the E-emission. Therefore it can be concluded that the excitation energy decays via non-radiative channels if the molecules cannot change into the E-excimer geometry. Furthermore it was observed that for very ragged oxide structures (not shown in this thesis) in some cases the emission spectrum and its low temperature behavior is different from that on comparably smooth LAO oxide surfaces. Obviously there is a strong dependence of the dye aggregation on the surface topography which also favors the geometric explanation attempt rather than the trapping approach. A systematic study concerning the influence of the oxide roughness on the spectra of the bound sf-PBI dyes would be very interesting, though it would necessitate a very high experimental effort as the oxide roughness is very hard to control. Additionally, an influence of the lateral roughness on a molecular scale (some nanometers) has to be assumed which is only accessible by high resolution AFM measurements and cannot be probed by optical methods (diffraction limited laser spot). In conclusion, it is clearly evident that the special conditions on the charged LAO oxide lead to a quenching of the E-emission at low temperatures. This process is at least partially reversible by thermal annealing, though the observed recovery times are rather long (several 10 hours). In consideration of the current experimental data, a reorganization of the sf-PBI molecules on the surface seems to be the most promising explanation. However, a systematic and more detailed study of the low-temperature behavior as well as the interplay between aggregation and surface topography would be necessary in order to develop a self-contained model of sf-PBI aggregation on LAO oxide nanostructures.

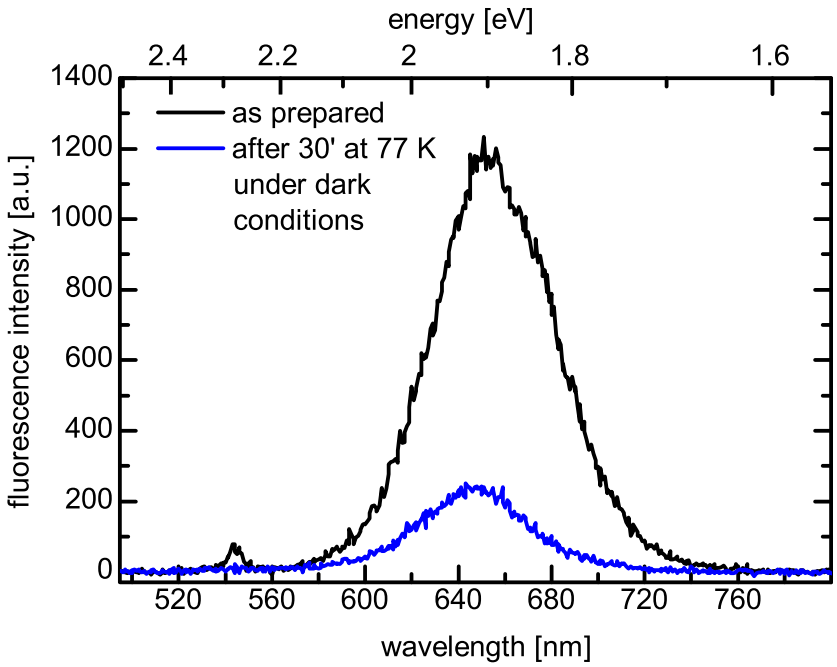

Figure 6.14: Emission spectra of sf-PBI on an LAO oxide nanostructure measured in vacuum at room temperature after preparation (black) and after freezing for 30 minutes at 77 K under dark conditions (blue) using LSCM with an excitation wavelength of 488 nm with an excitation power of 250 nW. Spectra have been integrated for 10 s. The small feature at 544 nm is due to stray light from the environment which could not be removed completely by a background correction.

6.3.4 Fluorescence life time investigations of bound sf-PBI dyes

In order to further investigate the interaction of the sf-PBI molecules bound to a LAO nanostructure, the life time of their excited state has been probed via time-resolved fluorescence microscopy. Figure 6.15 shows a typical fluorescence decay curve of sf-PBI on an LAO oxide nanostructure (red curve) compared to the decay in solution (blue curve). In aqueous solution, the fluorescence decay is nearly mono-exponential which is expressed by a linear shape of the decay curve in a log-lin diagram. The fluorescence life time was determined to be (4.1 ± 0.1) ns which is in agreement with previous investigations of the dye [Rehm10]. In contrast, the decay of sf-PBI bound electrostatically to a nanostructure is clearly multi-

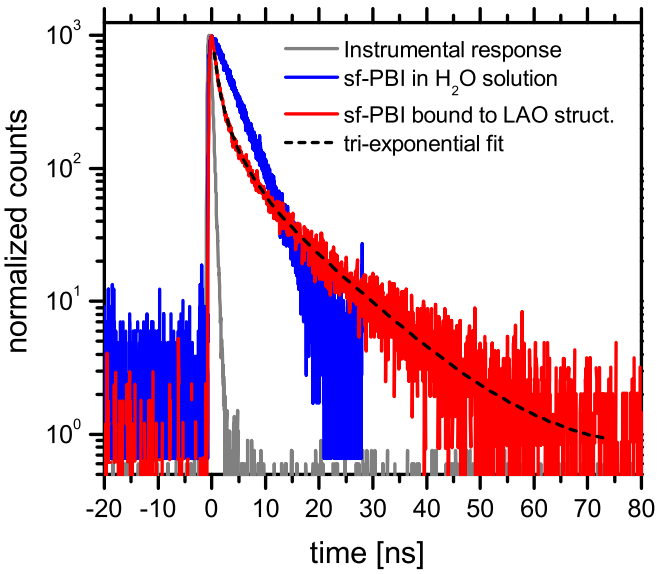

Figure 6.15: Log-lin plot of the normalized fluorescence decay curve of sf-PBI in a 10^{-7} M aqueous solution (blue) and bound electrostatically to a LAO oxide nanostructure (red) including a tri-exponential fit (dotted black). The decay has been measured over the whole spectral range. The instrumental response function for the LAO measurement is displayed as a gray curve.

exponential. At least three different life time components are required to deliver a satisfactory fit result over the whole curve (black dotted curve in fig. 6.15). Fit functions in the following form have been used for evaluation of the decay curves:

$$I(t) = A_1 e^{-t/\tau_1} + A_2 e^{-t/\tau_2} + A_3 e^{-t/\tau_3} \tag{6.1}$$

The shortest time constant τ_1 is typically in the order of 1 ns, the medium time constant τ_2 is around 4 ns and the long decay time τ_3 is in the order of 14 ns. To understand the multi-exponential nature of the fluorescence decay, three different mechanisms have to be considered:

(i) As it is evident from the spectral investigations, there are at least two different species of sf-PBI present on the LAO nanostructure: monomer-like (or Y-type) emitting molecules as well as molecules that show E-type emission. Both species possess quite different fluorescence life times, for the monomer or Y state it should be very similar to that in solution (4 ns) whereas the fluorescence life time for the E-emission of perylene crystals is in the order of 100 ns [Walk85].

(ii) An efficient excitation energy transfer is expected for dye molecules that are close

to each other (as it is the case for electrostatically bound sf-PBI) which leads to a decrease of the fluorescence life time. It has been shown that upon increase of the perylene dye concentration in LB films, there is a decrease of the life time as well as a transition from mono-exponential to a bi-exponential decay [Akim97]. This was explained by energy transfers between monomers, two different excimers as well as monomers and excimers. Also for chemically designed u-shaped PBI dimers, a double-exponential decay of the fluorescence has been found [Veld08]. Here the authors attributed this to the existence of two excited states of the dimerized PBI.

(iii) As the sf-PBI molecules on the nanostructures are separated from the underlying silicon only by the oxide height (a few nm), a very strong energy transfer between the dyes and the silicon is expected by classical electromagnetic theory [Dext79, Aliv87] that should decrease the measured fluorescence life time dramatically.

As a result of all three processes, the fluorescence decay of sf-PBI bound to the nanostructures is in average faster than in solution and possesses at least tri-exponential characteristics. In the following, the different aspects will be investigated and discussed in greater detail.

As a control experiment in order to exclude the quenching of the underlying silicon, again films of sf-PBI spincoated on silicon wafers with a 100 nm thick thermal silicon oxide layer were investigated. The fluorescence decay curves of sf-PBI films prepared from different concentrations ($1.6 \cdot 10^{-3}$ M to $1.6 \cdot 10^{-8}$ M) of sf-PBI in ethanol solution are displayed in figure 6.16. The life time investigations have been carried out parallel to the spectral investigations, so each curve at a certain concentration refers to the corresponding spectrum in figure 6.6.

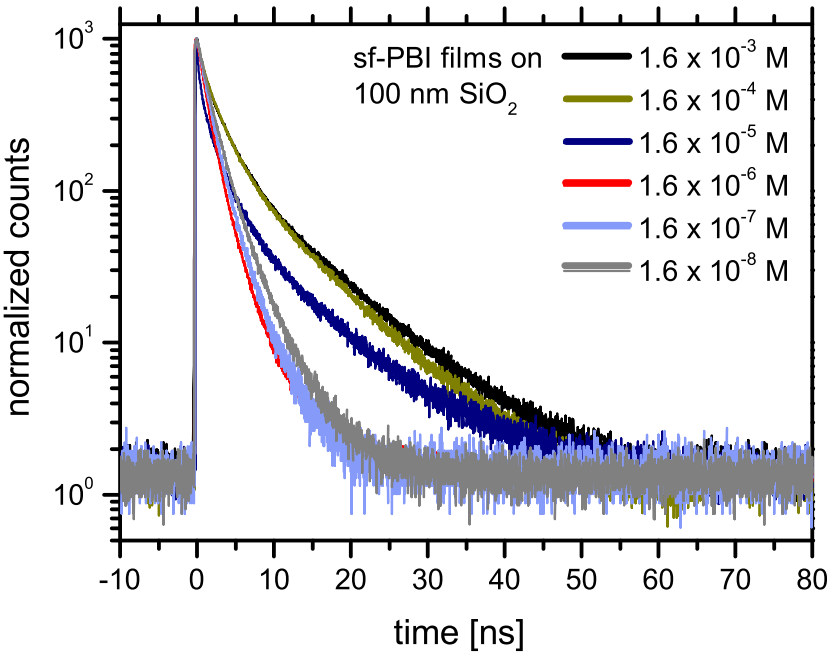

Figure 6.16: Log-lin plot of the normalized fluorescence decay of sf-PBI films on 100 nm thermal silicon oxide on silicon substrates for dye concentrations of $1.6 \cdot 10^{-8}$ M (gray), $1.6 \cdot 10^{-7}$ M (light blue), $1.6 \cdot 10^{-6}$ M (red), $1.6 \cdot 10^{-5}$ M (dark blue) $1.6 \cdot 10^{-4}$ M (yellow) and $1.6 \cdot 10^{-3}$ M (black) in the spincoated solution. The decay has been measured over the whole spectral range.

At first glance, the decay curves seem to become more and more multi-exponential with an increasing amplitude of longer time constants for an increasing concentration of sf-PBI in the spin-coating solution and therefore also on the surface. Also the general qualitative characteristics of the spectral development can be found in these curves. For µM concentrations and below, the curves are very similar to each other and can be attributed to the monomer emission (see also figure 6.6). At a concentration of 10^{-5} M, there is a transition to a stronger multi-exponential behavior of the fluorescence decay (spectrally there is a conjunction of monomer or Y-fluorescence and E-excimer spectrum) and at a concentration of 10^{-4} M and above the curves are again very similar to each other (predominant E-excimer spectrum). However, even for low concentrations the decay curves are not purely mono-exponential. The reason for this is still unclear but may be connected to differences of the dielectric environment of the dye molecules on the silicon oxide surface. In any case, the curves have been evaluated by a tri-exponential fit according to equation 6.1 which has turned out to be sufficient in order to retrace the decay sat-

isfactorily. The obtained life times and amplitudes from those fits are displayed in figure 6.17. The evaluation of the decay also confirms the conclusions from above.

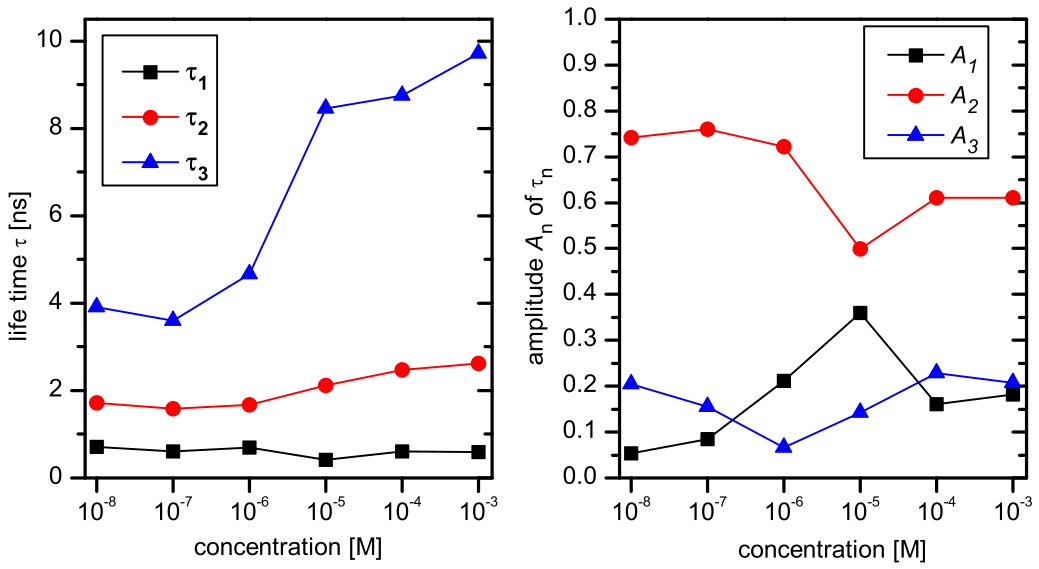

Figure 6.17: Obtained life times τ_n (left)and their respective amplitudes A_n (right) for tri-exponential fits of the fluorescence decay curves in figure 6.16 according to equation 6.1.

For concentrations above 10^{-6} M, the longest time constant increases significantly (by more than a factor of two) and also the medium decay time becomes larger. Yet there is no clear change in the amplitudes of the different decay components. The medium time constant has the strongest weighting of the three components (roughly two-thirds) and the other decay times share the remaining third. This means that though the magnitude of the three time constants changes for different concentrations, their distribution remains rather similar. As the spectral properties are changing dramatically from low concentrations (monomer emission) to high concentrations (E-type emission), it can be concluded that the mere existence of three different decay times cannot be attributed directly to the three different emissive states (monomer, Y state, E state). The multi-exponential nature of the decay seems to be a result of the system itself (sf-PBI on silicon oxide) and independent of the origin of the emission (isolated molecules, dimers or excimers). In order to unravel the origin of the multi-exponential decay as well as the correlation between spectral properties and life time, a more detailed analysis of spincoated sf-PBI films (preferentially using spectrally resolved life time measurements) would be very interesting. Especially the transition region between monomer and E-type emission (around 10^{-5} M) should be analyzed in smaller concentration intervals

as the strongest qualitative difference of the curves seems to occur here. At a concentration of 10^{-5} M a decrease of the amplitude of the long time constant and an increase of the amplitude of the shortest decay time is observed (see figure 6.17 and also figure 6.16). This may be a hint for a fast energy transfer between monomer sf-PBI molecules and aggregates that coexist on the surface at this concentration.
As a next step, the quenching of the underlying silicon has been the subject of investigation. Therefore, LAO line structures with a different height have been prepared followed by binding of sf-PBI and investigation by time-resolved fluorescence microscopy. The results of these investigations are displayed in figure 6.18.

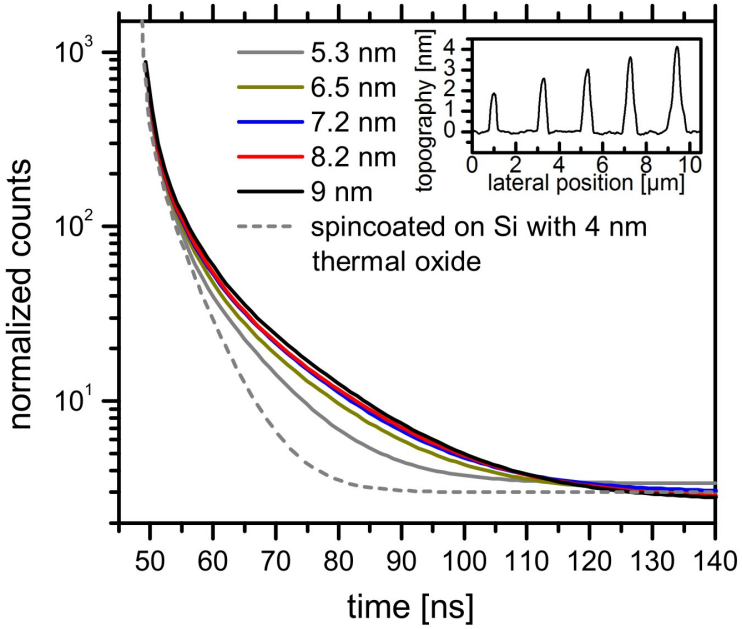

Figure 6.18: Log-lin plot of the normalized tri-exponential fluorescence decay fits of the decay curves of sf-PBI bound to LAO nanostructures with different thickness ranging from 5.3 to 9 nm (solid curves) and spincoated from a $1.6 \cdot 10^{-5}$ M solution on silicon with a 4 nm thermal oxide layer (dashed curve). The decay has been measured over the whole spectral range. The inset shows an AFM height profile of the used LAO line structures. Note that the oxide height is larger than the detected topographic height as 40% of the LAO oxide is below the silicon surface and the self-assembled monolayer leads to an additional virtual decrease of the height. For details see chapter 6.1.

As the measurement exhibits a rather low signal-to-noise-ratio, differences between the curves are small (the oxide height can be adjusted only in a rather narrow win-

dow). Therefore, not the measured data is displayed but the tri-exponential fits of the curves. The inset in figure 6.18 shows also the AFM profile of the line structures. To exclude local difference within the oxide lines, several measurements on different spots on each line have been performed and the fluorescence decay curves have been averaged for each line. The obtained parameters from the tri-exponential fits for different oxide thickness are displayed in figure 6.19. All three

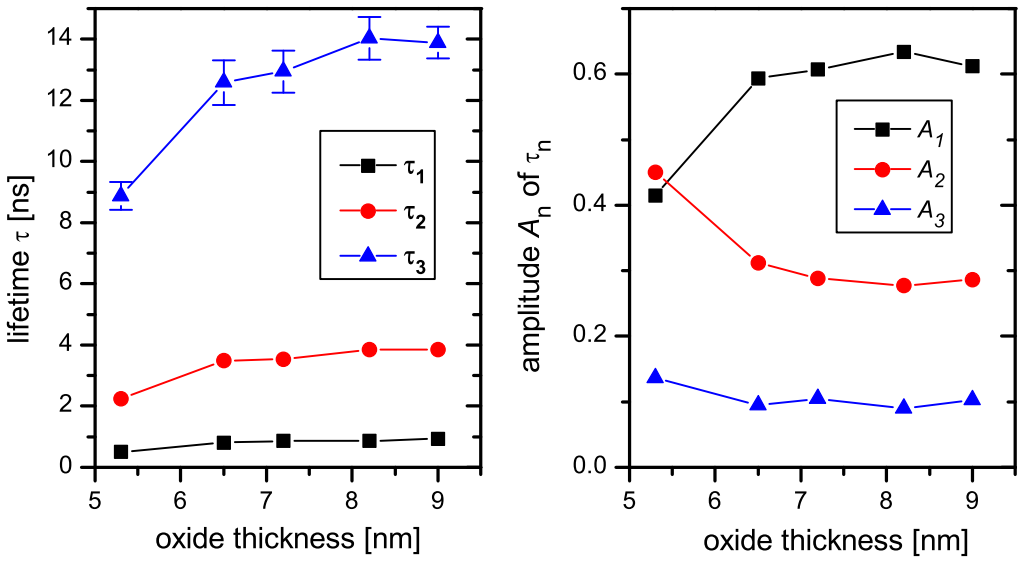

Figure 6.19: Obtained excited state life times τ_n and their respective amplitudes A_n for tri-exponential fits according to equation 6.1 of the fluorescence decay curves of bound sf-PBI depending on the oxide thickness.

life time components are becoming larger for an increasing oxide thickness. This is just as expected because the energy transfer between excited molecules and the underlying silicon depends strongly on their distance [Aliv87]. Therefore also the shortest life time component possesses the largest amplitude in contrast to the sf-PBI films on 100 nm oxide. To get a more quantitative analysis of the quenching, the evaluated data was compared with predictions from a theoretical model.
The energy transfer rate between excited molecules and a metal or semiconductor surfaces and the consequential lowering of the fluorescence life time has been described by several classical and quantum mechanical approaches [Chan78, Chan76, Pers82, Stav85]. Briefly, those models generally regard an electronically excited molecule as oscillating point dipole, separated by a spacer with a certain thickness d from the acceptor medium (see figure 6.20). The dipole field incident on the acceptor is partially reflected and partially absorbed in a manner governed by the dielectric constant ε of the involved media. Thus the imaginary part of the electric

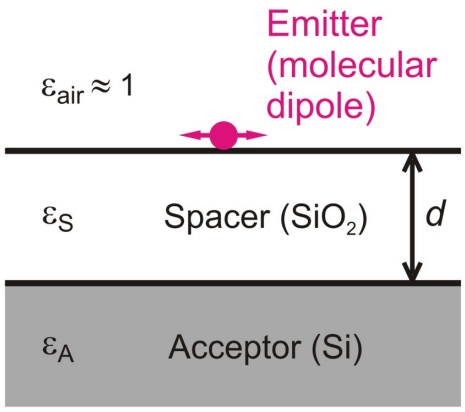

Figure 6.20: Schematic geometry relevant for molecule-semiconductor or metal energy transfer. The εs denote the complex dielectric constants of the involved media.

field at the dipole can be related to the life time of the molecule. In general, such models yield to the result that the fluorescence life time is related to the spacer thickness d by a d^{-4}-dependency in the case of metal acceptor substrates or a d^{-3}-relation in the case of a semiconductor respectively. Several experimental studies of distance dependent lowering of the fluorescence life time through molecule-semiconductor energy transfer have found a good agreement with a simple cubic relation in the form of equation 6.2 [Sluc95, Haya83, Dano08].

$$\tau_d = \frac{\tau_0}{1 + (d_0/d)^3} \tag{6.2}$$

Here τ_d is the distance dependent life time, τ_0 is the 'free' life time of the emitter without the presence of the acceptor and d_0 is the critical transfer distance where the rate constant for the energy transfer is equal to that for fluorescence of the molecule in absence of the acceptor. However, the d^{-3}-relation in this form is too arbitrary in order to be compared to the obtained data points as there is no information about the value of d_0 which would remain a fitting parameter which is hardly assessable. Therefore, a more fundamental model has been used to compare the experimental results with the theoretically expected behavior. The employed theory has been established by Persson and co-workers [Pers78, Pers80, Pers82, Avou84] and was already used by other groups to evaluate the distance dependency of the fluorescence life time of rhodamine 6G on aluminum [Cnos93] and rhodamine B on silicon substrates [Ishi98]. In this theory, the excited state life time $\tau_d(d)$ of an

oscillating dipole at a small ($kd \ll 1$) distance above a metal surface is given by:

$$\tau_d^{-1}(d) = \tau_\infty^{-1}\left\{1 + \frac{\eta}{8}(dk)^{-3}\left[2\mathbf{Im}\left(\frac{\varepsilon_A(\omega)-\varepsilon_1}{\varepsilon_A(\omega)+\varepsilon_1}\right) + 6\xi\frac{1}{k_F d}\frac{\omega}{\omega_p} + 18\frac{\omega_F}{\omega_p}\frac{\omega}{\omega_p}\frac{1}{k_F d}\right]\right\} \tag{6.3}$$

where τ_∞ is the fluorescence life time at an infinite distance from the acceptor, k is the magnitude of the wave vector at the emitted frequency ω, $\varepsilon_A(\omega)$ is the complex dielectric constant of the acceptor medium, ε_1 is the dielectric constant of the medium in which the dipole is embedded, η is an orientational parameter, k_F is the Fermi wave vector of the electron gas, ω_F the Fermi frequency, ω_p is the plasma frequency and ξ a constant which depends on the electron gas density. The last two terms in the square brackets contain electron-gas parameters and for very small molecule-surface separations ($d < 5$ nm) those terms are dominant and cause the d^{-4}-dependency in the case of nearly free-electron-like metals [Cnos93]. The first term is describes the bulk scattering contribution to the dampening of the emissive rate and shows a d^{-3}-dependence. A derivation and detailed discussion of the different terms in equation 6.3 is beyond the scope of this thesis and can be found in the mentioned literature [Pers78, Pers80, Pers82, Avou84]. As the thickness of the LAO nanostructures is above 5 nm and the substrate is not a metal with a free electron gas but a semiconductor, only the first term is important for the following analysis and consequently the last two terms in equation 6.3 can be omitted [Ishi98]. Thus equation 6.3 simplifies to:

$$\tau_d^{-1}(d) = \tau_\infty^{-1}\left\{1 + \frac{\eta}{8}(dk)^{-3}\left[2\mathbf{Im}\left(\frac{\varepsilon_A(\omega)-\varepsilon_1}{\varepsilon_A(\omega)+\varepsilon_1}\right)\right]\right\} \tag{6.4}$$

For the involved parameters, the following values can be assumed: As the sf-PBI molecules are most likely oriented in parallel fashion to the substrate, the orientational parameter η is 0.75 [Cnos93]. The complex dielectric constant of the acceptor is a function of the energy of the dipole radiation. Unfortunately, the spectrum of the sf-PBI emission is rather wide, so there is no discrete dipole energy. For a coarse approximation, an energy of 1.91 eV ($\approx$ 650 nm) was assumed, as this is roughly the maximum position of the dominant E-type emission. The imaginary part of ε_A of weakly doped silicon is about 0.126 for this energy [Aspn83]. In equation 6.3 and 6.4, ε_1 denotes the dielectric constant of the medium that surrounds the dipole. As the dipole is situated at the interface between silicon oxide ($\varepsilon_{Si} \approx 2.1$ [Phil71]) and air ($\varepsilon_{air} \approx 1$), theoretical curves have been calculated for both values as limiting cases of ε_1. Values for τ_∞ have been taken from the investigations of sf-PBI films on 100 nm oxide at a concentration of 10^{-5} M (see figure 6.17). For these films the quenching by the underlying silicon is negligible because for spacer thicknesses above 40 nm, there is nearly no influence of the substrate [Sluc95, Aliv87]. The determined theoretical curves for the long life time

($\tau_\infty = 8.46$ ns [1] and the medium life time $\tau_\infty = 2.12$ ns [1] are displayed in figure 6.21 together with the measured values from figure 6.19. Evidently, the distance-

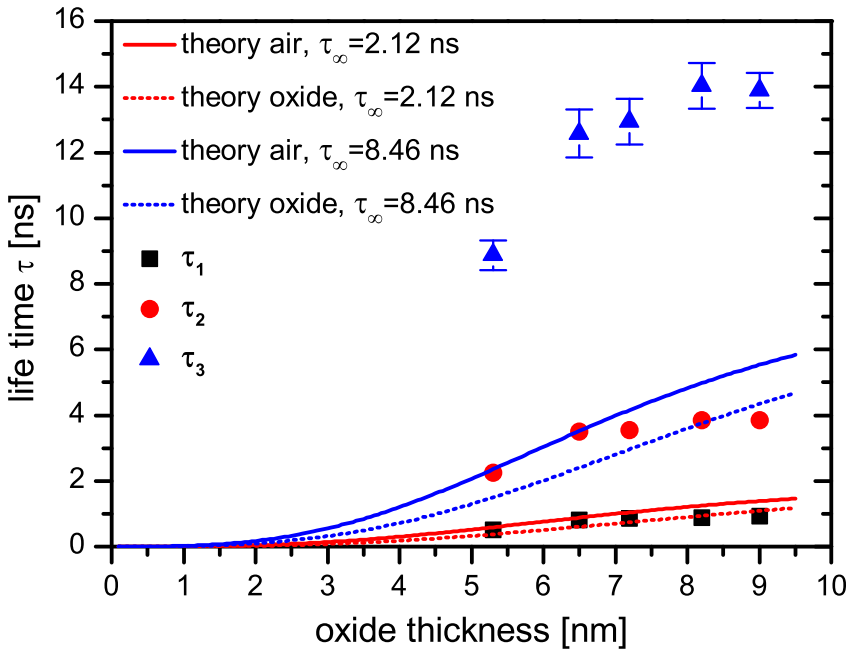

Figure 6.21: Fluorescence life times of sf-PBI for different LAO oxide thickness from figure 6.19 compared to the theoretically expected curves according to equation 6.4 for different free life times τ_∞ and surrounding media.

dependence of the middle time constant τ_2 and the short time constant τ_1 of sf-PBI on the nanostructures corresponds to the long (8.46 ns) and the middle (2.12 ns) time constant of the emission in absence of the quenching substrate. The shortest decay component (0.4 ns) of the sf-PBI film emission on 100 nm oxide is likely to be quenched below the detection limit and is not observable anymore. However, the existence of the third time constant τ_3 is completely unexpected. As it is even larger than the long decay component of the films far away from the silicon, it would be related to a substantially slower decay which is only present for sf-PBI bound to the LAO structures. However, the relatively low amplitude (≈ 0.1; see figure 6.19) of this long component makes such a conclusion arguable. Although the theoretical curves show a reasonable agreement with the measured decay times, an examination of the decay times for oxide thicknesses over several magnitudes would be necessary in order to provide a verifiable survey of the model. Since the controlled LAO oxide thickness is limited to one order of magnitude at the most,

[1] value from figure 6.17, 10^{-5} M

such an investigation is unfortunately not possible with the investigated systems. Furthermore, there are many factors that provide a certain scope for uncertainties. First of all, the theoretical model was derived for a single emitter on a flat and infinite dielectric surface. The LAO oxide surface on the other hand is laterally confined and the molecules are packed densely on it. The oligomerization of the sf-PBI molecules, as evident from the spectral investigations, and a possible energy transfer between them may further influence the true distance dependency of the quenching by the silicon substrate. As mentioned above, the model has been derived for a dipole which is isotropically surrounded by the dielectric medium with ε_1. In the present experimental case, the sf-PBI molecules are located at the silicon oxide/air interface. This has been tried to be accounted for by the calculation for both ideal cases and the measured values are indeed mostly within the intermediate region of both curves. Nevertheless, possibly occurring surface effects that are not included in the calculations may lead to a deviation from the pure d^{-3}-dependence. Last but not least equation 6.4 is only valid for a dipole with a discrete energy. The emission spectrum of sf-PBI on the LAO nanostructures is rather wide though. This means that the influence of the underlying silicon on the dampening of the emissive rate should also have a rather broad distribution. In figure 6.18, also the fluorescence decay fit of a sf-PBI film spincoated from a $1.6 \cdot 10^{-5}$ M solution on silicon with a 4 nm thermal oxide layer is displayed (dashed curve). As expected, the fluorescence decay is faster than for the 5.3 nm LAO nanostructure (especially the long time component has a smaller amplitude and is shorter). A spectrally correlated life time measurement would be very helpful in order to assign the different life time components to different spectral features or emissive states. Unfortunately, this was not possible with the available equipment. Instead a different sample has been investigated time-resolved while separating the fluorescence emission into two regions by utilizing a 570 nm short pass (SP) filter and a 585 nm long pass (LP) filter (see figure 6.22). Figure 6.23 shows the normalized fluorescence decay curves for both spectral regimes. Again, the decay can only be fitted satisfactorily by using a tri-exponential function in the form of equation 6.1. The obtained fit parameters are given in table 6.1.

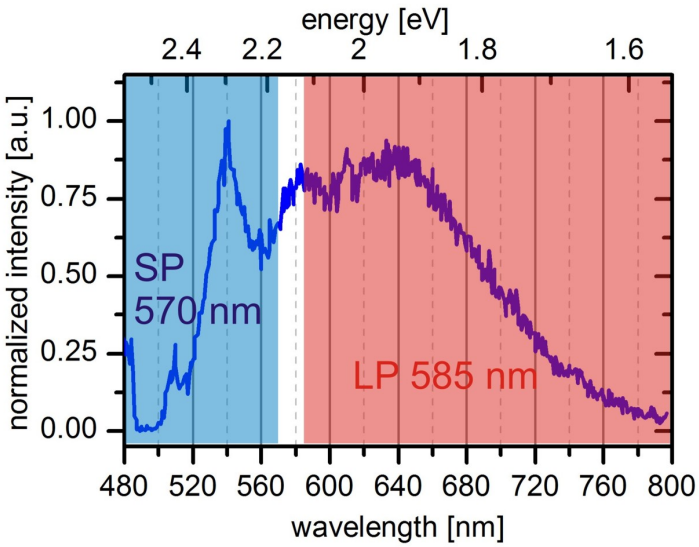

Figure 6.22: Spectral partition of the sf-PBI emission on the nanostructures by a 570 nm short pass (SP) and a 585 nm long pass (LP) filter.

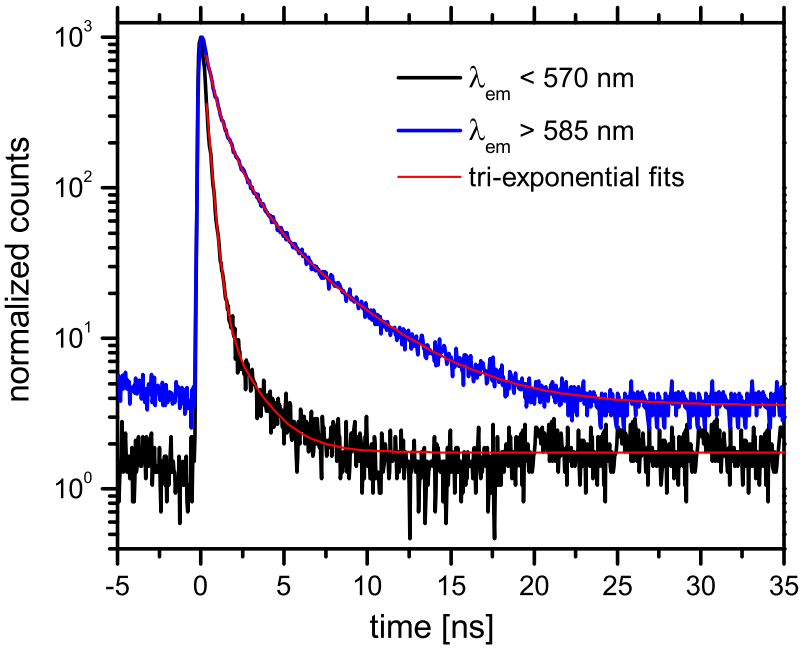

Figure 6.23: Decay curves and tri-exponential fits (red) of the fluorescence emission below 570 nm (black) and above 585 nm (blue) of sf-PBI bound to a LAO nanostructure.

The fluorescence emission below 570 nm, which is attributed mostly to the monomer-like emission, is dominated mainly by a very short decay time constant of 0.32 ns. This can be understood in terms of a quenching by an energy transfer to the underlying silicon as well as to the close-by dye aggregates or monomers. Consequently, the already short life time component of the monomers is further decreased. It should be mentioned that the short life time for this regime ($\tau_1 = 0.11$ ns) is below the temporal resolution of the detector (IRF-width $\approx$200 ps) and therefore should not be regarded as 'real' value. The emission above 585 nm consists to nearly equal parts of the two decay components 0.43 ns and 1.22 ns. From that as well as the visual impression of the decay curves in figure 6.23 it can be concluded that even for a close proximity to the silicon, the E-emissive states are significantly longer-lived than the monomer-like sf-PBI molecules as it was already indicated by the temporal investigations of sf-PBI films on 100 nm silicon oxide. Furthermore, it seems that the fluorescence decay of the monomers possess a rather mono-exponential character whereas the E-type excimers show a broader distribution of life times.

Table 6.1: Life times τ_n and relative amplitudes A_n of the decay components of the tri-exponential fits in figure 6.23.

	short component		medium component		long component	
spectral regime	τ_1/ns	A_1	τ_2/ns	A_2	τ_3/ns	A_3
$<$ 570 nm (monomer/Y state)	0.11	16.5%	0.32	80%	1.68	3.5%
$>$ 585 nm (E-excimer)	0.43	43.7%	1.22	42.7%	4.23	13.6%

In summary, all measurements show that the fluorescence decay of sf-PBI bound to LAO nanostructures is clearly multi-exponential. This may be partly caused by energy transfer between the different species and/or states on the structure (monomers, dimers). A theoretically expected dependency of the emissive rate dampening on the dipole energy further enhances the multi-exponential character. The broad spectral and decay time distributions indicate that there is a multitude of different involved molecular states which may be understood in terms of a configurational disorder within the electrostatically assembled sf-PBI films. Such an assumption is also substantiated by the observation that for different samples with comparable LAO oxide height but different preparation conditions (LAO oxidation parameters, immersion time in the dye solution) the measured decay times differ slightly. The

investigation of the influence of different preparation and system parameters on the decay characteristics with a high spectral resolution would be very beneficial for a deeper understanding of the true nature behind the assembly of sf-PBI on local anodic oxide nanostructures. Time resolved experiments at low temperatures may also help to further unravel the aggregation behavior. It should also be mentioned that in the course of the sf-PBI investigations, experiments have not only been conducted on pure silicon samples but also on SOI (silicon on insulator) substrates. The used SOI wafers consist of three layers. The two bottom layers are just like a usual 500 µm thick silicon wafer with a 100 nm thermal silicon oxide layer. On top of the silicon oxide a third layer is deposited which is again silicon. This layer is only 27 nm thick. The question was whether the local anodic oxidation and dye binding techniques known from pure silicon substrates can also be performed on this type of substrate. This may be especially interesting since the thickness of the underlying silicon layer should also have an impact on the quenching of the emitters bound to the LAO structures. The obtained results of the experiments on SOI are briefly discussed in the following passage. First of all, the alkyl-monolayer termination and following local anodic oxidation of SOI substrates was possible in principle. However, the fabrication of smooth and homogeneous structures turned out to be much more difficult than in the case of pure silicon substrates. This is likely to be caused by difficulties with the electric contacting of the substrate. The 100 nm thick insulating silicon oxide middle layer prevents a direct contact between the bottom of the substrate and the top silicon layer. Therefore, a contacting of top layer by using conductive silver paint has been employed. Nevertheless, much higher voltages are needed to perform the LAO compared to pure silicon samples. Using AC instead of a DC voltage has been found to improve the oxidation result significantly. However, the LAO lithographic structures on SOI substrates are much wider compared to those on pure Si, which is ascribed to a dispersion of the electric field between substrate and AFM tip due to the dielectric spacer. It was also possible to functionalize the structures by electrostatic binding of sf-PBI molecules. Contrary to expectations, however, the decay characteristics of sf-PBI on LAO nanostructures on SOI substrates did not show fundamental differences compared to those on pure silicon. Obviously, even the 27 nm silicon layer is sufficient for an effective quenching of the fluorescence and cannot be distinguished from bulk material. Also the spectral fluorescence properties are very similar to that for sf-PBI functionalized nanostructures on pure silicon. Considering the greater difficulties and lower controllability of LAO on SOI substrates, no systematic investigations with this type of substrates have been performed.

6.4 Conclusions

It could be demonstrated that a functionalization of LAO nanostructures with sf-PBI molecules by electrostatic binding is possible in a reproducible and easily feasible manner. Spectral and time-resolved investigation reveal that the fluorescence emission of such structures can in principle be compared to that of thin films prepared by spin-coating on silicon substrates. The fluorescence spectra of the sf-PBI-functionalized structures are a combination of an emission similar to that of sf-PBI monomers as well as E-type excimer luminescence. Obviously, some of the emitters exist in a state which is similar to the electronic configuration of monomeric sf-PBI molecules whereas others are able to relax into an E-type excimer geometry. The electrostatic binding itself seems to have an influence on the low-temperature behavior of the electronic and structural excimer kinetics. For sf-PBI bound to LAO nanostructures there was a strong decrease of the E-emission while cooling the sample to low temperatures whereas such a phenomenon could not be observed for the spincoated sf-PBI thin films. Even after heating the sample up to room temperature, it required days until the E-emission recovered to its initial value. Furthermore, there seems to be a certain aging of the sample which means that the ratio between monomeric peak and excimer peak in the emission spectrum depends not only on the preparation conditions but also changes over time. This may be understood in terms of a motional constriction due to the electrostatic forces that bind the sf-PBI molecules to the local anodic oxide surface. However, further studies of this temporal and temperature dependency as well as molecular dynamic simulations would be very interesting in order to explain the observed phenomena in detail. The decay process of the excited state has been found to be at least tri-exponential, both for the dense spincoated films as well as for the dye bound to LAO oxide. The multi-exponential nature seems to increase for the E-excimer part of the spectrum compared to the monomer-like emission. This can be explained by the fact that the excimer formation is influenced strongly by the steric situation of the molecules on the surface which is very likely rather inhomogeneous, especially for the electrostatically bound sf-PBI molecules. As expected, the excimers possess a larger life time than the sf-PBI monomers. The theoretically expected influence of close-by bulk silicon on the dampening of the emissive rate shows a satisfactory agreement with the experimental data. Also, the investigations of the fluorescence decay should not be regarded as fully concluded as they raise new and interesting questions. Especially fluorescence life time experiments at low temperatures and with spectral sampling would be very beneficial for a deeper understanding of the invoked processes and with theoretical models may also give insight into the interplay between conformation and electronic structure of the bound perylenes.

Acknowledgement

The authors are grateful to the Deutsche Forschungsgemeinschaft (DFG, GR 2695/4) for financial support and Prof. F. Würthner for the courtsey of providing the spermine-functionalized PBI molecules.

7 Covalent binding of a fluorescein dye using amino linkers

Abstract

This study investigates the controlled chemical functionalization of silicon oxide nanostructures prepared by AFM-anodization lithography of silicon terminated with organic monolayers. Different conditions for the growth of covalently bound mono-, multi-or sub-monolayers of distinctively functional silane molecules on the nanostructures have been identified using AFM-height investigations. Several routes for the preparation of methyl- or amino-terminated structures or silicon surfaces are presented and discussed. The formation of silane monolayers on nanoscopic silicon oxide nanostructures was found to be much more sensitive towards ambient humidity as e.g. silanization of larger OH-terminated silica surfaces. Amino-functionalized nanostructures have been successfully modified by covalent binding of functional fluorescein dye molecules. Upon excitation, the dye-functionalized structures show only weak fluorescence, which may be a hint for a relatively low surface coverage of the dye molecules on length scale which is not accessible by standard AFM measurements.

The content of this chapter is planned for publication:
T. Baumgärtel, C. v. Borczyskowski, M. Ara, H. Tada and H. Graaf: to be submitted

7.1 Introduction

A covalent binding of the functional molecules is superior to other attachment mechanisms in many aspects, as covalent bonds are much more stable and allow for surface functionalization in multiple steps (see also chapter 2). A direct binding of the functional material to the oxide nanostructure is possible if the material possesses an appropriate anchoring group that binds selectively to silicon oxide surfaces. Synthesis of e.g. a perylene unit with such an anchoring group is possible but not trivial. Therefore, only materials which are commercially available have been used for this part of the thesis. A standard material for chemical modification of silicon oxide surfaces are silane compounds such as trichlorosilanes or ethoxysilanes [Sagi80, Howa06]. In order to provide the possibility for further chemical modification by click chemistry, functional silanes are of major interest. Those molecules possess a functional head-group (e.g. carboxyl, amino or thiol group) in addition to the silane tail group. This functional head group can react with other molecules resulting in an immobilization of the desired material on the structure with the silane molecule as linker. The binding of diverse silanes to silicon oxide surfaces has been subject of several investigations [Ulma96, Fade00, Desb11]. A functionalization of an LAO nanostructure on the other hand, has so far not been investigated in detail. Ara *et al.* reported binding of octadecyl-trichlorosilane to an LAO structure, however, they only found a height increase of about 0.4 nm which indicates only a partial coverage (the molecules are not densely packed) [Ara02a]. In a diploma thesis [Viel06], Vieluf detected a height increase after exposing the nanostructures to a functional silane, yet the height increase was rather non-uniform and the AFM image acquisition parameters (used tip, setpoint) may have varied between the measurements.
This section will cover the covalent modification of the nanostructures with functional silane molecules and the successive binding of fluorescein-5-isothiocyanate (FITC) to amino-terminated silanes on the LAO oxide only. Several other attempts using different routes such as thiol-metal reactions to immobilize semiconductor nanocrystals or peptide bonding have been tested too but yielded a negative outcome. FITC is a fluorescein derivative with a N=C=S functional group. This group is reactive towards nucleophiles such as amine or thiol groups. This is e.g. used to bind the dye to proteins that possess such groups, and this way label them selectively. The attachment of FITC on the oxide nanostructures is realized in two steps, as depicted schematically in figure 7.1. First, the functional silane aminopropyltriethoxysilane (APTES) is bound to the LAO oxide which leads to an amino-functionalization of the structure. In a second step, FITC is introduced to the surface and binds with the N=C=S group to the amino group on the structure. As a first preliminary investigation, however, the focus was not on the immobilization

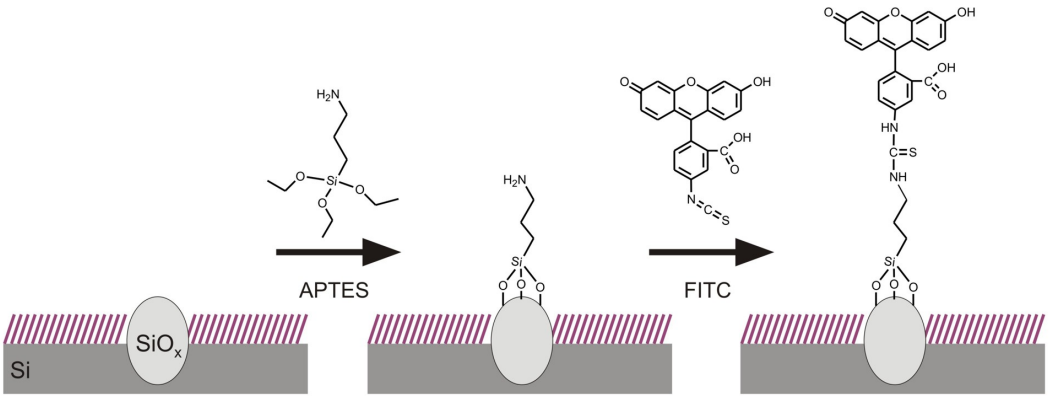

Figure 7.1: General route for covalent binding of FITC to a silicon oxide nanostructure on alkyl-terminated silicon via APTES linker.

of FITC on the LAO nanostructure but on a whole amino-functionalized silicon surface. These experiments have been conducted during a visit at the laboratory of Prof. H. Tada at Osaka University, Japan. The Tada laboratory has previously developed a chemical route in order to prepare amino-terminated alkyl monolayers on a silicon surface which was confirmed by IR spectroscopy [Ara07]. They also demonstrated the attachment of FITC to such a surface by fluorescence measurements [Tada03]. The measured fluorescence intensity on the other hand was very weak which can be attributed to a strong luminescence quenching by the underlying silicon and the fluorescence spectrum did not allow for a clear assignment to FITC emission. Therefore, comparative AFM measurements with local anodic oxide as absolute height mark have been conducted.

7.2 Experimental

7.2.1 FITC monolayers on silicon(111)

Prior to the monolayer formation the n-type silicon(111) substrates with a resistivity of (1-10) Ωcm have been cleaned by a very careful procedure. First, organic residues have been removed by ultrasonic baths in acetone and propanol for 5 minutes. Subsequently, the native oxide was etched with a 5% hydrofluoric acid solution and the sample was cleaned and oxidized again for 30 minutes in a 3:2 mixture of sulfuric acid and hydrogen peroxide ('piranha-solution'). Finally, the

oxide was removed by anisotropic etching for 40 minutes in a 40% NH_4F solution and a hydrogen-terminated silicon(111) surface was obtained. To prepare amino-terminated monolayers, the etched samples have been transferred into a 1 M solution of N-Vinylphthalimide (Sigma Aldrich) in mesitylene at room temperature for 24 hours. After removal from the solution, the sample has been ultrasonicated in dichloromethane and propanol as well as rinsed with ultrapure water in order to remove any physical adsorbates. Hydrolysis of the phthalimide group was carried out by immersion in a 40% aqueous solution of methylamine for 1 hour and subsequent rinsing with tri-ethylamine. The binding of FITC (Sigma Aldrich) has been performed by immersion of the sample in a 0.5 M solution of FITC in H_2O for 1 hour and subsequent repeated rinsing with ultrapure water. A "JSPM-5200" AFM (Joel, Japan) has been used for topography investigations as well as structuring of the samples. The microscope was operated in contact mode for the LAO experiments and non-contact mode for topography investigations. Ti-Pt coated AFM tips with a resonance frequency of 70 kHz have been used as probes ("NSC36", Mikromash, Estonia).

7.2.2 Silanization and functionalization of LAO nanostructures

Local anodic oxidation and AFM topography measurements have been carried out as described in 6.2 and 6.3.1. Binding of OTS (octadecyl-trichlorosilane) and other trichlorosilanes (ABCR, Germany) has been carried out by immersion of the structured into a 10 mM solution of the silane in toluene (spectroscopic grade, Merck). After a specific amount of time, the sample was removed from the solution and rinsed thoroughly in ultrasonic baths of toluene, dichloromethane and ethanol (all: spectroscopic grade, Merck). APTES (aminopropyltriethoxysilane, Sigma Aldrich) was bound by immersion under the same conditions and preparation steps as the trichlorosilanes. For sparging of the silane / toluene solutions, argon has been used as inert gas. Binding of FITC to the APTES-functionalized structures was achieved by immersion of the samples in a low mM solution of FITC in acetone (spectroscopic grade, Merck) for 90 minutes and subsequent cleaning in ultrasonic baths of acetone, dichloromethane and ethanol. Optical investigations of the samples have been performed with the SSCM setup described in chapter 3.

7.3 Results and Discussion

7.3.1 FITC monolayers on silicon

Amino-terminated alkyl monolayers on Si(111) substrates have been prepared as proposed by Ara *et al.* [Ara07]. A direct reaction of amino-terminated alkene molecules to a hydrogen-terminated silicon surface is not possible in a controlled manner as not only the double bond but also the amino groups are reactive towards the silicon [Bitz96]. To avoid such a binding the amino group has to be rendered inert with a protective group. Figure 7.2 shows the used route: first, vinylphthalimide is bound to the Si-H surface which results in a vinylphthalimide monolayer. In a next step, the phthalimide is hydrolyzed using methylamine, leading to an amino-terminated monolayer on silicon. At last, FITC is bound to the amino groups and a FITC-monolayer is obtained.

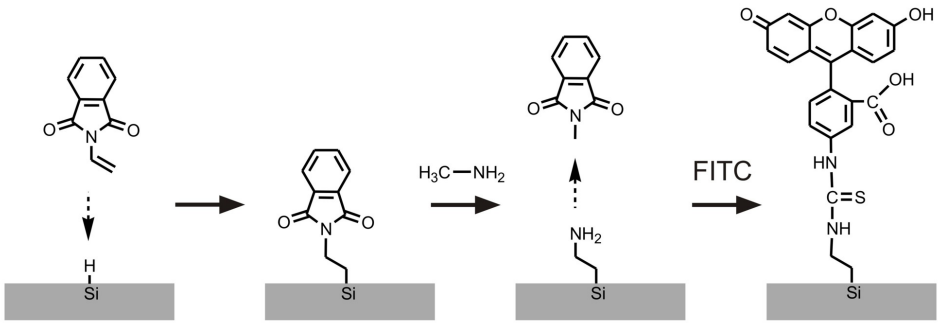

Figure 7.2: Covalent binding of FITC to a silicon surface via amino functionalized alkenes.

An AFM image of a hydrogen-terminated silicon surface is displayed in figure 7.3A. Clearly visible terraces with a monotonic step height of 3 Å are typical for the Si(111) surface which has been etched anisotropically by NH_4F [Flid99, Fu03]. After the formation of a vinylphthalimide monolayer on the surface (figure 7.3B), the image is considerably blurred. Though single terraces are still distinguishable, their edges are not as sharp as for the Si-H surface. This effect may be due to two main reasons: First of all, the carbonyl groups possess a negative partial charge resulting in an effective repulsion between these groups of neighboring molecules. Thus the vinylphthalimide molecules may not arrange in a monolayer as densely packed and uniform as e.g. alkyl chains due to the molecular geometry. This leads

to a slight increase in surface roughness and the underlying surface structure (terraces) is blurred. Secondly, the vinylphthalimide surface is much more hydrophilic (water contact angle below 10°) compared to the H-Si surface (water contact angle 110°). Since the AFM measurements have been conducted under ambient condi-

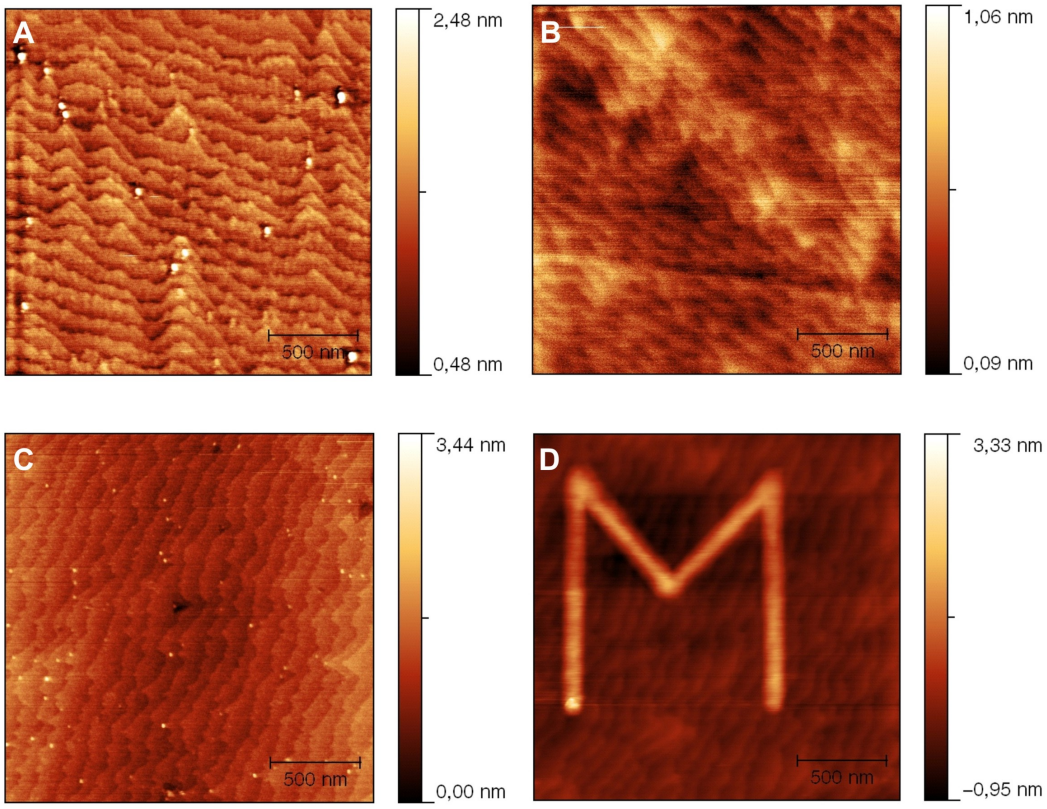

Figure 7.3: NC-AFM images of a Si(111) surface after different chemical modifications. **A:** Si-H surface after anisotropic etching. **B:** After binding of vinylphthalimide **C:** amino-terminated surface after hydrolysis of phthalimide **D:** LAO nanostructure on the vinylphthalimide-terminated silicon.

tions, humidity from the surrounding air will condensate on the surface and form a water layer especially on the hydrophilic vinylphthalimide surface. The surface water leads to a damping of the AFM cantilever oscillation whenever the tip is close to the surface and thus decreases the imaging resolution due to a decrease of the Q-factor (similar to measurements in liquids [Hans94]). After hydrolysis of the phthalimide, again clearly visible and sharp edged terraces are observed (figure 7.3C). As the residual amino-terminated hydrocarbon chain is relatively short, the underlying surface structure is not concealed as much as in the case of vinylphthalimide termination. Furthermore, the contact angle of the amino surface became

significantly larger (about 60°) which is in agreement with previously reported values [Hozu01]. As AFM measurements of the uniformly covered surface only provide such indirect insight in the binding or unbinding of different species, an LAO oxide structure has been implemented as a height mark. Local anodic oxidation of vinylphthalimide-terminated silicon is possible and an exemplarily structure is shown in figure 7.3D. Analogous to LAO on alkyl-terminated silicon, the vinylphthalimide monolayer is first degraded and then the underlying silicon is oxidized resulting in a silicon oxide structure. The general measurement principle is depicted in figure 7.4. After the generation of a local oxide structure (figure 7.4B), the hydrolysis of the phthalimide leads to a height increase of the structure when measured via AFM as the rest of the surface lowers (figure 7.4C). In turn, the subsequent binding of FITC leads to a decrease in height (figure 7.4D). Four oxide

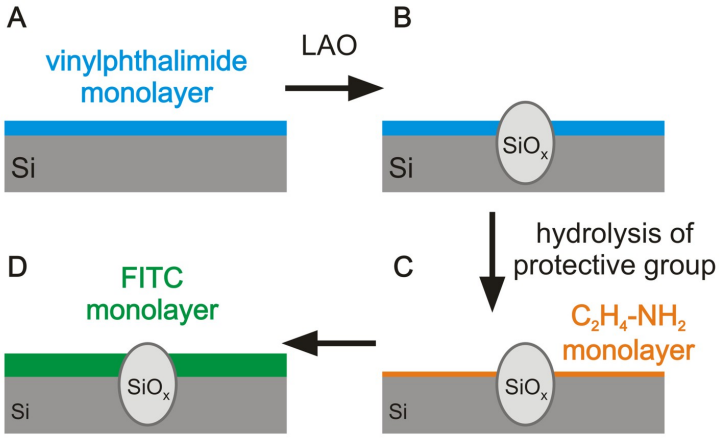

Figure 7.4: Comparative topography measurements using local anodic oxide as a height mark. **A:** vinylphthalimide monolayer on silicon **B:** after local oxidation **C:** amino-terminated monolayer after hydrolysis of phthalimide **D:** attachment of FITC.

lines with different height have been created. The line profiles measured from the AFM images after each stage are displayed in figure 7.5. The irregular appearance of some curves may be the result of the uneven silicon substrate (terraces) and residual contaminations on the AFM tip after LAO. For a better comparability of the height images (maintaining a similar sample-tip interaction, driving frequency and Q-factor), all AFM images have been measured with the same tip, though it may have been contaminated. The initial height of the oxide structures above the vinylphthalimide surface is about 1.9 nm for the largest line and about 0.5 nm for the smallest one (black curve). As expected, after hydrolysis of the phthalimide there is a relative height increase (red curve). However, the absolute value of this increase is about (1.5 ± 0.5) nm which is more than twice the length of a phthalim-

ide molecule (about 0.6 nm). After the binding of FITC to the surface (blue curve), the relative oxide height decreases about (2 ± 1) nm. This is also about twice the height of an upright standing FITC molecule (ca. 1 nm). It is unlikely that the deviation from the expected height variations are caused by the formation of multilayer since the functional molecules possess only one binding site and the sample has been washed thoroughly multiple times in an ultrasonic bath with different organic solvents. Seemingly, the influence of the different surface terminations on the tip-sample interaction and/or the water adsorption layer on the surface has such a strong influence on the measured height. Another unexpected peculiarity is that the relative height variation depends also on the absolute oxide height. For higher oxide nanostructures the increase or decrease is larger than for smaller structures. This may be a result of the double tip. When scanning over the oxide structure, the second peak of the AFM tip is still above the hydrophilic vinylphthalimide or FITC surface which influences the cantilever oscillation. The higher the oxide, the farther away is this second peak from the surface and the weaker is its influence on the cantilever oscillation. Though the absolute height values from this measurement are most likely not accurate due to the double tip and the influence of the different tip-surface interactions, the qualitative results confirm the hydrolysis of phthalimide as well as the binding of FITC.

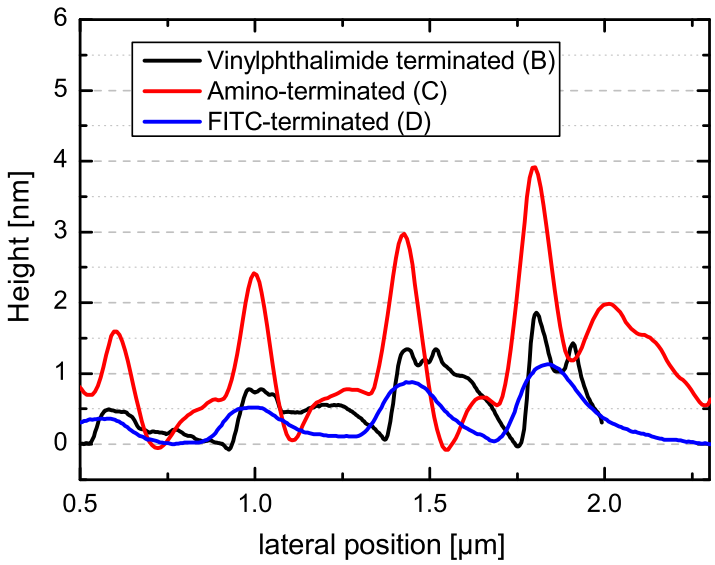

Figure 7.5: NC-AFM topography profiles of four LAO oxide lines after generation on a vinylphthalimide-terminated silicon surface (black), on the amino-terminated surface after hydrolysis of phthalimide (red) and after binding of FITC (blue). The profiles have been measured perpendicular to the line direction and averaged over a width of 20 pixels.

7.3.2 Successful routes towards silane functionalization of nanostructures

After the binding of FITC to amino-terminated silicon surfaces has been proved, a suitable route had to be found for the functionalization of LAO oxide with amino groups by selective binding of APTES. For a better evaluation of the AFM height measurements, octadecyl-trichlorosilane (OTS) was used for the first experiments because of the larger molecular length. Furthermore, under suitable conditions, OTS molecules tend to assemble into densely packed monolayers on silicon oxide surfaces [Mirj06]. Figure 7.6 shows the NC-AFM images of a square oxide structure before (A) and after (B) 40 h in a 10 mM OTS solution in toluene under ambient conditions. After the OTS treatment, the measured structure height increases from about 2 nm up to 50 nm (figure 7.6D and 7.6E). Additionally this increase is very nonuniform: there is a formation of clusters of different height (figure 7.6E and 7.6C) and the RMS roughness on the structure increases more than one order of magnitude (0.5 to 10). As the height increase is much larger than the chain length of an OTS molecule (2.6 nm), OTS is not forming closed monolayers on the nanostructure (figure 7.7A) but rather a vertical or 3D polymerization of OTS has to be assumed (figure 7.7B). Such a vertical polymerization is known for tri- and di-functional silanes, especially alkoxysilanes and alkylchlorosilanes [Fade00, Bran93, Plue91] under certain conditions. In order to understand why the 3D polymerization is preferred to the monolayer formation on the LAO structure under ambient conditions, one has to go further into the details of the reaction mechanism of trichlorosilanes with silica surfaces. In the presence of water, the Si-Cl bonds of an OTS molecule undergo hydrolysis forming Si-OH groups. If the OTS molecule is close to the substrate, these Si-OH groups react with OH groups on the silicon oxide surface forming a Si-O-Si bond and water. Such a reaction is of course also possible between two OTS molecules leading to a cross-linking of the layer molecules. Thus, the presence of a surface water layer on the silicon oxide is a necessary condition for the monolayer formation, but too much water on the surface also promotes vertical polymerization. Besides the availability of water, the surface density of OH-groups (silanole groups) on the silica surface has a very strong impact on whether there is a monolayer formation or a vertical polymerization [Fade00]. If the density of such groups is sufficiently large, the hydrolyzed OTS molecules should tend to react preferentially with the surface due to steric reasons. A 3D polymerization requires a certain twisting of the molecules out of their equilibrium conformation. In order to obtain high quality monolayers, silica substrates are usually cleaned in an oxidizing acid (e.g. 'piranha' solution) to provide a maximum coverage of the surface with OH groups. However, such a method is not possible for LAO nanostructures on alkyl-terminated silicon as the

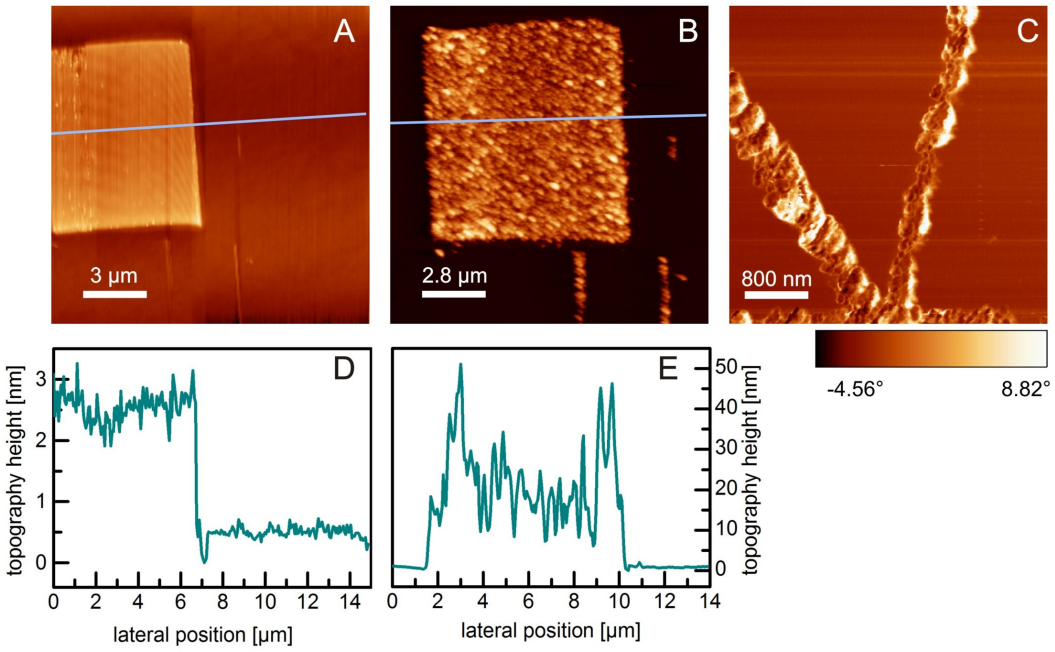

Figure 7.6: NC-AFM height images of LAO oxide structures before (**A**) and after (**B**) 40 h in a 10 mM OTS solution in toluene under ambient conditions. **C**: AFM phase image of line structures after the 40 h in OTS. **D, E:** topography profile along the lines in A and B.

protecting monolayer would also be oxidized. The strong tendency towards vertical polymerization in the presence of ambient water however, is an indirect evidence for a rather low density of OH groups on the lithographic oxide. This is further supported by the fact that for smaller immersion times of the substrate within the OTS solution, also a very non-uniform increase in height with clear local differences was observed. The few surface hydroxyl groups also lead to a much slower binding rate of OTS to the LAO oxide. Even after several hours in the OTS solution, the surface was not fully covered with OTS, whereas for 'piranha'-cleaned silica a fractional surface coverage near unity was reported within a few minutes [Mirj06, Belg10].

As the OH group density on the LAO oxide cannot be altered, the only way to prevent vertical polymerization is to completely remove the water from the silane solution in toluene. This was achieved by further drying of the solvent (sparging of the solution with an inert gas for 1 hour before the reaction) and placing the vessel in a desiccator during reaction. Under such conditions, a much more uniform coverage of the silicon oxide nanostructures could be achieved (see figure 7.8). The small amount of water which is necessary for the hydrolysis of the trichlorosilane may originate from residual water in the dried solution or a very thin water

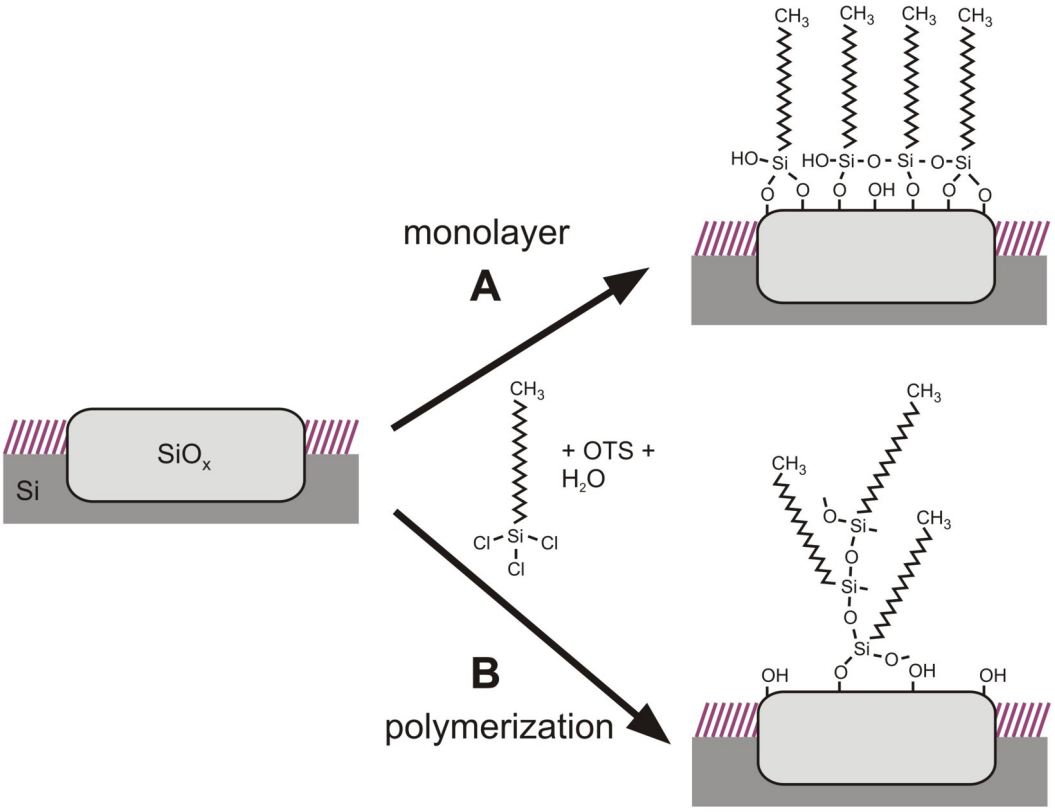

Figure 7.7: Schematic illustration of the two different possible covalent binding mechanisms of OTS with a silicon oxide surface. **A:** formation of a smooth OTS monolayer, **B:** vertical polymerization.

film which is adsorbed on the oxide surface during transfer under ambient conditions. Since the rest of the alkyl-terminated silicon is much more hydrophobic than the local oxide, surface water will condensate preferentially on the nanostructures. Compared to the binding under ambient conditions, the height increase is much more uniform under dry conditions. In the case of a square structure, the formed silane layer (here: 11-bromo-undecyltrichlorosilane was used) possesses a thickness of about 1.6 nm to 2 nm (figure 7.8A, B and E). This is in very good agreement with the thickness of 11-bromo-undecyltrichlorosilane monolayers on silica substrates which was determined to a value of 1.81 nm by ellipsometry measurements [Sawo08]. There are also very few larger elevations which may be due to polymerization within the solution. However, such impurities could be avoided using better anhydrous conditions and controlled process conditions. They are not crucial for the general observations and their physicochemical interpretation. The height increase of the line structures (figure 7.8C, D and F) is also within a reasonable range of 0.5 to 2.5 nm. Silane layer thicknesses smaller than the molecular

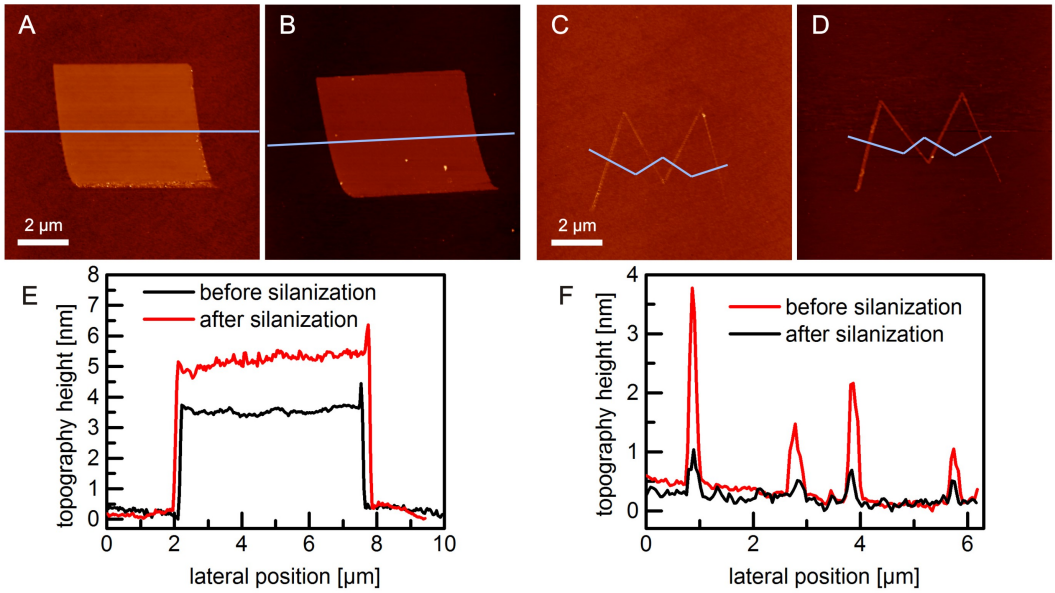

Figure 7.8: NC-AFM height images of LAO oxide structures before (**A, C**) and after (**B, D**) 16 h in a 10 mM 11-bromo-undecyltrichlorosilane solution in dry toluene under dry conditions. **E, F**: topography profile along the lines in A-D averaged over a width of 10 pixels.

length can be explained by a low surface coverage. If the monolayer is not densely packed, the molecules will not stand nearly upright (in all-trans conformation) but the alkyl chains will orient more parallel to the surface which leads to a decrease of the measured layer thickness [Mirj06]. A height increase of more than the thickness of a densely packed monolayer can only be explained by a beginning vertical polymerization. It is striking that there is a clear correlation between initial structure height and width with the thickness of the silane layer: The higher and wider the initial oxide, the larger is also the height increase by binding of silane molecules. Obviously the surface geometry has a strong influence on the reaction mechanism.

7.3.3 FITC bound to silicon oxide nanostructures

Once suitable conditions for the controlled silanization of LAO nanostructures have been found, functionalization with fluorescent FITC molecules according to the route displayed in figure 7.1 has been carried out. Figure 7.9 shows the results of comparative AFM height measurements after different functionalization steps. After binding of APTES, there is a height increase of approximately 0.3 nm

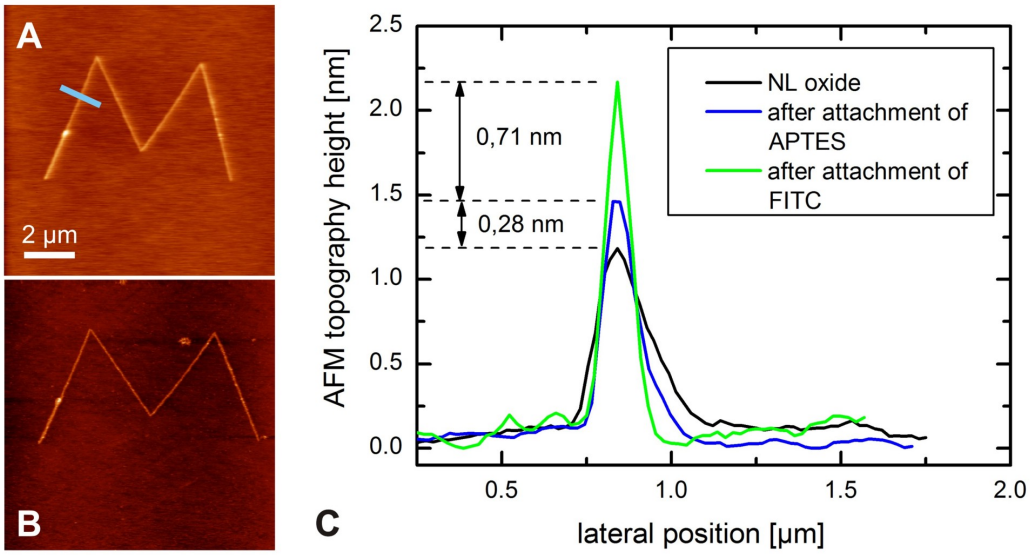

Figure 7.9: **A** and **B:** NC-AFM height images of LAO oxide line structures before any functionalization (A) and after binding of FITC (B). **C:** Height profile of an LAO oxide structure (black curve) after 6 h in 10 mM APTES solution dry toluene under dry conditions (blue curve) and after subsequent binding of FITC in aqueous solution (green curve). The profiles were measured and averaged over a width of 20 pixels along the path indicated by the blue line in figure (A).

(blue curve) which is in good agreement with the length of a hydrolyzed APTES molecule (∼0.3 nm). The subsequent binding of FITC to the amino-functionalized nanostructure leads to a further increase in height of about 0.7 nm. As the length of a single FITC molecule is about 1 nm, it can be concluded that the molecules are not standing upright but are tilted from the surface normal. The tilt is most likely caused by the thiocarbonyl group (planar trigonal geometry due to binding sp^2 orbitals). A calculation of the tilt from the height measurements is not straightforward though, as too many assumptions about the 3D orientation and bending of the bound FITC molecules would have to be made. Further theoretical considerations (e.g. molecular dynamic simulations) could be employed in order to

investigate the molecular orientation on the surface but it has to be kept in mind that AFM measurements of such systems are always influenced by many other factors like tip-sample interactions and the formation of water layers that strongly depend on the chemical nature of the surface, as mentioned in the previous chapters. FITC functionalized nanostructures have been investigated using fluorescence microscopy which further confirms the successful binding. Figure 7.10B shows a confocal microscope image of the fluorescence from the FITC-terminated structure in figure 7.10A (AFM image). There is a clear luminescence signal which

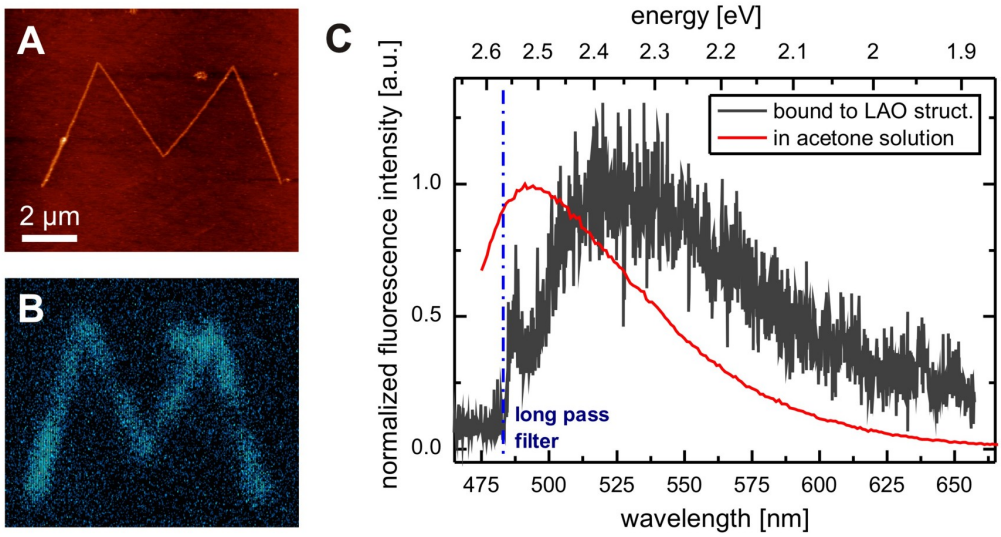

Figure 7.10: **A:** NC-AFM height image of an LAO oxide line structure after binding of FITC. **B:** confocal microscope image of the same structure (λ_{exc}=465 nm, excitation power: 11 µW, integration time: 1 ms/px) and **C:** fluorescence spectrum from the FITC-functionalized structure (dark gray curve) compared to FITC fluorescence in acetone solution (red curve).

originates from the nanostructure only. The spectral shape of the fluorescence light resembles that of FITC in acetone solution and is shifted about 36 nm to the red (figure 7.10C) due to the different dielectric environment (the small signal close to the filter edge at 485 nm is not part of the FITC fluorescence but probably scattered light from the environment). The fluorescence signal is comparable weak (roughly a factor of 10 above the background noise level). Main reason for this is the quenching by the underlying silicon. Nevertheless, other high quantum yield xanthene dyes (e.g. rhodamine 6G) that are bound to the nanostructures by electrostatic interactions, show a much higher signal-to-noise ratio for similar structure heights and excitation powers. Thus the quenching by the underlying silicon does not explain the measured low fluorescence intensities. Another important factor that influences the absorption and emission of radiation by the bound molecules is

the orientation of their transition dipole moment. For xanthene derivatives such as fluorescein or rhodamine, the transition dipole moment $\vec{\mu}$ for the $S_1 \rightarrow S_0$ transition is typically oriented along the xanthene unit [Penz80, Arbe06]. As this unit is perpendicular to the binding axis of the molecule, it should be oriented rather parallel to the surface (tilt angle $\alpha = 0°$, see figure 7.11). Since the directional char-

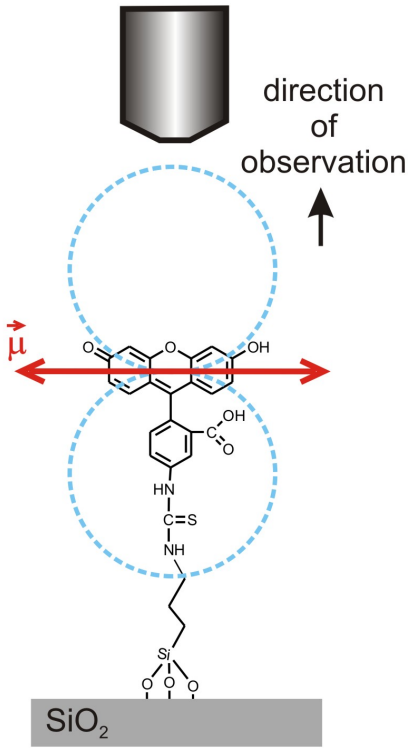

Figure 7.11: Schematic of the transition dipole moment orientation $\vec{\mu}$ (red arrow) of FITC bound to a SiO_2 surface.

acteristic of a dipole scales with $\cos^2 \alpha$, a very large tilting (α close to 90°) would be necessary to explain the much lower fluorescence intensities. Such a large tilt is very unlikely due to steric reasons as well as the molecular structure and would also be contradictory to the AFM-investigations. It may also be possible that the fluorescence is quenched by an efficient energy transfer between densely packed FITC molecules on the structure. This can be excluded by comparison to a study of Imhof *et al.* [Imho99] They investigated FITC bound to silica spheres and found a quenching of the fluorescence intensity for increasing dye concentration which was attributed to an interaction between neighboring molecules. This interaction however, also causes a lowering of the excited state energy which was observed as a 10 nm red shift of the emission spectrum from 531 nm to 541 nm for increasing dye concentration. Although it is difficult to exactly determine the peak position

in figure 7.10C due to the low signal-to-noise ratio of the spectrum, the maximum position clearly seems to be rather in the range of 530 nm than 540 nm. The absence of the red-shift as well as the agreement of the approximate peak position and spectral shape with the results of Imhof *et al.* for low dye concentrations, leads to the conclusion that the observed low fluorescence intensity is likely not caused by a dense packing of the FITC molecules on the oxide structure. Measurements of the excited state lifetime are likely not suitable to investigate the intermolecular interactions because of the predominant quenching by the silicon below. Consequently the most likely reason for the strong difference in fluorescence intensity between the electrostatically bound dyes and the covalently bound FITC is also the most evident one: the concentration of FITC bound to the LAO structure seems to be much lower than that of dyes which attach through electrostatic interactions. Of course this conclusion, though plausible, is based on many uncertainties and assumptions. Yet a more precise quantification is very difficult due to the unknown quenching by the underlying silicon and the unavailability of suitable measurement techniques of the surface coverage for such small geometries. If the density of FITC molecules on the structures is really much lower than that of electrostatically attracted dyes then this may be a hint that either the APTES monolayer is not closed on a nanoscopic scale or the molecules in the monolayer are not well-ordered. The latter would lead to a rather low density of surface amino groups [Past08] which are available for reaction with the functional group of FITC. However, the next neighbor distance between two adjacent surface amino groups has to be below the AFM tip diameter ($\sim$ 30 nm) as no distinct height steps or islands could be observed in the AFM images. A resolution of the density of bound molecules may be possible by using novel techniques such as the measurement of AFM amplitude-phase-distance curves [Diet08]. From such experiments, the dissipated energy of the AFM tip oscillation can be calculated which depends on the local elastic and therefore structural surface properties of the substrate. The surface coverage of the relatively rigid silicon oxide with 'softer' organic molecules should in principle be distinguishable by the amplitude-phase-distance curve technique.

7.4 Conclusions

In conclusion, a route for a controlled covalent functionalization of silicon oxide nanostructures with an amino-terminated silane and FITC dye molecules has been realized successfully. The formation of silane monolayers on nanoscopic silicon oxide nanostructures has proven to be much more sensitive towards ambient humidity as e.g. silanization of larger OH-terminated silica surfaces. This is most likely

due to a lower density of surface hydroxyl groups which requires a longer reaction time for the formation of a closed monolayer. Optical investigations of the bound FITC dye on the other hand, seem to indicate that the forming APTES monolayer is not well-ordered. Pasternack *et al.* found that the ordering of APTES monolayers can be improved through in situ heating during the functionalization reaction [Past08]. An elevation of the reaction temperature seems to be a promising step for future experiments in order to obtain more densely packed FITC monolayers on the silicon oxide nanostructures. Also a formation of silane monolayers from the gas phase should be considered, as this technique enables a controlled formation of highly ordered films under appropriate conditions [Dong06, Sugi02, Hozu01].

Acknowledgement

The authors are grateful to the Deutsche Forschungsgemeinschaft (DFG, GR 2695/4) for financial support.

8 Summary and Prospects

8.1 Summary

The main objective of this thesis was to investigate different routes for the selective functionalization of silicon oxide nanostructures created by local anodic oxidation of alkyl-terminated silicon. Thereby two different general mechanisms for the binding of optically active molecules have been pursued, attachment of different dyes via electrostatic interactions and covalent binding. Both approaches could be successfully realized and in this process new insights into the physiochemical modification of nanoscopic surfaces were obtained. This especially is a very interesting and important topic for a future development and design of functional nanoscale materials or devices by combined up-down and bottom-up techniques. Furthermore, the fluorescence properties of the generated functional structures have been investigated for the first time in such a great detail. By interpreting these properties through adaptation of existing models and the development of new conceptions, a deeper understanding of this class of systems could be achieved. In the following, general and specific new findings presented within this thesis will be summarized briefly.

(I) The recently verified negative space charge within the local oxide structures is stable at least over several days. A found decrease of the Kelvin probe force microscopy contrast over time at ambient conditions could be clearly attributed to an adsorption of ambient humidity on the structure which leads to a screening of the charge. The high stability of the charge was also confirmed by fluorescence measurements of a charge sensitive dye. Though both methods showed a good qualitative agreement, special attention should be paid to their quantitative validity which cannot be easily derived for such systems.

(II) The negative space charge allows for a reliable and easily applicable binding of different classes of cationic dye molecules. For the first time, a perylene derivative could be selectively immobilized on LAO nanostructures by using spermine-functionalized PBI molecules that have been synthesized by the Würthner-group.

(III) In the case of electrostatically bound rhodamine 6G, the number of bound dye molecules is nearly proportional to the surface area of the dye-covered nanostructures. This emphasized the impact of the surface charge density on the dye attachment rather than the volume charge density.

(IV) The spectral emission characteristics of electrostatically bound R6G is very similar to that in solution or a physisorbed thin film on silicon oxide. However, there is a small yet clearly verified blue shift which was attributed to the interaction between the R6G molecules and the negative charges. No distinct influence of the electrostatic binding on the photophysical degradation (bleaching) of rhodamine 6G could be found.

(V) Emission spectra of sf-PBI functionalized LAO nanostructures can be interpreted as a combination of monomer-like emission and E-type excimer luminescence. Thus it can be concluded that some of the emitters exist in a state which is similar to the electronic configuration of monomeric sf-PBI molecules whereas others are able to relax into an E-type excimer geometry. The spectral findings for the electrostatically attached PBIs could also be compared to those of thin films spincoated on silicon with a 100 nm silicon oxide layer.

(VI) The relative strength of the E-emission from the nanostructures decreases gradually by cooling the sample down to 77 K. This may be understood in terms of a motional constriction due to the electrostatic forces that bind the sf-PBI molecules to the local anodic oxide surface.

(VII) The decay process of the excited state has been found to be at least tri-exponential, both for the dense spincoated films as well as for the dye bound to LAO oxide. This indicates a multitude of different involved molecular states which may be understood in terms of a configurational disorder within the electrostatically assembled sf-PBI films. The E-excimers possess a larger life time than the sf-PBI monomers which is also in agreement with previous findings as well as the investigations of the spincoated films.

(VIII) The influence of the underlying close-by silicon on the dampening of the emissive rate shows a reasonable agreement with an existing theoretical model. It has also been found that even a 27 nm thin silicon film is sufficient to cause a dampening compared to bulk silicon.

(IX) For the first time, a covalent attachment of an optically active material (in this case the functional fluorescein derivative FITC) to the LAO nanostructures via an amino-terminated silane linker has been successfully demonstrated. The binding

was confirmed by AFM height measurements and fluorescence microscopy.

(**X**) Photoluminescence intensity and spectral investigations, however, indicate that the density of the bound FITC molecules is rather low compared to the electrostatic binding mechanisms of rhodamine 6G or sf-PBI. This may be connected to a poor order within the formed silane layer on a nanometer scale.

8.2 Prospects and open questions

Although within this thesis many of the occurring problems concerning the functionalization of LAO nanostructures with optically active materials are solved, it is only natural in the context of scientific discourse that it raises new questions which should be addressed in future experiments. The most essential ones will be discussed in the following.

- The stability of the space charge within the nanostructures has been verified for time periods of days, yet it would be very interesting whether it is also stable even for longer times. If so, applications could be conceived, where once bleached or otherwise de-functionalized species could be removed and replaced easily by a new self-assembly process through providing a fresh solution containing the respective functional cationic molecules (self-healing of the functional structures).

- A suitable 'calibration' procedure for the use of the charge sensitive dyes would be very beneficial, as those are strongly local probes that are not as easily influenced by forming water films as e.g. KPFM measurements.

- A theoretical calculation of the influence of the negative charge on the spectral properties of the attached dyes (electrochromic effect) may not only explain the observed spectra but could also provide new insights in the binding strength and orientation of the attached molecules.

- Elaborate theoretical simulations should also be conducted in order to explain the interplay between structural and electronic properties of bound sf-PBI molecules (excimer formation).

- The interpretation of such calculations could also be supported by low-temperature life time investigations. This may help to understand the found decrease of the E-excimer peak while cooling the sample as well as the found thermal relaxation

kinetics.

- The design of dye molecules with defined binding sites could be used to covalently bind them in a very controllable way to the LAO oxide structures. A synthesis of a perylene derivative with a reactive NCS-group at the imide position is attempted at the moment but did not yield to a positive result so far. With different functional dyes available, it should be possible to create nanostructures with distinct functionalities on a very small scale in a multi-step combined top-down / bottom-up approach.

- In order to gain further insights into the coverage of the LAO structures on a length scale below the optical resolution limit, other techniques such as AFM amplitude-phase-distance curves should be tested on the fabricated systems.

REFERENCES

[Ahre04] M. Ahrens, L. Sinks, B. Rybtchinski, W. Liu, B. Jones, J. Giaimo, A. Gusev, A. Goshe, D. Tiede, and M. Wasielewski. *J. Am. Chem. Soc.*, Vol. 126, pp. 8284–8294, 2004.

[Akim97] S. Akimoto, A. Ohmori, and I. Yamazaki. *J. Phys. Chem. B*, Vol. 101, pp. 3753–3758, 1997.

[Albo08] C. Albonetti, J. Martinez, N. Losilla, P. Greco, M. Cavallini, F. Borgatti, M. Montecchi, L. Pasquali, R. Garcia, and F. Biscarini. *Nanotechnology*, Vol. 19, p. 435303, 2008.

[Aliv87] A. Alivisatos, M. Arndt, S. Efrima, D. Waldeck, and C. Harris. *J. Chem. Phys.*, Vol. 86, pp. 6540–6549, 1987.

[Ara02a] M. Ara, H. Graaf, and H. Tada. *Appl. Phys. Lett.*, Vol. 80, pp. 2565–2567, 2002.

[Ara02b] M. Ara, H. Graaf, and H. Tada. *Jpn. J. Appl. Phys.*, Vol. 41, p. 4894, 2002.

[Ara07] M. Ara, M. Tsuji, and H. Tada. *Surf. Sci.*, Vol. 601, pp. 5098–5102, 2007.

[Arbe06] F. Arbeloa and V. Martínez. *Chem. Mater.*, Vol. 18, pp. 1407–1416, 2006.

[Aspn83] D. Aspnes and A. Studna. *Phys. Rev. B*, Vol. 27, pp. 985–1009, 1983.

[Avou84] P. Avouris and B. Persson. *J. Phys. Chem.*, Vol. 88, pp. 837–848, 1984.

[Avou97] P. Avouris, T. Hertel, and R. Martel. *Appl. Phys. Lett.*, Vol. 71, pp. 285–287, 1997.

[Barn98] W. Barnes. *J. Mod. Optic*, Vol. 45, pp. 661–699, 1998.

[Baum07] T. Baumgärtel. “Diplomarbeit: AFM-induced Nanolithography on Alkyl-Terminated Silicon for Selective Binding of Dye Molecules”. Chemnitz University of Technology, 2007.

[Baum10] T. Baumgärtel, C. von Borczyskowski, and H. Graaf. *Nanotechnology*, Vol. 21, p. 475205, 2010.

[Baum11a] T. Baumgärtel and H. Graaf. *Lithography: Principles, Processes and Materials*, Chap. Local Anodic Oxidation Nanolithography on Silicon: Chemical Routes to Functional Nanostructures, pp. 175–193. Nova Science Publishers, Hauppauge NY 11788-3619, USA, 2011.

[Baum11b] T. Baumgärtel, H. Graaf, and C. von Borczyskowski. *Thin Solid Films*, Vol. 519, pp. 3443–3447, 2011.

[Baum12] T. Baumgärtel, C. von Borczyskowski, and H. Graaf. *Nanotechnology*, Vol. 23, p. 095707, 2012.

[Belg10] C. Belgardt, H. Graaf, T. Baumgärtel, and C. von Borczyskowski. *Physica Status Solidi C*, Vol. 7, pp. 227–230, 2010.

[Binn86] G. Binnig, C. F. Quate, and C. Gerber. “Atomic Force Microscope”. *Phys. Rev. Lett.*, Vol. 56, pp. 930–933, Mar 1986.

[Bish96] P. Bisht, K. Fukuda, and S. Hirayama. *Chem. Phys. Lett.*, Vol. 258, pp. 71–79, 1996.

[Bitz96] T. Bitzer, T. Alkunshalie, and N. Richardson. *Surf. Sci.*, Vol. 368, pp. 202–207, 1996.

[Bran93] S. Brandriss and S. Margel. *Langmuir*, Vol. 9, pp. 1232–1240, 1993.

[Buh01] G. Buh, H. Chung, and Y. Kuk. *Appl. Phys. Lett.*, Vol. 79, p. 2010, 2001.

[Bulo96] V. Bulović, P. Burrows, J. C. S.R. Forres and, and M. Thompson. *Chem. Phys.*, Vol. 210, pp. 1–12, 1996.

[Buri99] J. Buriak. *Chem. Commun.*, pp. 1051–1060, 1999.

[Call00] M. Calleja and R. Garcia. *Appl. Phys. Lett.*, Vol. 76, pp. 3427–3429, 2000.

[Cava03] M. Cavallini, P. Mei, F. Biscarini, and R. Garcia. *Appl. Phys. Lett.*, Vol. 83, pp. 5286–5288, 2003.

[Chan76] R. Chance, A. Prock, and R. Silbey. *J. Chem. Phys.*, Vol. 65, pp. 2527–2531, 1976.

[Chan78] R. Chance, A. Prock, and R. Silbey. *Advances in Chemical Physics*, pp. 1–65. Vol. 37, Wiley-Interscience, New York, 1978.

[Char08] D. Charrier, M. Kemerink, B. Smalbrugge, T. de Vries, and R. Janssen. *ACS Nano*, Vol. 2, p. 622, 2008.

[Chen08] Z. Chen, Y.-J. Tang, T.-T. Xie, Y. Chen, and Y.-Q. Li. *J. Fluoresc.*, Vol. 18, pp. 93–100, 2008.

[Chen99] C. Chen, C. Yet, H. Wang, and C. Chao. *Langmuir*, Vol. 15, pp. 6845–6850, 1999.

[Chie10] M. Chiesa and R. Garcia. *Appl. Phys. Lett.*, Vol. 96, p. 263112, 2010.

[Cnos93] G. Cnossen, K. Drabe, and D. Wiersma. *J. Chem. Phys*, Vol. 98, pp. 5276–5280, 1993.

[Daga04] J. A. Dagata, F. Perez-Murano, C. Martin, H. Kuramochi, and H. Yokoyama. *J. Appl. Phys.*, Vol. 96, No. 4, pp. 2386–2392, 2004.

[Daga95] J. Dagata. *Science*, Vol. 270, p. 1625, 1995.

[Daga98] J. A. Dagata, T. I. Inoue, J. Itho, K. Matsumoto, and H. Yokoyama. *J. Appl. Phys.*, Vol. 84, No. 12, pp. 6891–6899, 1998.

[Dano08] L. Danos, R. Greef, and T. Markvart. *Thin Solid Films*, Vol. 516, pp. 7251–7255, 2008.

[Desb11] S. Desbief, L. Patrone, D. Goguenheim, D. Guérin, and D. Vuillaume. *Phys. Chem. Chem. Phys.*, Vol. 13, pp. 2870–2879, 2011.

[Dext79] D. Dexter. *J. Luminescence*, Vol. 18/19, pp. 779–784, 1979.

[Diet08] C. Dietz, M. Zerson, C. Riesch, M. Franke, and R. Magerle. *Macro-*

molecules, Vol. 41, pp. 9259–9266, 2008.

[Dong06] J. Dong, A. Wang, K. Ng, and G. Mao. *Thin Solid Films*, Vol. 515, pp. 2116–2122, 2006.

[Dubo00] E. Dubois and J.-L. Bubendorff. *J. Appl. Phys.*, Vol. 87, No. 11, pp. 8148–8154, 2000.

[Ebel07] A. Ebel, W. Donaubauer, F. Hampel, and A. Hirsch. *Eur. J. Org. Chem.*, Vol. 2007, pp. 3488–3494, 2007.

[Enik04] E. Enikov and A. Palaria. *Nanotechnology*, Vol. 15, p. 1211, 2004.

[Fade00] A. Fadeev and T. McCarthy. *Langmuir*, Vol. 16, pp. 7268–7272, 2000.

[Fauc07] A. Faucheux, A. C. Gouget-Laemmel, P. Allongue, C. H. de Villeneuve, C. Ozanam, and J.-N. Chazalviel. *Langmuir*, Vol. 22, pp. 153–162, 2007.

[Flid99] J. Flidr, Y.-C. Huang, and M. A. Hines. *J. Chem. Phys.*, Vol. 111, pp. 6970–6981, 1999.

[Fluh85] E. Fluhler, V. Burnham, and L. Loew. *Biochemistry*, Vol. 24, p. 5749, 1985.

[Font98] P. Fontaine, E. Dubois, and D. Stievenard. *J. Appl. Phys.*, Vol. 84, No. 4, pp. 1776–1781, 1998.

[Ford87] W. Ford and P. Kamat. *J. Phys. Chem.*, Vol. 91, pp. 6373–6380, 1987.

[Fres04] Z. Fresco, I. Suez, S. Backer, and J. Frechet. *J. Am. Chem. Soc.*, Vol. 126, pp. 8374–8375, 2004.

[Fres05] Z. Fresco and J. Frechet. *J. Am. Chem. Soc.*, Vol. 127, pp. 8302–8303, 2005.

[Frey78] E. von Freydorf, J. Kinder, and M. Michel-Beyerle. *Chem. Phys.*, Vol. 27, pp. 199–209, 1978.

[Fu03] J. Fu, H. Zhou, J. Kramar, R. Silver, and S. Gonda. *Appl. Phys. Lett.*, Vol. 82, pp. 3014–3016, 2003.

[Gang10] V. Gangilenka, L. Titova, L. Smith, H. Wagner, L. DeSilva, L. Gisslen, and

R. Scholz. *Phys. Rev. B*, Vol. 81, p. 155208, 2010.

[Gao11] F. Gao, Y. Zhao, and W. Liang. *Phys. Chem. B*, Vol. 115, pp. 2699–2708, 2011.

[Garc06] R. Garcia, R. Martinez, and J. Martinez. *Chem. Soc. Rev.*, Vol. 35, p. 29, 2006.

[Gavr06] V. Gavrilenko and M. Noginov. *J. Chem. Phys.*, Vol. 124, p. 044301, 2006.

[Giai08] J. Giaimo, J. Lockard, L. Sinks, A. Scott, T. Wilson, and M. Wasieliewski. *J. Phys. Chem. A*, Vol. 112, pp. 2322–2330, 2008.

[Graa07] H. Graaf, M. Vieluf, and C. v. Borczyskowski. *Nanotechnology*, Vol. 18, p. 265306, 2007.

[Graa08a] H. Graaf, T. Baumgärtel, M. Vieluf, and C. von Borczyskowski. *Superlat. Microstruct.*, Vol. 44, pp. 402–410, 2008.

[Graa08b] H. Graaf, T. Unold, C. Mattheus, and D. Schlettwein. *J. Phys. D: Appl. Phys.*, Vol. 41, p. 105112, 2008.

[Graa11] H. Graaf, F. Friedriszik, C. Wagner, and C. von Borczyskowski. *Phys. Chem. C*, Vol. 115, pp. 8150–8154, 2011.

[Grim08] S. Grimme. *Angew. Chem. Int. Ed.*, Vol. 47, pp. 3430–3434, 2008.

[Gu04] J. Gu, C. Yam, S. Li, and C. Cai. *J. Am. Chem. Soc.*, Vol. 126, pp. 8098–8099, 2004.

[Haen09] C. Haensch, S. Hoeppener, and U. Schubert. *Nanotechnology*, Vol. 20, p. 135302, 2009.

[Han09] J. Han, D. Kasahara, T. Ichii, K. Murase, and H. Sugimura. *J. Vac. Sci. Technol. B*, Vol. 27, pp. 928–933, 2009.

[Hans94] P. Hansma, J. Cleveland, M. Radmacher, D. Walters, P. Hillner, M. Bezanilla, M. Fritz, D. Vie, H. Hansma, C. Prater, J. Massie, L. Fukunaga, J. Gurley, and V. Elings. *Appl. Phys. Lett.*, Vol. 64, pp. 1738–1740, 1994.

[Haya83] T. Hayashi, T. Castner, and R. Boyd. *Chem. Phys. Lett.*, Vol. 94, pp. 461–466, 1983.

[Henn99] M. Hennessy, Z. Soos, R. P. Jr., and A. Girlando. *Chem. Phys.*, Vol. 245, pp. 199–212, 1999.

[Herb97] W. Herbst and K. Hunger. *Industrial Organic Pigments: Production, Properties, Applications*. WILEY-VCH, 2nd Ed., 1997.

[Hern04] J. Hernando, P. de Witte, E. van Dijk, J. Korterik, R. Nolte, A. Rowan, M. Garcia-Parajo, and N. van Hulst. *Angew. Chem. Int. Ed.*, Vol. 43, pp. 4045–4049, 2004.

[Hoep05] S. Hoeppener and U. Schubert. *small*, Vol. 1, pp. 628–632, 2005.

[Howa06] J. Howarter and J. Youngblood. *Langmuir*, Vol. 22, pp. 11142–11147, 2006.

[Hozu01] A. Hozumi, Y. Yokogawa, T. Kameyama, H. Sugimura, K. Hayashi, H. Shirayama, and O. Takai. *Vac. Sci. Technol. A*, Vol. 19, pp. 1812–1816, 2001.

[Hutt93] J. Hutter. *Rev. Sci. Instrum.*, Vol. 64, pp. 1868–1873, 1993.

[Imho99] A. Imhof, M. Megens, J. Engelberts, D. de Lang, R. Sprik, and W. Vos. *J. Phys. Chem. B*, Vol. 103, pp. 1408–1415, 1999.

[Ishi98] M. Ishikawa, O. Yogi, J. Ye, T. Yasuda, and Y. Maruyama. *Anal. Chem.*, Vol. 70, pp. 5198–5208, 1998.

[Jali04] N. Jalili and K. Laxminarayana. "A review of atomic force microscopy imaging systems: application to molecular metrology and biological sciences". *Mechatronics*, Vol. 14, No. 8, pp. 907 – 945, 2004.

[Jone04] B. Jones, M. Ahrens, M.-H. Yoon, A. Facchetti, T. Marks, and M. Wasielewski. *Angew. Chem. Int. Ed.*, Vol. 43, pp. 6363–6366, 2004.

[Jone07] B. Jones, A. Facchetti, M. Wasielewski, and T. Marks. *J. Am. Chem. Soc.*, Vol. 129, pp. 15259–15278, 2007.

[Kais09] T. Kaiser, V. Stephanenko, and F. Würthner. *J. Am. Chem. Soc.*, Vol. 131, pp. 6719–6732, 2009.

[Kash65] M. Kasha, H. Rawls, and M. El-Bayoumi. *Pure Appl. Chem.*, Vol. 11, pp. 371–392, 1965.

[Kolb01] H. Kolb, M. Finn, and K. Sharpless. *Angew. Chem. Int. Ed.*, Vol. 40, pp. 2004–2021, 2001.

[Kowe09] D. Kowerko, J. Schuster, and C. von Borczyskowski. *Mol. Phys.*, Vol. 107, pp. 1911–1921, 2009.

[Kras11] C. Krasselt, J. Schuster, and C. von Borczyskowski. *Phys. Chem. Chem. Phys.*, Vol. 13, pp. 17084–17092, 2011.

[Krau11] S. Krause, D. Kowerko, R. Börner, C. Hübner, and C. von Borczyskowski. *Chem. Phys. Chem.*, Vol. 12, pp. 303–312, 2011.

[Kura03] H. Kuramochi, K. Ando, and H. Yokoyama. *Surf. Sci.*, Vol. 542, pp. 56–63, 2003.

[Lee99] S. Lee, Y. Zu, A. Herrmann, Y. Geerts, K. Müllen, and A. Bard. *J. Am. Chem. Soc.*, Vol. 121, pp. 3513–3520, 1999.

[Ley96] L. Ley, T. Teuschler, K. Mahr, S. Miyazaki, and M. Hundhausen. *J. Vac. Sci. Technol., B*, Vol. 14, pp. 2845–2849, 1996.

[Lian84] Y. Liang, P. Moy, J. Poole, and A. P. Goncalves. *J. Phys. Chem.*, Vol. 88, pp. 2451–2455, 1984.

[Lian85] Y. Liang and A. P. Goncalves. *J. Phys. Chem.*, Vol. 89, pp. 3290–3294, 1985.

[Lin10] H. Lin, R. Camacho, Y. Tian, T. Kaiser, F. Würthner, and I. Scheblykin. *Nano Lett.*, Vol. 10, pp. 620–626, 2010.

[Linf95] M. Linford, P. Fenter, P. Eisenberger, and C. Chidsey. *J. Am. Chem. Soc.*, Vol. 117, No. 11, pp. 3145–3155, 1995.

[Liu02] S. Liu, R. Maoz, G. Schmid, and J. Sagiv. *Nano Lett.*, Vol. 2, pp. 1055–1060, 2002.

[Loew78] L. Loew, G. Bonneville, and J. Surow. *Biochemistry*, Vol. 17, p. 4065, 1978.

[Loew81] L. Loew and L. Simpson. *Biophys. J.*, Vol. 34, p. 353, 1981.

[Losi08] N. Losilla, N. Oxtoby, J. Martinez, F. Garcia, R. Garcia, M. Mas-Torrent, J. Veciana, and C. Rovira. *Nanotechnology*, Vol. 19, p. 455308, 2008.

[Losi09] N. Losilla, J. Martinez, and R. Garcia. *Nanotechnology*, Vol. 20, p. 475304, 2009.

[Lu07] Y.-S. Lu, H.-I. Wu, S. Wu, and Y.-R. Ma. *Surf. Sci.*, Vol. 601, pp. 3788–3791, 2007.

[Macq99] D. Macquarrie, S. Taverner, G. Gray, P. Heath, J. Rafelt, S. Saulzet, J. Hardy, J. Clark, P. Sutra, D. Brunel, F. di Renzo, and F. Fajula. *New J. Chem.*, Vol. 23, p. 725, 1999.

[Mahr94] J. Mahrt, F. Willig, W. Storck, D. Weiss, R. Kietzmann, K. Schwarzburg, B. Tufts, and B. Troesken. *J. Phys. Chem.*, Vol. 98, pp. 1888–1894, 1994.

[Maoz00a] R. Maoz, E. Frydman, S. Cohen, and J. Sagiv. *Adv. Mater.*, Vol. 12, pp. 424–429, 2000.

[Maoz00b] R. Maoz, E. Frydman, S. Cohen, and J. Sagiv. *Adv. Mater.*, Vol. 12, pp. 725–731, 2000.

[Maoz99] R. Maoz, S. Cohen, and J. Sagiv. *Adv. Mater.*, Vol. 11, pp. 55–61, 1999.

[Mart05] J. Martin, F. Cichos, and C. von Borczyskowski. *Optics and Spectroscopy*, Vol. 99, p. 281, 2005.

[Mart08] J. Martinez, R. Martinez, and R. Garcia. *Nano Lett.*, Vol. 8, p. 3636, 2008.

[Mirj06] S. Mirji. *Surf. Interface Anal.*, Vol. 38, pp. 158–165, 2006.

[Mo09] Y. Mo, Y. Wang, J. Pu, and M. Bai. *Langmuir*, Vol. 25, pp. 40–42, 2009.

[Mont89] V. Montana, D. Farkas, and L. Loew. *Biochemistry*, Vol. 28, p. 4536, 1989.

[Must01] T. Muster, C. Prestidge, and R. Hayes. *Colloids and Surfaces A: Physicochem. Eng. Aspects*, Vol. 176, p. 254, 2001.

[Nonn91] M. Nonnenmacher, M. O'Boyle, and H. Wickranmashinghe. *Appl. Phys. Lett.*, Vol. 58, p. 2921, 1991.

[Noy95] A. Noy, C. Frisbie, L. Rosznyai, M. Wrighton, and C. Lieber. *J. Am. Chem. Soc.*, Vol. 117, p. 7943, 1995.

[Noy97] A. Noy, D. Vezenov, and C. Lieber. *Annu. Rev. Mater. Sci.*, Vol. 27, pp. 381–421, 1997.

[Oria06] A. Orians, C. Clemons, D. Golovaty, and G. Young. *Surf. Sci.*, Vol. 600, pp. 3297–3312, 2006.

[Pal73] M. Pal and S. Ash. *J. Phys. Chem.*, Vol. 78, No. 5, pp. 536–540, 1973.

[Pale06] V. Palermo, M. Palma, and P. Samori. *Adv. Mater.*, Vol. 18, p. 145, 2006.

[Park04] J. Park and H. Lee. *Mater. Sci. Eng. C*, Vol. 24, pp. 311–314, 2004.

[Past08] R. Pasternack, S. Amy, and Y. Chabal. *Langmuir*, Vol. 24, pp. 12963–12971, 2008.

[Patt09] A. Pattantyus-Abraham, H. Qiao, J. Shan, K. Abel, T.-S. Wang, F. van Veggel, and J. Young. *Nano Lett.*, Vol. 9, pp. 2849–2854, 2009.

[Penz80] A. Penzkofer and J. Wiedmann. *Opt. Commun.*, Vol. 35, pp. 81–86, 1980.

[Pers78] B. Persson. *J. Phys. C*, Vol. 11, pp. 4251–4269, 1978.

[Pers80] B. Persson and M. Persson. *Surf. Sci.*, Vol. 97, pp. 609–624, 1980.

[Pers82] B. Persson and N. Lang. *Phys. Rev. B*, Vol. 26, pp. 5409–5415, 1982.

[Phil71] H. Philipp. *J. Phys. Chem. Solids*, Vol. 32, pp. 1935–1945, 1971.

[Pign03] B. Pignataro, A. Licciardello, S. Cataldo, and G. Marletta. *Mat. Sci. Eng. C*, Vol. 23, pp. 7–12, 2003.

[Plue91] E. Plueddemann. *Silane Coupling Agents*. Springer, Berlin, 2nd Ed., 1991.

[Pols10] D. Polster, H. Graaf, T. Baumgärtel, C. von Borczyskowski, U. Benedkit, and A. Auer. *Langmuir*, Vol. 26, pp. 8301–8308, 2010.

[Prat01] S. Prathapan, S. Yang, J. Seth, M. Miller, D. Bocian, D. Holten, and J. Lindsey. *J. Phys. Chem. B*, Vol. 105, pp. 8237–8248, 2001.

[Proe04] H. Proehl, T. Dienel, R. Nitsche, and T. Fritz. *Phys. Rev. Lett.*, Vol. 93, p. 097403, 2004.

[Puec96] K. Puech, H. Fröob, M. Hoffman, and K. Leo. *Opt. Lett.*, Vol. 21, pp. 1606–1608, 1996.

[Putm94] C. A. J. Putman, K. O. Van der Werf, B. G. De Grooth, N. F. Van Hulst, and J. Greve. "Tapping mode atomic force microscopy in liquid". *Applied Physics Letters*, Vol. 64, No. 18, pp. 2454 –2456, may 1994.

[Ravo09] B. Ravoo. *J. Mater. Chem.*, Vol. 19, pp. 8902–8906, 2009.

[Rehm10] S. Rehm, V. Stepanenko, X. Zhang, T. Rehm, and F. Würthner. *Chem. Eur. J.*, Vol. 16, pp. 3372–3382, 2010.

[RF K82] R.F. Kubin and A.N. Fletcher. "Fluorescence quantum yield of some rhodamine dyes". *J. Lumin.*, Vol. 27, pp. 455–462, 1982.

[Sagi80] J. Sagiv. *J. Am. Chem. Soc.*, Vol. 102, pp. 92–98, 1980.

[Sasa01] A. Sasahara, H. Uetsuka, and H. Onishi. "Noncontact atomic force microscope topography dependent on the electrostatic dipole field of individual molecules". *Phys. Rev. B*, Vol. 64, p. 121406, Sep 2001.

[Sawo08] S. Sawoo, P. Dutta, A. Chakraborty, R. Mukhopadhyay, O. Bouloussa, and A. Sarkar. *Chem. Commun.*, pp. 5957–5959, 2008.

[Schu07] J. Schuster, J. Brabandt, and C. v. Borczyskowski. *J. Luminescence*, Vol. 127, pp. 224–229, 2007.

[Schu56] M. Schubert and D. Hamerman. *J. Histochem. Cytochem.*, Vol. 4, pp. 159–189, 1956.

[Send95] T. Senden and C. Drummond. *Colloids and Surfaces A: Physicochem. Eng.*

Aspects, Vol. 94, pp. 29–51, 1995.

[Shen08] Y. Shen, D. Barnett, and P. Pinsky. *Rev. Sci. Instrum.*, Vol. 79, p. 023711, 2008.

[Sheu05] J. Sheu, C. Chen, P. Huang, and M. Hsu. *Microelectron. Eng.*, Vol. 78/79, pp. 294–299, 2005.

[Siev00] A. Sieval, R. Linke, H. Zuilhof, and E. Sudhoelter. *Adv. Mater.*, Vol. 12, No. 19, pp. 1457–1460, 2000.

[Siev98] A. Sieval, A. Demirel, J. Nissink, M. Linford, J. van der Maas, W. de Jeu, H. Zuilhof, and E. Sudhoelter. *Langmuir*, Vol. 14, No. 7, pp. 1759–1768, 1998.

[Sluc95] M. Sluch, A. Vitukhnovsky, and M. Petty. *Phys. Lett. A*, Vol. 200, p. 61, 1995.

[Snow00] E. Snow, G. Jernigan, and P. Campbell. *Appl. Phys. Lett*, Vol. 76, pp. 1782–1784, 2000.

[Snow94] E. Snow and P. Campbell. *Appl. Phys. Lett.*, Vol. 64, pp. 1932–1934, 1994.

[Somo06] M. Somoza. "Licensed: GFDL. Source: http://en.wikipedia.org/wiki/File:Franck-Condon-diagram.png". 2006.

[Stav85] M. Stavola, D. Dexter, and R. Knox. *Phys. Rev. B*, Vol. 31, pp. 2277–2289, 1985.

[Stra05] E. Strassbourg, A.Boag, and Y. Rosenwaks. *Rev. Sci. Instrum.*, Vol. 76, p. 083705, 2005.

[Sugi02] H. Sugimura, Y. Ishida, K. Hayashi, and O. Takai. *Appl. Phys. Lett.*, Vol. 80, p. 1459, 2002.

[Sugi09] H. Sugimura, S. Nanjo, H. Sano, and K. Murase. *J. Phys. Chem. C*, Vol. 113, pp. 11643–11646, 2009.

[Sugi97] H. Sugimura and N. Nakagiri. *Nanotechnology*, Vol. 8, pp. A15–A18, 1997.

[Sumi89] H. Sumi. *Chem. Phys.*, Vol. 130, pp. 433–449, 1989.

[Sung97] M. Sung, J. Kluth, O. Yauw, and R. Maboudian. *Langmuir*, Vol. 13, pp. 6164–6168, 1997.

[Sze81] S. Sze. *Physics of Semiconductor Devices*, Chap. 7. John Wiley & Sons, New York, 2nd Ed., 1981.

[Tada03] H. Tada, M. Ara, and S. Tanaka. In: *Mat. Res. Soc. Proc. Vol. 739*, p. H7.37.1, Materials Research Society, 2003.

[Tana63] J. Tanaka. *Bull. Chem. Soc. Japan*, Vol. 36, pp. 1237–1249, 1963.

[Tell03] M. Tello and R. Garcia. *Appl. Phys. Lett.*, Vol. 83, pp. 2339–2341, 2003.

[Teus95] T. Teuschler, K. Mahr, S. Miyazaki, M. Hundhausen, and L. Ley. *Appl. Phys. Lett.*, Vol. 67, No. 21, pp. 3144–3146, 1995.

[Tleu05] D. Tleugabulova, J. Sui, P. Ayers, and J. Brennan. *J. Phys. Chem. B*, Vol. 109, pp. 7850–7858, 2005.

[Tsen05] A. Tseng, A. Notargiacomo, and T. Chen. *J. Vac. Sci. Technol. B*, Vol. 23, pp. 877–894, 2005.

[Tsuk98] M. Tsukada, N. Sasaki, R. Yamura, N. Sato, and K. Abe. *Surf. Sci.*, Vol. 401, pp. 355–363, 1998.

[Ulma96] A. Ulman. *Chem. Rev.*, Vol. 96, pp. 1533–1554, 1996.

[Vale02] B. Valeur. *Molecular Fluorescence Principles and Applications*. WILEY-VCH, 2002.

[Veld08] D. Veldman, S. Chopin, S. Meskers, M. Groeneveld, R. Williams, and R. Janssen. *J. Phys. Chem. A*, Vol. 112, pp. 5846–5857, 2008.

[Viel06] M. Vieluf. “Diplomarbeit: Nanolithographische Strukturierung an selbstassemblierten organischen Monolagen zur selektiven Modifizierung - Diploma Thesis”. Technische Universität Chemnitz, 2006.

[Walk85] B. Walker, H. Port, and H. Wolf. *Chem. Phys.*, Vol. 92, pp. 177–185, 1985.

[Wars74] A. Warshel and E. Huler. *Chem. Phys.*, Vol. 6, pp. 463–468, 1974.

[Watt05] F. Watt, A. A. Bettiol, J. A. van Kan, E. J. Teo, and M. B. H. Breese. *Int. J. Nanoscience*, Vol. 4, pp. 269–286, 2005.

[Weis89] A. L. Weisenhorn, P. K. Hansma, T. R. Albrecht, and C. F. Quate. "Forces in atomic force microscopy in air and water". *Applied Physics Letters*, Vol. 54, No. 26, pp. 2651 –2653, jun 1989.

[Weis92] D. Weiss, R. Kietzmann, J. Mahrt, B. Tufts, W. Storck, and F. Willig. *J. Phys. Chem.*, Vol. 96, pp. 5320–5325, 1992.

[Whit83] P. Whitmore, A. Alivisatos, and C. Harris. *Phys. Rev. Lett.*, Vol. 50, pp. 1092–1094, 1983.

[Wilb95] J. Wilbur, H. Biebuyck, J. MacDonald, and G. Whitesides. *Langmuir*, Vol. 11, pp. 825–831, 1995.

[Wout03] D. Wouters and U. Schubert. *Langmuir*, Vol. 19, pp. 9033–9038, 2003.

[Wout05] D. Wouters, R. Willems, S. Hoeppener, C. Flipse, and U. Schubert. *Adv. Funct. Mater.*, Vol. 15, pp. 938–944, 2005.

[Wout09] D. Wouters, S. Hoeppener, and U. Schubert. *Angew. Chem. Int. Ed.*, Vol. 48, pp. 1732–1739, 2009.

[Wurt04] F. Würthner. *Chem. Commun.*, pp. 1564–1579, 2004.

[Yang06a] M. Yang, Z. Zheng, Y. Liu, and B. Zhang. *J. Phys. Chem. B*, Vol. 110, pp. 10365–10373, 2006.

[Yang06b] M. Yang, Z. Zheng, Y. Liu, and B. Zhang. *Nanotechnology*, Vol. 17, pp. 330–337, 2006.

[Yang09] M. Yang, D. Wouters, M. Giesbers, U. Schubert, and H. Zuilhof. *ACS Nano*, Vol. 3, p. 2887, 2009.

[Zhan07] X. Zhang, Z. Chen, and F. Würthner. *J. Am. Chem. Soc.*, Vol. 129, pp. 4886–4887, 2007.

[Zond03] R. Zondervan, F. Kulzer, S. Orlinskii, and M. Orrit. *J. Phys. Chem. A*, Vol. 107, pp. 6770–6776, 2003.

[Zond04] R. Zondervan, F. Kulzer, M. Kol'chenko, and M. Orrit. *J. Phys. Chem. A*, Vol. 108, pp. 1657–1665, 2004.

Acknowledgement

This thesis was prepared as a part of the DFG project ”Präparation und Charakterisierung ein- und zwei-dimensionaler optisch aktiver Nanostrukturen mittels Rastersondenlithographie” at the chair of ”Optical Spectroscopy and Molecular Physics” at Chemnitz University of Technology between January 2008 and February 2012.
It is a pleasure for me to thank those who made this thesis possible:

- **professor Christian von Borczyskowski and Dr. Harald Graaf for offering me the possibility to work independently on this most interesting topic and for the assistance with new ideas, helpful advices and alternative perspectives**
- **professor Hirokazu Tada (Osaka University) for giving me the opportunity to broaden my scientific and personal horizon during a six month stay at his lab as well as many fruitful discussions**
- **professor Robert Magerle for the generous provision of the atomic force microscopes of his group and reviewing this thesis as the second referee**
- **professor Frank Würthner and co-workers for providing the spermine-functionalized PBI dye**
- **my colleagues and friends at the Chemnitz University of Technology and the OSMP group for their help, stimulating discussions and a pleasant working atmosphere**
- **the German Science Foundation (DFG) for financial support (grant GR 2695/4-1)**

Selbstständigkeitserklärung

Hiermit erkläre ich, dass ich die vorliegende Arbeit selbstständig angefertigt, nicht anderweitig zu Prüfungszwecken vorgelegt und keine anderen als die angegebenen Hilfsmittel verwendet habe. Sämtliche wissentlich verwendete Textausschnitte, Zitate oder Inhalte anderer Verfasser wurden ausdrücklich als solche gekennzeichnet.

Chemnitz, den 20.02.2012

Thomas Baumgärtel

Lebenslauf

Name	**Thomas Baumgärtel**
Geburtsdatum	**17.11.1982**
Geburtsort	**Karl-Marx-Stadt**
2002 - 2007	**Studium der Physik an der Technischen Universität Chemnitz**
2007	**Diplomarbeit zum Thema ”Rasterkraftmikroskopisch induzierte Nanolithographie an alkylterminiertem Silizium zur selektiven Anbindung von Farbstoffmolekülen”**
2008-2012	**Wissenschaftlicher Mitarbeiter an der Professur ”Optische Spektroskopie und Molekülphysik” an der Technischen Universität Chemnitz**
2012	**Promotion zum Thema ”Binding and characterization of fluorescent nano-aggregates on structured surfaces”**